STRUCTURAL SYSTEMS

RESEARCH PROJECT

Report No.
SSRP–06/18
Final

SEISMIC RESPONSE OF PRECAST SEGMENTAL BRIDGE SUPERSTRUCTURES

by

MARC J. VELETZOS

JOSÉ I. RESTREPO

FRIEDER SEIBLE

Final Report Submitted to the California Department of Transportation (Caltrans) Under Contract No. 59A0337

December 2006

Department of Structural Engineering
University of California, San Diego
La Jolla, California 92093-0085

University of California, San Diego
Department of Structural Engineering
Structural Systems Research Project

Report No. SSRP–06/18

SEISMIC RESPONSE OF PRECAST SEGMENTAL BRIDGE SUPERSTRUCTURES

by

Marc J. Veletzos
Graduate Student Researcher

José I. Restrepo
Professor of Structural Engineering

Frieder Seible
Dean of the Jacobs School of Engineering
Professor of Structural Engineering

Final Report Submitted to the California Department of Transportation (Caltrans) Under Contract No. 59A0337

Department of Structural Engineering
University of California, San Diego
La Jolla, California 92093-0085

December 2006

Technical Report Documentation Page

1. Report No.	2. Government Accession No.	3. Recipient's Catalog No.

4. Title and Subtitle	5. Report Date
Seismic Response of Precast Segmental Bridge Superstructures	December, 2006
	6. Performing Organization Code UCSD/ SSRP-06/18
7. Author(s) Marc J. Veletzos, José I. Restrepo, Frieder Seible	8. Performing Organization Report No. UCSD / SSRP- 06/18
9. Performing Organization Name and Address Department of Structural Engineering School of Engineering University of California, San Diego La Jolla, California 92093-0085	10. Work Unit No. (TRAIS) 11. Contracts or Grant No. 59A0337
12. Sponsoring Agency Name and Address California Department of Transportation Division of Engineering Services 1801 30th St., West Building MS #9-2/5I Sacramento, California 95807	13. Type of Report and Period Covered Final Report 14. Sponsoring Agency Code

15. Supplementary Notes

Prepared in cooperation with the State of California Department of Transportation.

16. Abstract

Precast segmental construction of bridges can accelerate construction and minimize the cost of bridges in highly congested urban environments and environmentally sensitive regions. Despite their proven benefits, the use of precast segmental bridges in seismic regions of the United States remains very limited. A main obstacle to their use is the concern about the seismic response of segment joints. Recent research has shown that segment joints can undergo very large rotations that open up gaps in the superstructure, without significant loss of strength. While the ultimate performance of segment joints was investigated, the expected response during a significant seismic event remains uncertain. Using models of precast segmental bridges, similar to the Otay River Bridge and the San Francisco-Oakland Bay Bridge Skyway as case studies, this report will investigate the response of segment joints using detailed non-linear time-history analyses. A suite of ten near field earthquake records were used to determine the median joint response as well as to quantify the effect of vertical motion on the joint response.

17. Key Words	18. Distribution Statement
post-tensioning, precast, segmental construction, balanced cantilever, seismic, superstructures, segment joints, analysis	Unlimited

19. Security Classification (of this report)	20. Security Classification (of this page)	21. No. of Pages	22. Price
No restrictions	Unclassified	~94	

Form DOT F 1700.7 (8-72)

Disclaimer

The contents of this report reflect the views of the authors who are responsible for the facts and the accuracy of the data presented herein. The contents do not necessarily reflect the official views or policies of the State of California. This report does not constitute a standard, specifications or regulation.

Acknowledgments

This research project was made possible by funding from the California Department of Transportation under contract No. 59A0337. The input of Dr. Charly Sikorsky and others at Caltrans was greatly appreciated.

The authors would like to express their gratitude to Dr. Athol Carr at the University of Canterbury, New Zealand for his assistance with developing a suitable finite element model, Benjamin Soule and Daniel Tassin at International Bridge Technologies for their assistance with design details of the Otay River Bridge, and Dr. Sajid Abbas at T.Y. Lin International for his assistance with design details of the San Francisco-Oakland Bay Bridge Skyway.

Abstract

Precast segmental construction of bridges can accelerate construction and minimize the cost of bridges in highly congested urban environments and environmentally sensitive regions. Despite their proven benefits, the use of precast segmental bridges in seismic regions of the United States remains very limited. A main obstacle to their use is the concern about the seismic response of segment joints. Recent research has shown that segment joints can undergo very large rotations that open up gaps in the superstructure, without significant loss of strength. While the ultimate performance of segment joints was investigated, the expected response during a significant seismic event remains uncertain. Using models of precast segmental bridges, similar to the Otay River Bridge and the San Francisco-Oakland Bay Bridge Skyway as case studies, this report will investigate the response of segment joints using detailed non-linear time-history analyses. A suite of ten near field earthquake records were used to determine the median joint response as well as to quantify the effect of vertical motion on the joint response.

Table of Contents

List of Figures

List of Tables

1. Introduction

Precast segmental construction methods can ease construction costs by reducing construction time while maintaining quality. In addition, the absence of falsework can minimize traffic congestion and environmental impact, adding to the benefits of this construction method. While the popularity of precast segmental construction has increased throughout the United States, and the world, its use in seismic regions of the country has been hampered by a lack of research on the seismic response. The California Department of Transportation supported a research program to address this concern. This report summarizes recent research that builds upon the previous experimental phases and investigates the response of two full scale segmental bridges using detailed finite element analyses.

1.1. Summary of Previous Research

The research presented in this report builds upon previous research at the University of California, San Diego. To help explain the motivation for the current research it is important to summarize the findings of the previous phases of the research program.

1.1.1. Phase I – High Moment and Low Shear Experiments

Four 2/3 scale test units were tested under vertical loading to failure to investigate the performance of precast segments in superstructure regions of high moment and low shear (Megally et al., 2002). The test set-up is shown in Figure 1-1. The test units investigated different post tensioning layouts as shown in Figure 1-2. In addition, one test unit was constructed with a cast-in-place deck closure and 100% internal tendons. All test units achieved large rotations prior to failure. The failure modes varied from rupture of the

post-tensioning (PT), to crushing of the extreme concrete fibers to buckling of the deck rebar and subsequent compression failure of the cast-in-place deck.

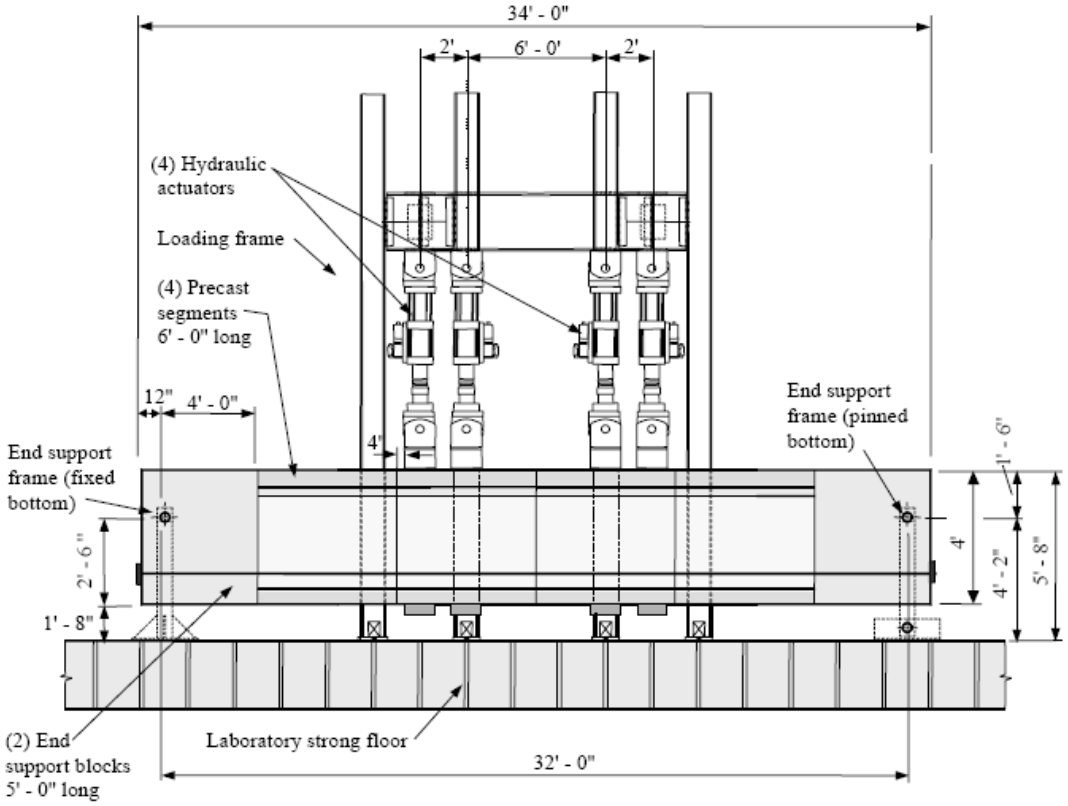

Figure 1-1 Phase I Experimental Test Set-Up (Megally et al., 2002)

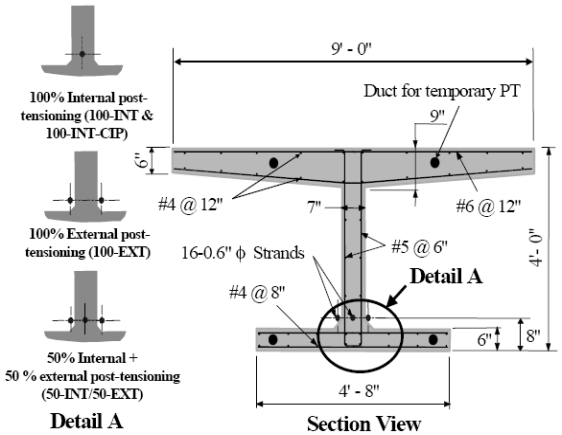

Figure 1-2 Phase I Test Unit Cross Section (Megally et al., 2002)

1.1.2. Phase II – High Moment and High Shear Experiments

This phase of the research program utilized similar test units as in Phase I, but with different PT details and test set-up (Megally et al., 2002). The test units and test set-up are shown in Figure 1-3 and Figure 1-4, respectively. The results of this phase were similar to the previous phase in that all test units achieved large rotations prior to failure. In addition, no relative shear slip between segments was observed prior to flexural failure. All test units experienced crushing of the bottom soffit under negative bending. The final failure, however, varied from crushing of the top flange to rupture of the PT tendons.

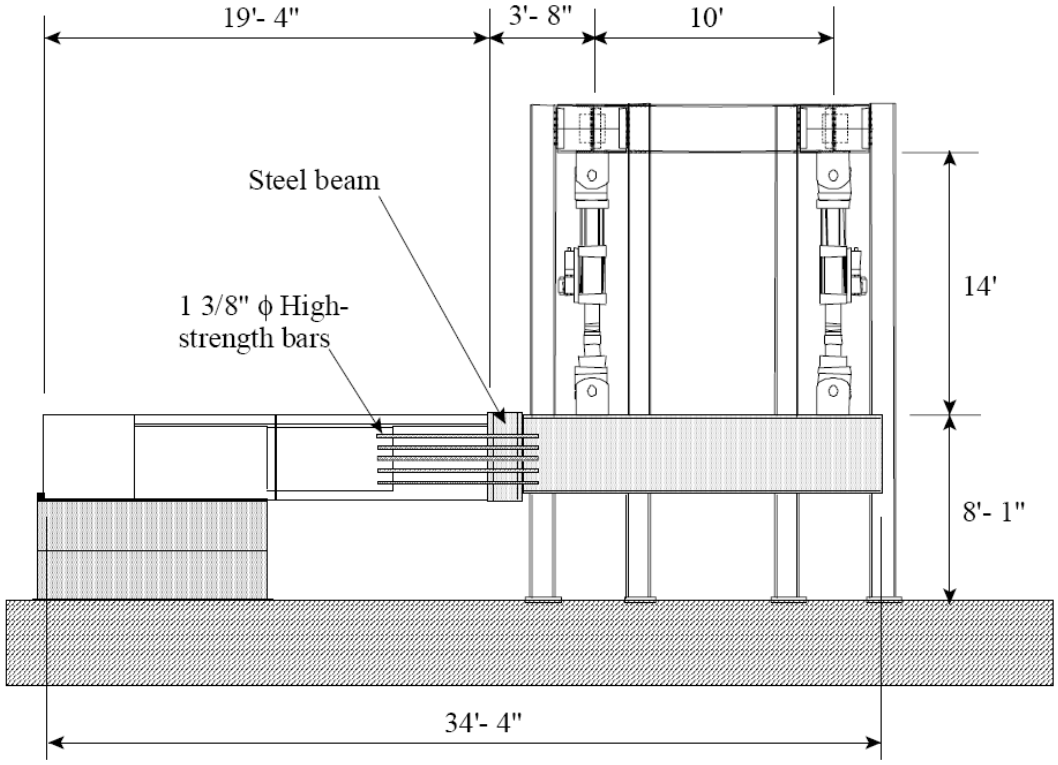

Figure 1-3 Phase II Test Set-Up (Megally et al., 2002)

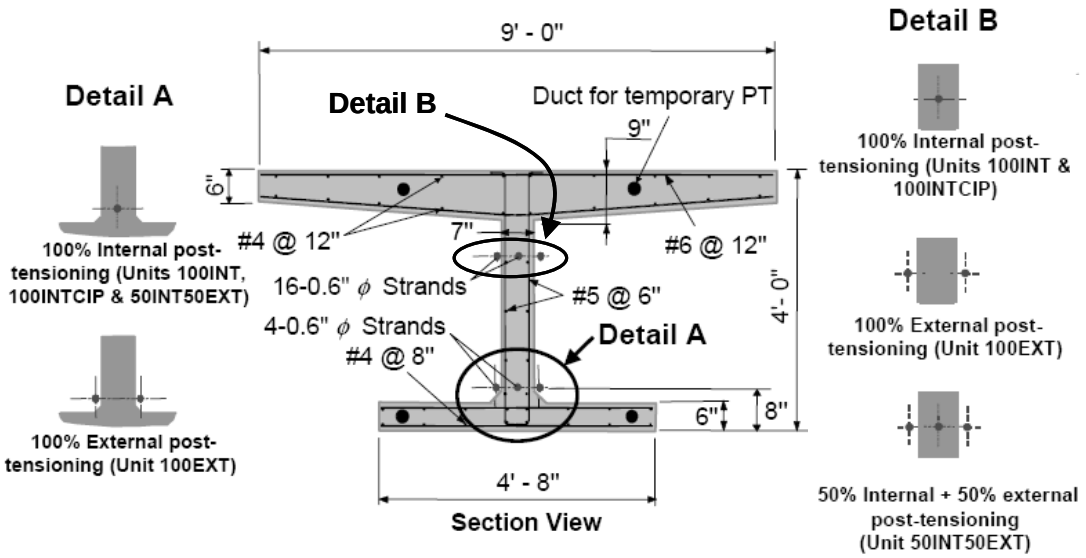

Figure 1-4 Phase II Test Unit Cross Section (Megally et al., 2002)

1.1.3. Phase III – System Test

This phase of the research program investigated the performance of a half-scale superstructure-pier system (Burnell et al., 2005). The test set-up and superstructure cross section are shown in Figure 1-5 and Figure 1-6, respectively. The testing program for this phase was split into two stages. The first stage achieved a column displacement ductility of 4 and utilized 100% of the design post-tensioning as well as 100% of the superstructure dead load. The results from this stage indicated that there was no significant opening of the segment-to-segment joints. A hairline crack was observed at a displacement ductility of 4, but this was adjacent to the cast-in-place closure pour, so the crack was likely initiated by shrinkage. The second stage of testing continued from displacement ductility 4 up to ductility 8 and utilized 175% of the superstructure dead load to account for vertical accelerations and approximately 75% of the longitudinal superstructure PT. The results from this stage indicated that segment-to-segment joints open during testing, but they closed when the earthquake demands were removed.

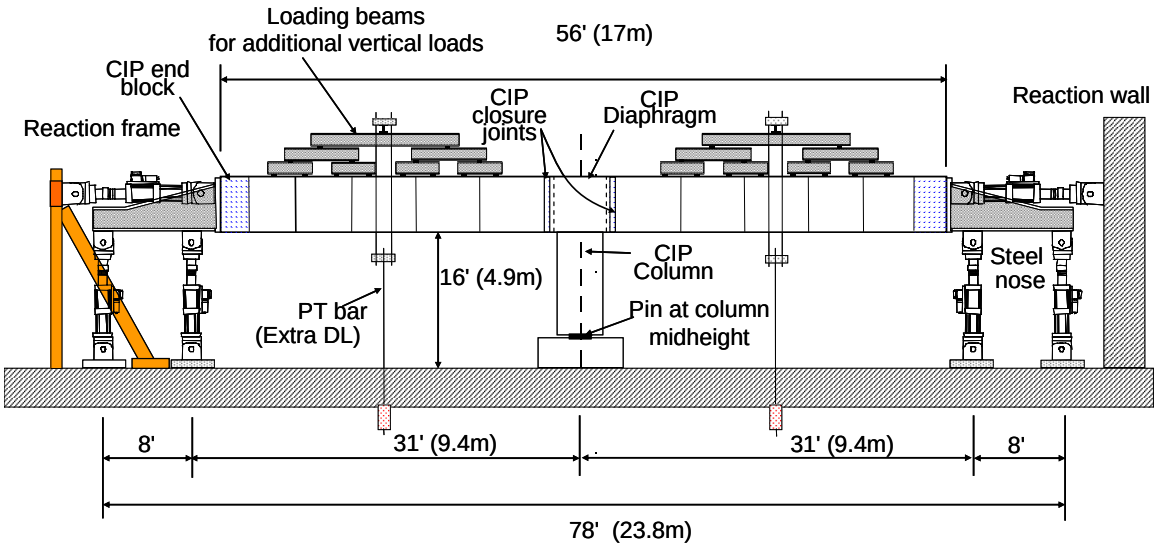

Figure 1-5 Phase III Experimental Test Set-Up (Burnell et al., 2005)

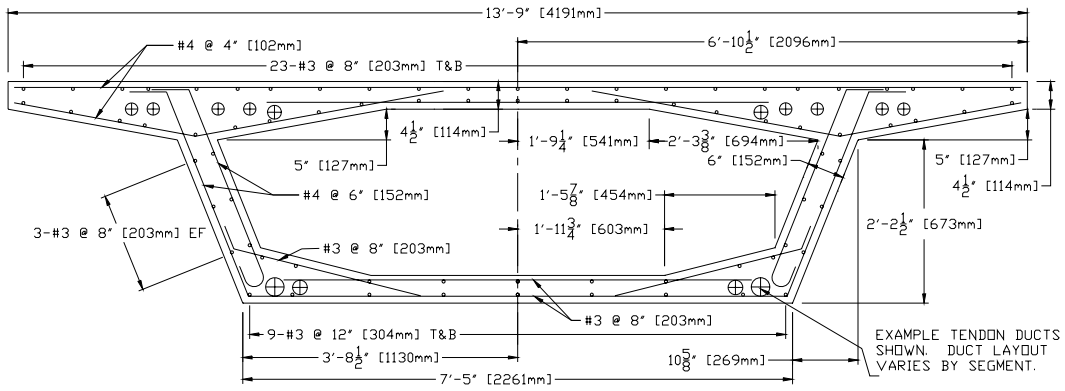

Figure 1-6 Phase III Test Unit Superstructure Cross Section (Burnell et al., 2005)

1.2. Issues Addressed in this Report

The previous three phases of this research program achieved their objectives and determined the crack patterns, failure modes and behavior of precast segmental bridge superstructure joints. However a number of issues remain and are outlined below. This report addresses these issues using detailed 2D non-linear time history analyses.

1.2.1. Contribution of Vertical Motions

Phase III - Stage 2 testing showed that precast segment joints open if the dead load of the superstructure was increased by 75% and the superstructure post tensioning was reduced by 25%, indicating that vertical motion contributed to joint opening. But this contribution was not decoupled from the effect of reducing the longitudinal PT. So the question remains, how much do vertical earthquake motions contribute to joint opening? Also, if joints open, what is the possibility of yielding the tendons and developing residual inter-segment cracks of significant width?

1.2.2. Joint opening

The Phase III – Stage 2 experiment indicated that segment joints will likely open when vertical motion is considered and when the longitudinal post tensioning is reduced. But what about when the PT is not reduced? Do the joints still open? If so, how much? What is the expected crack width?

1.2.3. Residual cracks and yielding of longitudinal post-tensioning

The Phase III experiment indicated that current design procedures, based on capacity design principles, prevent residual joint opening and protect the longitudinal post tensioning tendons from yielding when vertical earthquake motion was not considered. Does this remain true when vertical earthquake motions are considered? If not, how large of a residual crack width can be expected and how much of the post tensioning force has been lost?

1.3. Report Outline

Chapter 1 discussed the motivation for this report and summarizes previous phases of the research program. Chapter 2 discusses the validation of the joint model and summarizes the results of various sensitivity studies that were used to fully understand and optimize the joint model. The earthquake records used for the time history analyses are described in Chapter 3. Chapter 4 documents the full bridge models and discusses the discretization and results of all the various analyses for both the 300 foot and the 525 foot span models. The limitations of the models are outlined in Chapter 5. Chapters 6, 7 and 8 discuss conclusions, design recommendations and future research, respectively. Additional model results and a description of the Ruaumoko (Carr, 2004) finite element analysis program are included in the Appendix.

2. Joint Model Validation

In order to ensure that the analytical model accurately represents the physical world, the joint model must be validated with physical experiments. Two detailed finite element models of test unit 100-INT from the Phase I experiment were created using the computer software Ruaumoko (Carr, 2004). Ruaumoko was selected because of its extensive library of non-linear hysteresis and damping rules. A detailed description of the program is given in Appendix B. These models were developed to capture numerous physical characteristics of the segment-to-segment joints. These characteristics include: crushing of extreme concrete fibers, yielding of PT tendons at the true limit of proportionality, and energy dissipation due to bond slip of the grouted internal tendons.

2.1. Single Joint Model

The first model, shown in Figure 2-1, captured the moment rotation response of a single segment-to-segment joint. To concentrate deformations at the midspan joint, the rotations of the girder nodes were slaved to the rotation at the supports. The joint was modeled with six axial only elements at the top and bottom flanges and three axial only elements at the web. Each element captured concrete crushing and tensile cracking using an origin centered hysteresis rule to capture the loss of stiffness after cracking and crushing (see Figure 2-2a). The PT across the joint is modeled with three separate elements. One element captured the early onset of yielding at the true limit of proportionality of ASTM A416 (270 ksi) steel of 210 ksi. A second element captured the response of PT between the limit of proportionality and the idealized yield stress as well as the post yield response of PT strands (see Figure 2-2b). The third element captured the

bond slip behavior of PT across the joint. When a joint opens and the PT strands stretch, they lose their bond with the grout and energy is dissipated between the strands and the grout, via friction. The unbonded length of the PT was obtained by a trial and error process to match the experimental data. This is described in detail in Section 2.3.1. Rigid elements between the superstructure girder elements and the PT are used to ensure accurate PT deformations. At the joint locations, however, rigid elements are not used. Rather, the vertical deformations of the PT nodes are slaved to the girders. This will allow for tendon slip caused by strain penetration into the segments.

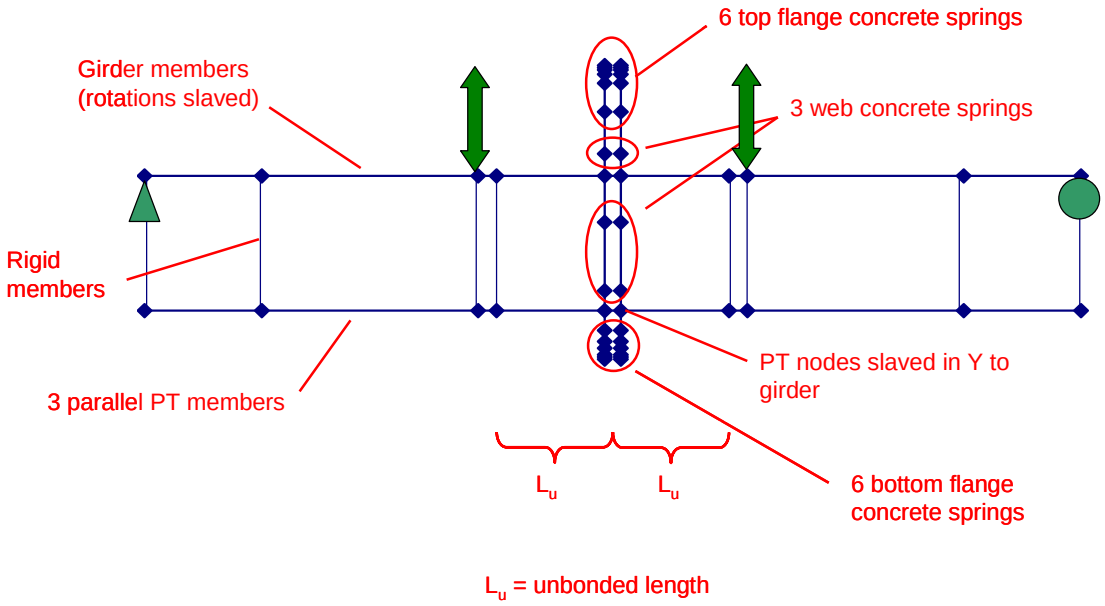

Figure 2-1 Single Joint Model

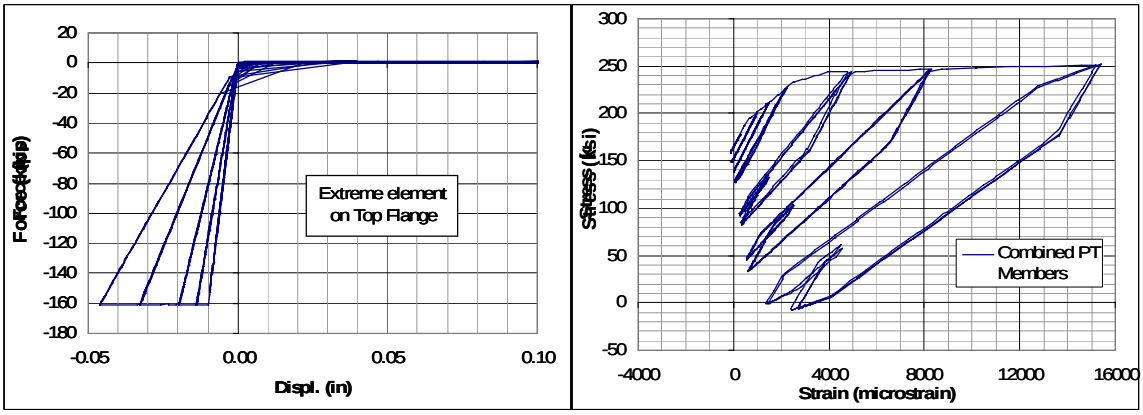

a) Joint Concrete b) Combined PT Members – Includes Bond Slip

Figure 2-2 Joint Concrete and Combined PT Hysteresis Model

Results from the single joint model are shown in Figure 2-3. The backbone curve, yield displacement and energy dissipation match very accurately the experimental results for both small and large rotations. Differences between the model and the experiment are such that the residual rotations in the model are larger that observed in the tests. Therefore the residual rotations obtained from the analyses will be accurate if not slightly over-predicted.

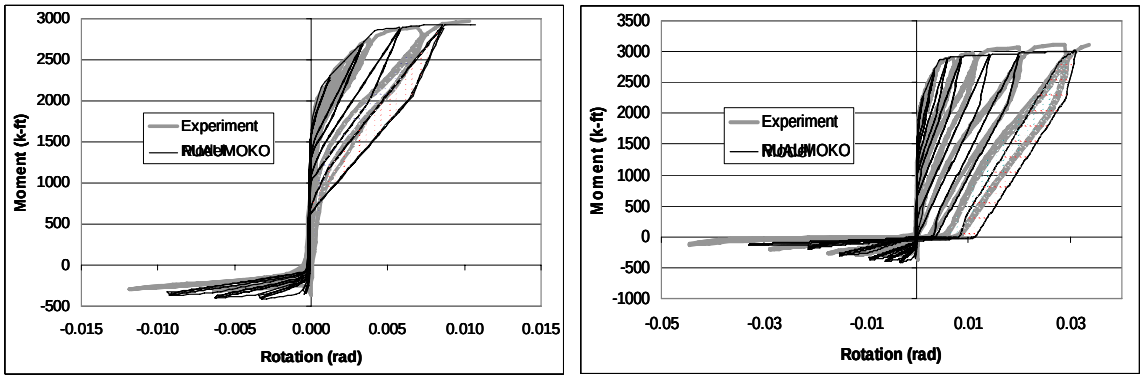

a) Small Rotations b) Large Rotations

Figure 2-3 Moment-Rotation Diagrams of Single Joint Model

2.2. Multiple Joint Model

The second validation model, shown in Figure 2-4, captures the response at the system level including deformations with the precast segments and joint opening. This model allows the superstructure girders to crack and captures shear deformations of the girders using a concentrated flexibility approach. That is, all the shear deformations are concentrated in two non-linear element located at segment-to-segment joints 2 and 4. Note that shear deformations are not expected to be significant in a full size bridge superstructure, because the shear span of a full size bridge is much larger. These elements were added to the model to capture effects observed in the experiment. The properties of the non-linear shear springs were estimated using the modified compression field theory.

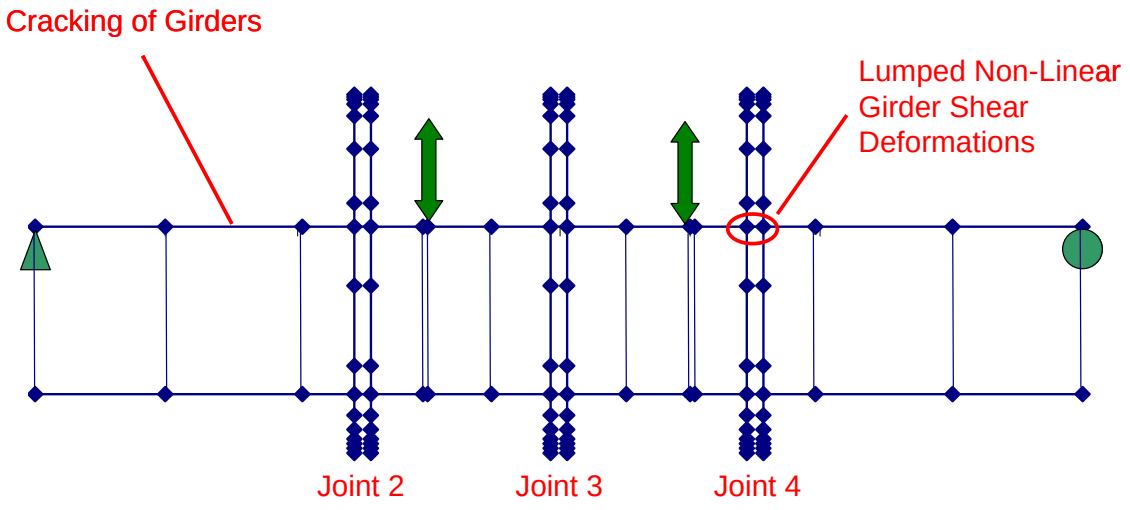

Figure 2-4 Multiple Joint Model

Results from the multi-joint model are shown in Figure 2-5 and Figure 2-6. Figure 2-5a shows the Moment-Rotation of the midspan joint for small rotations (less than 0.005

radians). This plot suggests that the computer model slightly under predicts the joint rotation. This, however, is not the case because the target displacement for the 1 inch cycle was not reached, as can be seen in Figure 2-5b.

Figure 2-6a shows the Moment-Rotation diagram for large rotations (greater than 0.0075 radians), while Figure 2-6b shows the Girder Shear-Midspan Deflection diagram. These diagrams indicate that the model overestimates the midspan joint rotations while matching the midspan vertical deformations. This suggests that the finite element model will provide conservative joint rotation estimates and is considered acceptable.

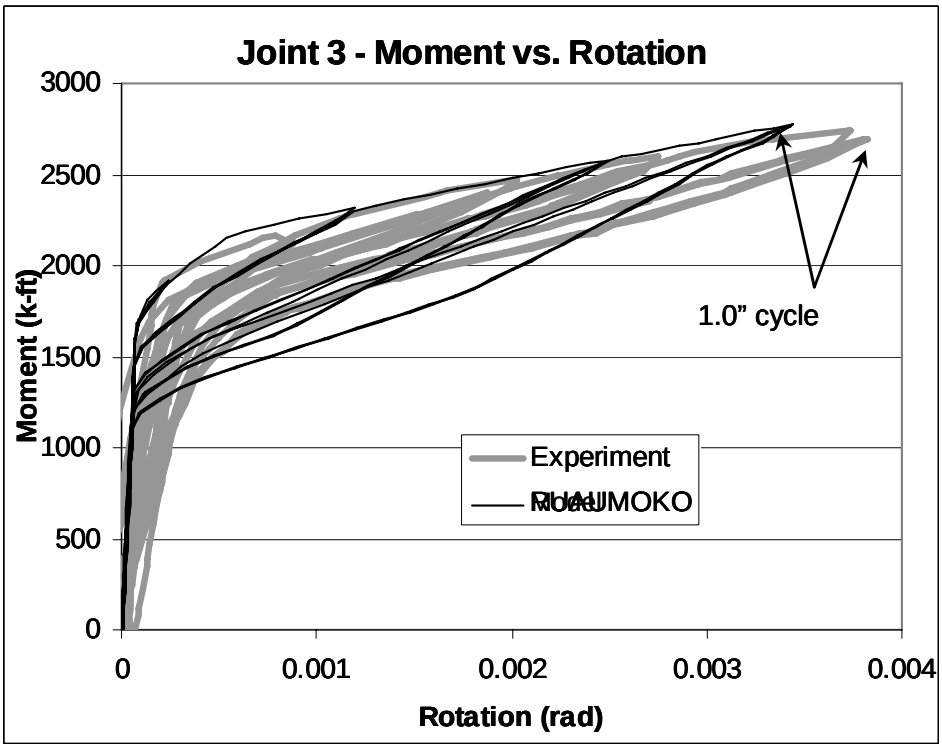

a) Midspan Moment-Rotations

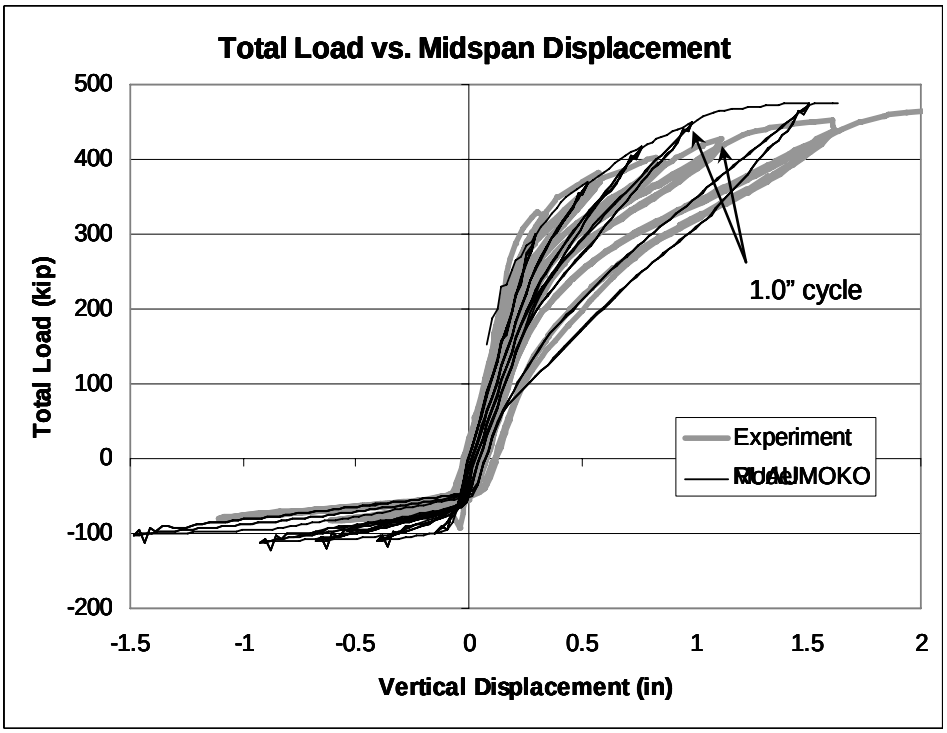

b) Girder Shear-Midspan Deflection

Figure 2-5 Small Deformation Results from the Multiple Joint Model

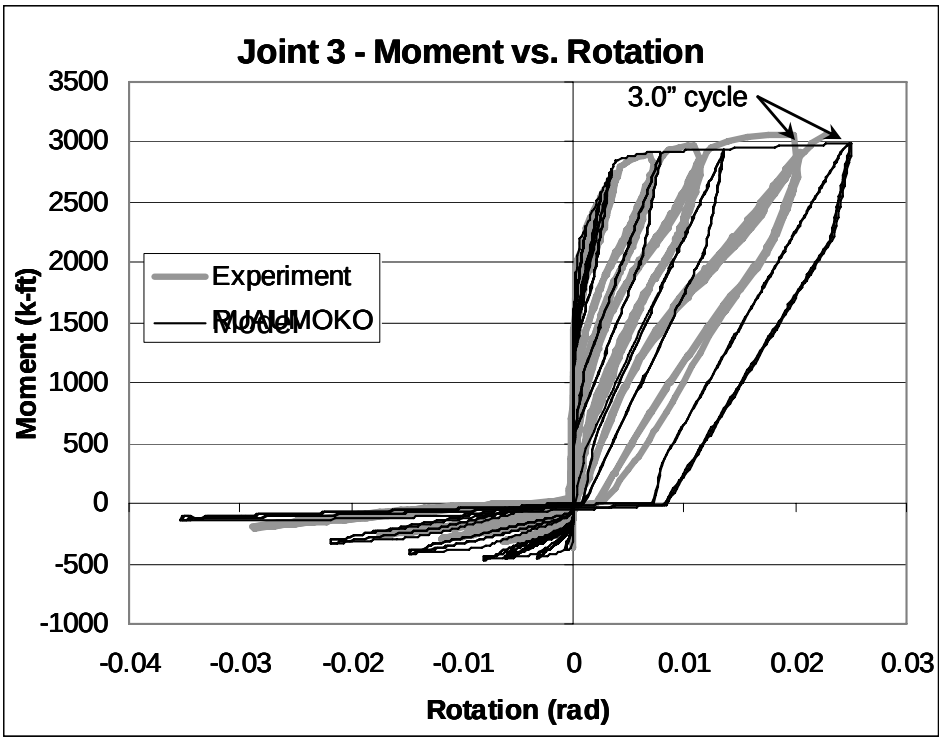

a) Midspan Moment-Rotations

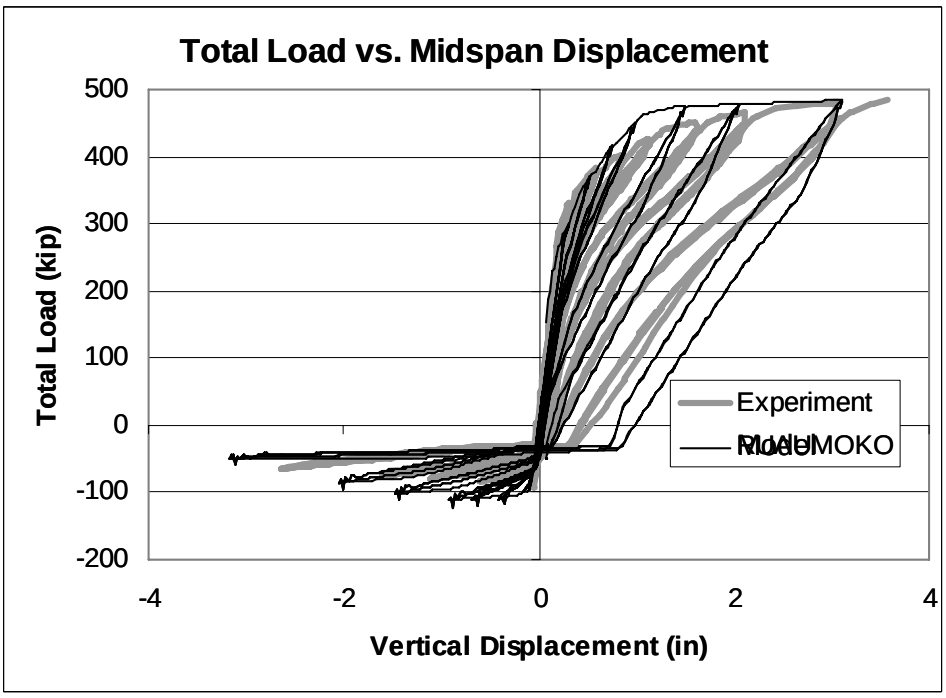

b) Girder Shear-Midspan Deflection

Figure 2-6 Large Deformation Results from the Multiple Joint Model

2.3. Sensitivity Studies

Three separate parameter studies were performed to investigate the influence of various variables and to optimize performance of the segment joint model. The parameters studied include the number of concrete springs across the segment-to-segment joints, the unbonded length of the grouted PT tendons, and the amount and type of damping.

2.3.1. Unbonded Length of the PT

The unbonded length of the PT tendons was determined using a trial and error approach to match the results from the Phase I experiments. The unbonded length was increased in 5 inch increments from 10 inches up to 45 inches, and the moment rotation response of the joint was compared to the experimental results. Figure 2-7 to Figure 2-9 show the comparisons of the 10 inch, 25 inch, and 40 inch unbonded lengths to test unit 100-INT of the Phase I experiment. An unbonded length of 25 inches matches the experiment best. The PT tendons yield at the same rotation and the energy dissipation is comparable. The 10 inch unbonded length is too stiff after joint opening and significantly under predicts the rotation at which the tendon yields. Conversely, the 40 inch unbonded length is too soft upon joint opening and significantly over predicts the rotation at which the tendon yields.

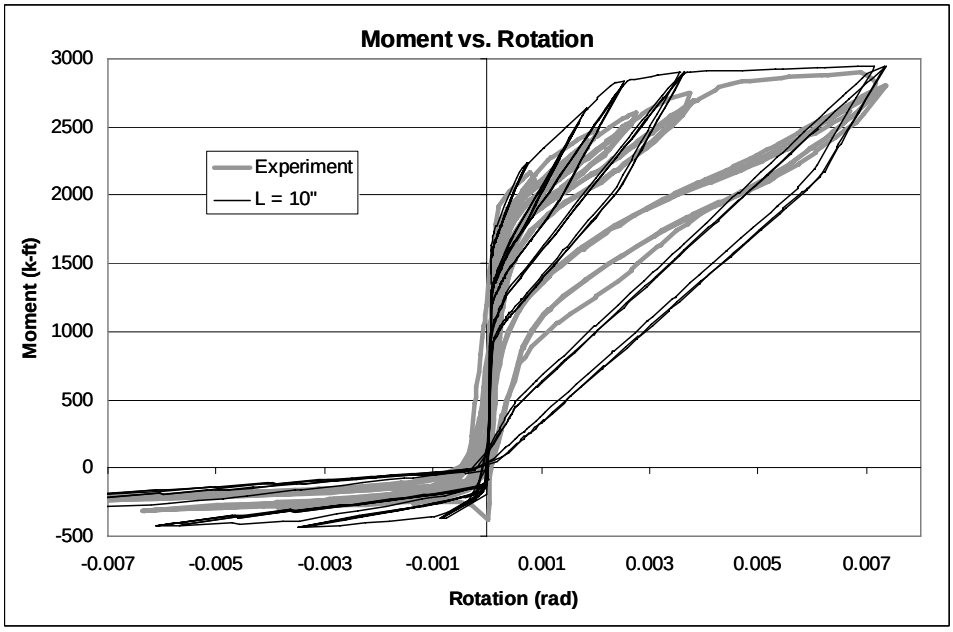

a) Small Rotations

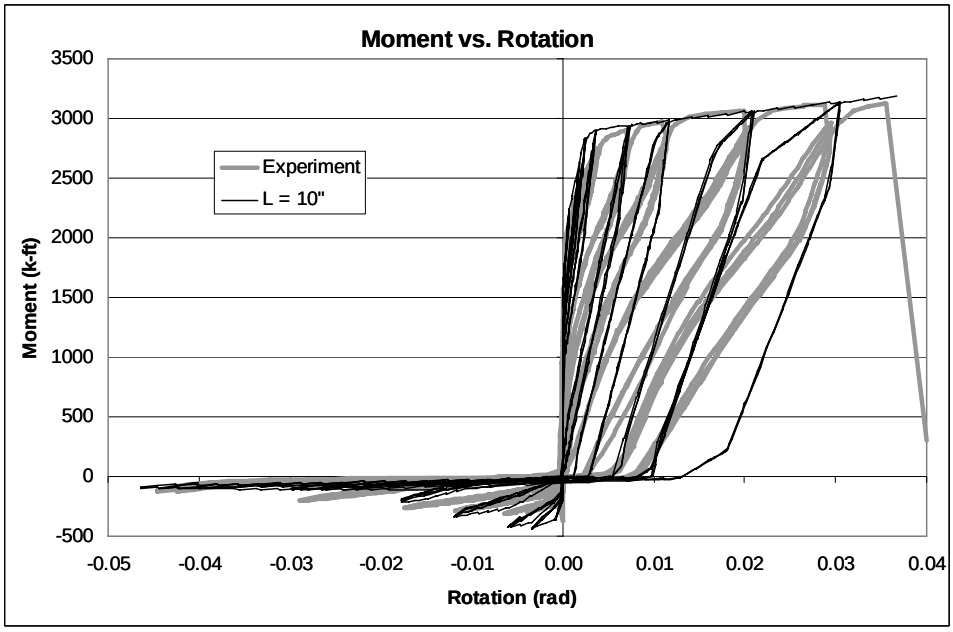

b) Large Rotations

Figure 2-7 Moment - Rotation Diagrams with 10" Unbonded Length

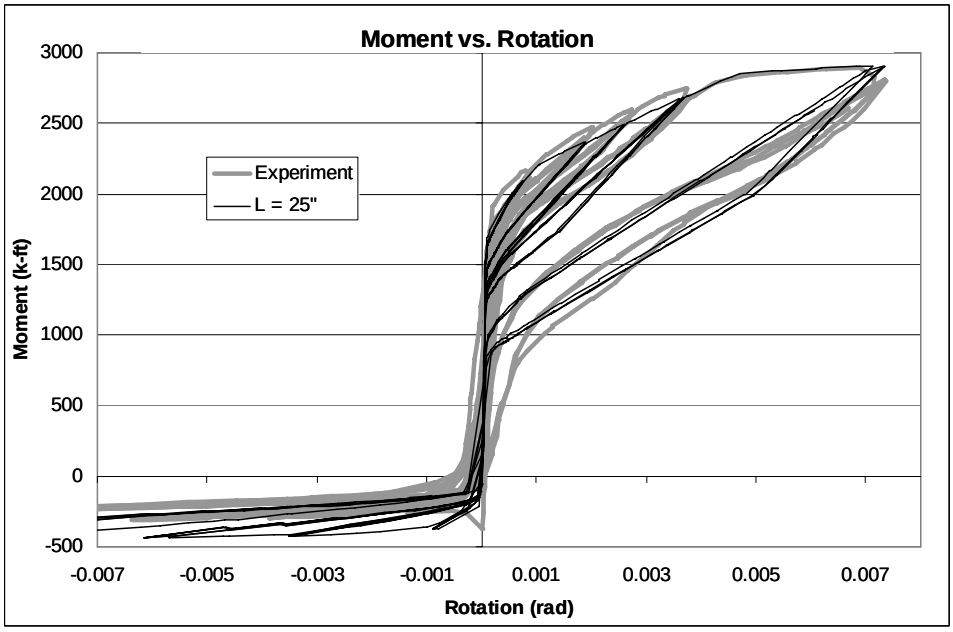

a) Small Rotations

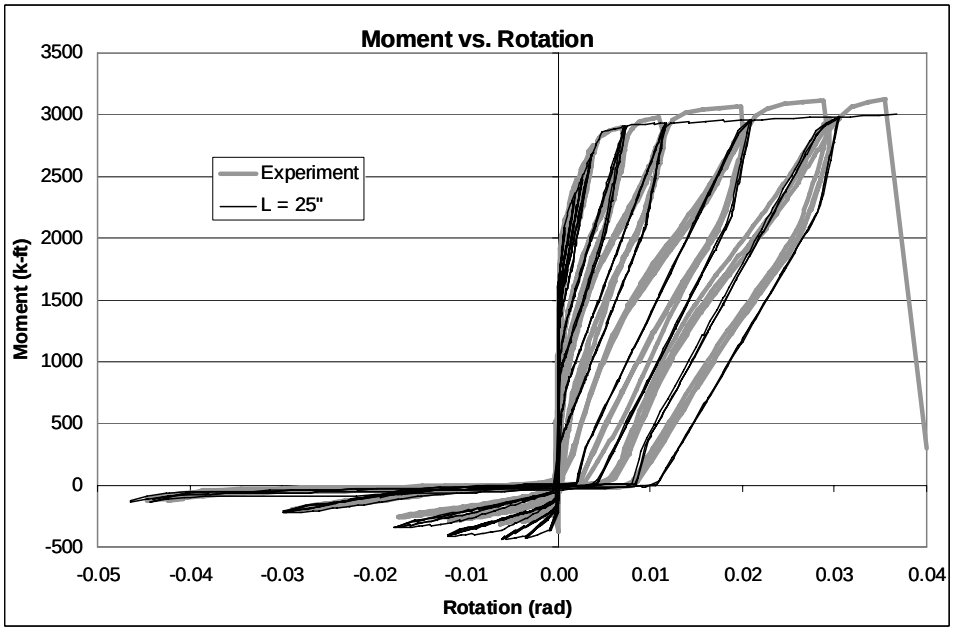

b) Large Rotations

Figure 2-8 Moment - Rotation Diagrams with 25" Unbonded Length

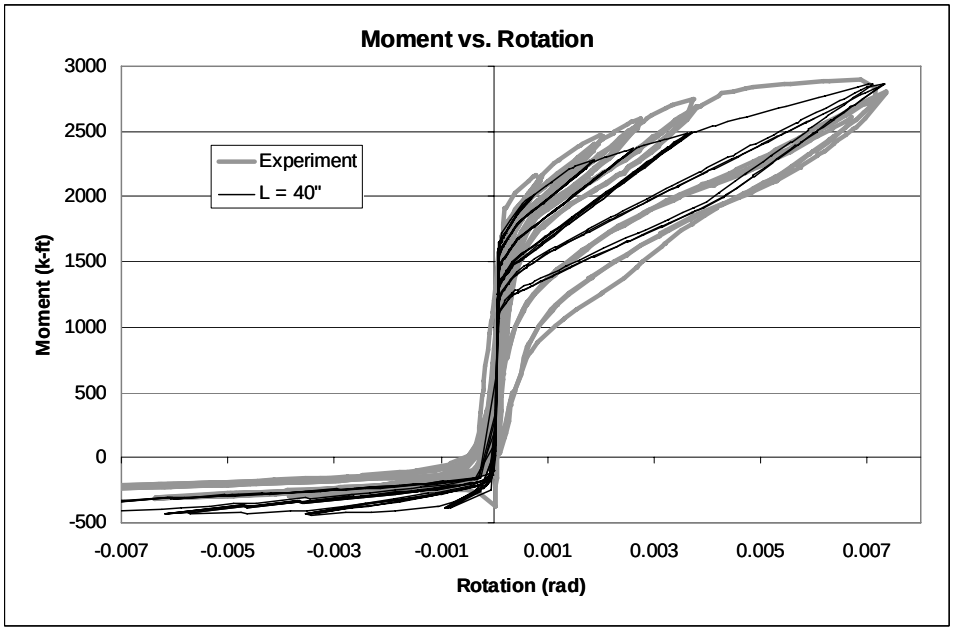

a) Small Rotations

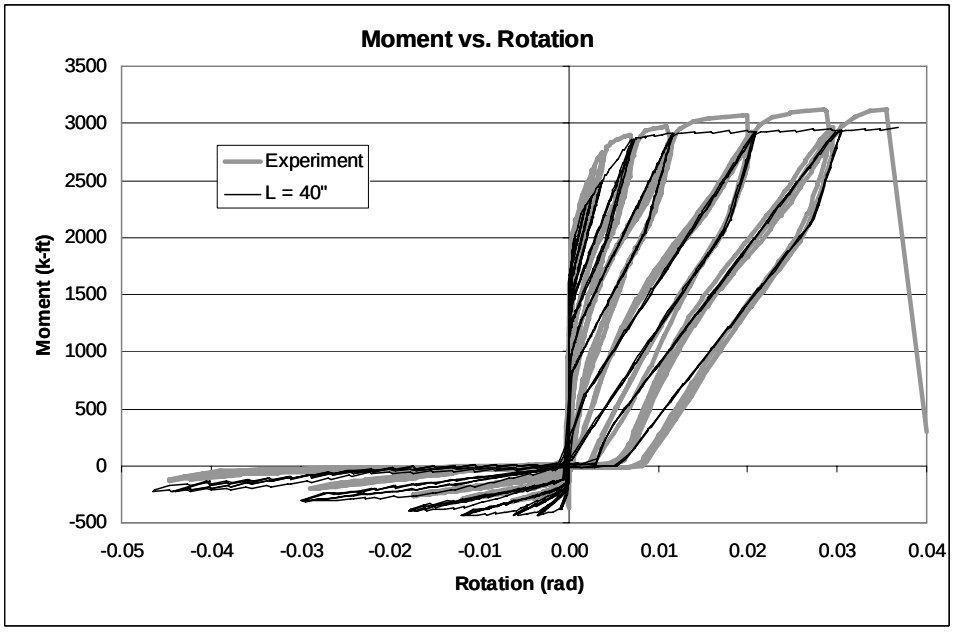

b) Large Rotations

Figure 2-9 Moment - Rotation Diagrams with 40" Unbonded Length

2.3.2. Number of Joint Springs

The initial number of concrete springs across the segment-to-segment joints was selected, somewhat arbitrarily, to be fifteen (six in both the top and bottom flanges and three in the web). The intention was to capture the energy dissipation and loss of stiffness due to crushing of the extreme concrete fibers. Using fifteen concrete springs across each joint will result in a very large stiffness matrix in a full bridge model. This may increase the likelihood of convergence problems and will require significant computational effort. If the number of concrete springs can be reduced without compromising the accuracy of the results, much time and effort will be saved.

With the goal of optimizing the number of concrete springs across the segment-to-segment joints, several models were developed with flange springs ranging from one to six and web springs ranging from one to three. Comments about each model are shown in Table 1.

Table 1 - Joint Spring Parameter Study Summary

Total Joint Springs	Flange Springs	Web Springs	Comments
15	6	3	Reference model.
14	6	2	No visible change in response.
13	6	1	No visible change in response.
11	5	1	Essentially no change.
9	4	1	Essentially no change. Stable if only 2 flange springs crush.
7	**3**	**1**	**Essentially no change. Stable if only 1 flange spring crushes.**
5	2	1	Slightly understimates the yield moment. Numerical problems at large rotations.
3	1	1	Understimates the yield moment. No concrete crushing

The seven spring model (three flange springs and 1 web spring) produced the best results as can be seen in Figure 2-10. The joint response is nearly identical to the fifteen spring model (six flange springs and 3 web springs), with a slight deviation at the onset of joint opening. The yield rotation and energy dissipation are identical. Further reducing the number of flange springs increases the likelihood of numerical instability and inaccuracies in the moment due to difficulties in modeling the centroid of the compression toe.

It should be noted that for tall girders, multiple web springs are required in order to accurately model the bending stiffness of the girder across the joints. By using only axial springs across the joint, the moment of inertia is calculated solely with the parallel axis theorem. For very large webs, the moment of inertia of the web itself (i.e. $bd^3/12$) is significant. Breaking the web up into smaller areas will reduce the error. It is for this reason that multiple web springs were used in the full bridge models.

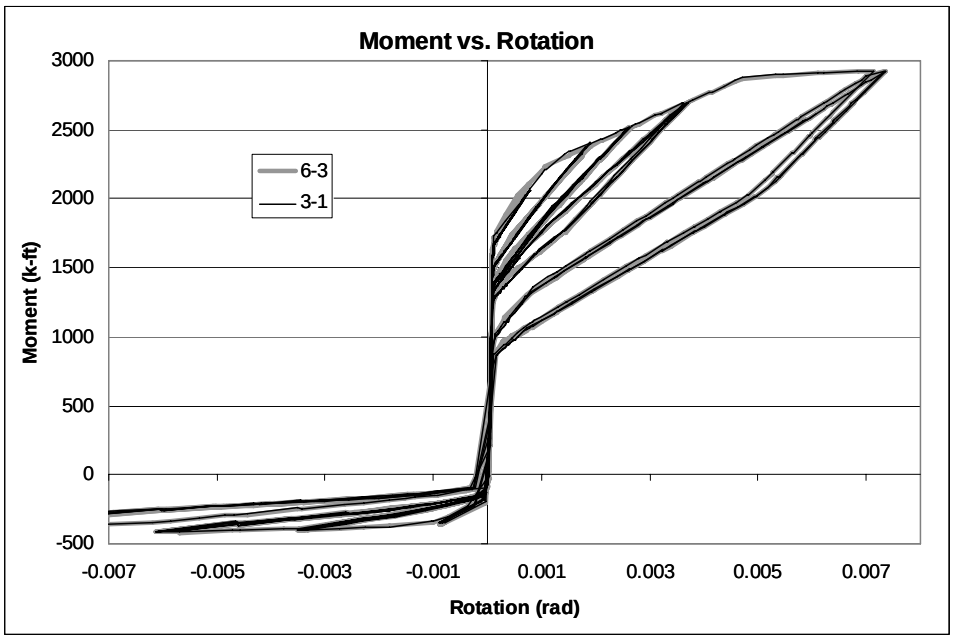

a) Small Rotations

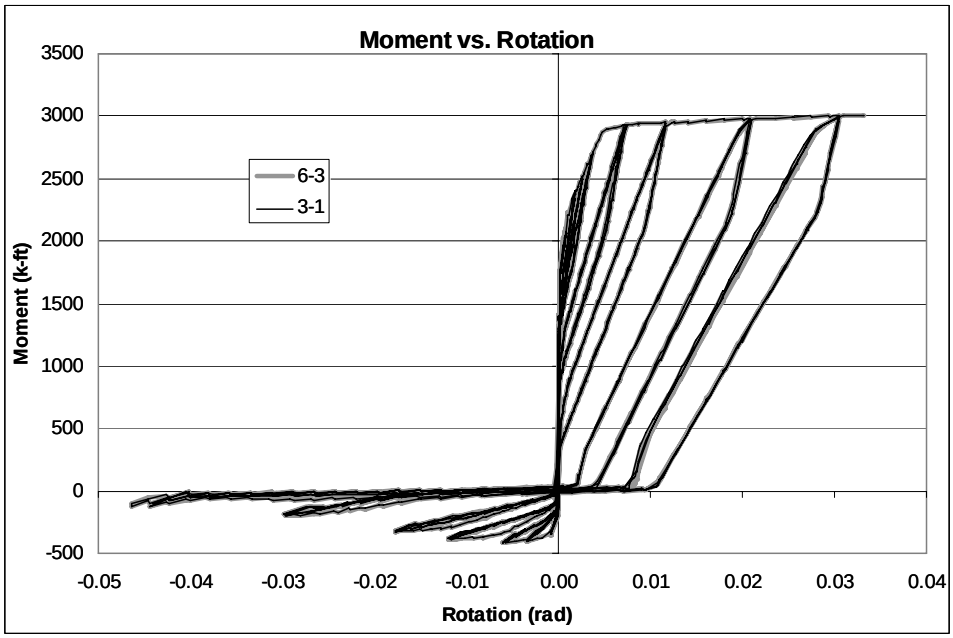

b) Large Rotations

Figure 2-10 Moment - Rotation Diagram - Comparison of 15 and 7 Joint Springs

2.3.3. Damping

The type and amount of damping play a significant role in the accuracy of jointed models. To investigate and understand the effects of damping on the model, we have run a number of analyses with different types and amount of damping. The damping types selected are constant modal damping, Rayleigh damping based on the initial stiffness of the structure, and Rayleigh damping based on the tangent stiffness of the structure as formulated in the computer program Ruaumoko (Carr, 2004). Damping levels were varied from 0.1% up to 10%.

The Rinaldi record from the 1994 Northridge earthquake was used as the excitation in the damping sensitivity study. The single joint model was used to ensure that observations are due solely to the modeling of the joint and not due to other modeling effects. Mass was added to the model at midspan to obtain a realistic primary vertical period of 0.4 seconds (see Figure 2-11). The record was reduced down to a PGA of 0.7g and then further reduced by a factor of 1/8 to account for scaling effects as this is a model of a half scale experiment. This reduction in the excitation produced reasonable joint rotations that ranged from 0.005 radians (i.e. the yield rotation) with 10% damping up to 0.03 radians with 0.1% damping.

It is important to note that a time step of 0.001 seconds was used for all analyses. A time step of 0.0001 seconds was also investigated, but this reduced time step had no effect on the results, yet increase the run time significantly.

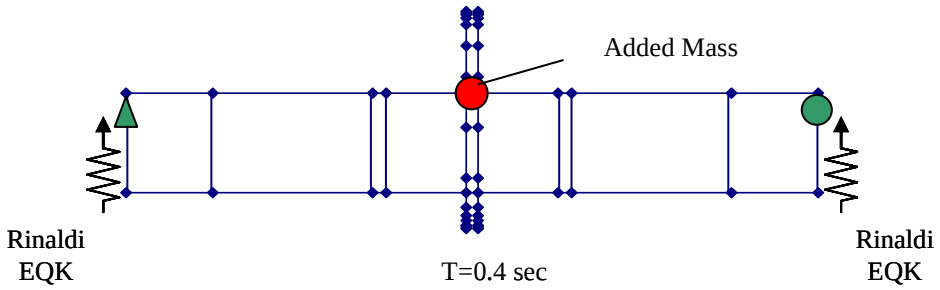

Figure 2-11 Damping Sensitivity Study Model

Results from the damping study are summarized on Figure 2-12. The tangent stiffness Rayleigh damping typically generated shear forces that are significantly higher than the other damping models. The initial stiffness Rayleigh and the Constant Modal damping models produced similar shear forces for damping values greater than 1%.

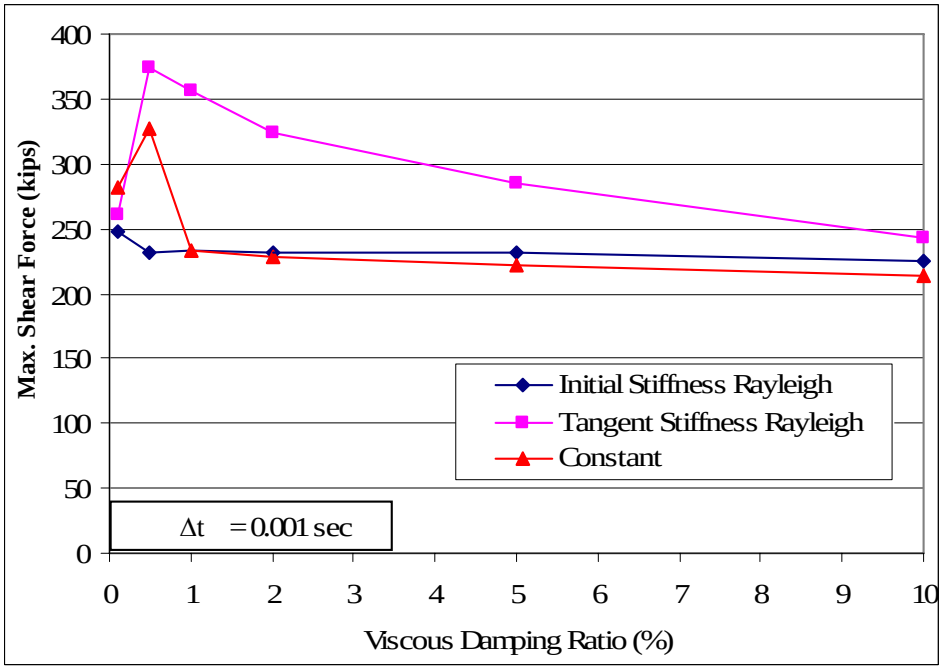

Figure 2-12 Influence of Amount of Damping on Peak Girder Shear Force

Figure 2-13 to Figure 2-15 compare the girder shear and midspan displacement time histories of the three damping models with damping values of 0.1%, 2%, and 10%, respectively. Note that the initial stiffness Rayleigh and constant damping models are typically similar to each other, while the tangent stiffness Rayleigh can differ significantly.

The initial Rayleigh damping model appears to be the most stable and will minimize computation effort in the full bridge analysis as it does not require a full damping matrix. For these reasons, the initial Rayleigh damping model with 1% damping was selected as the damping model of choice for all future analyses.

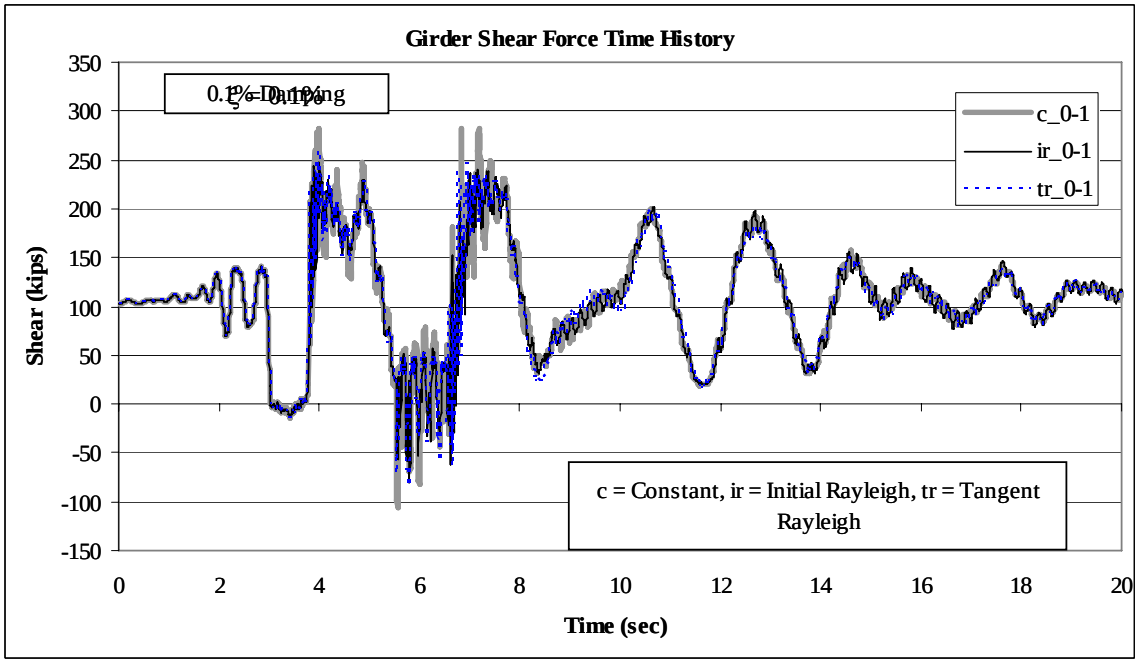

a) Girder Shear Force

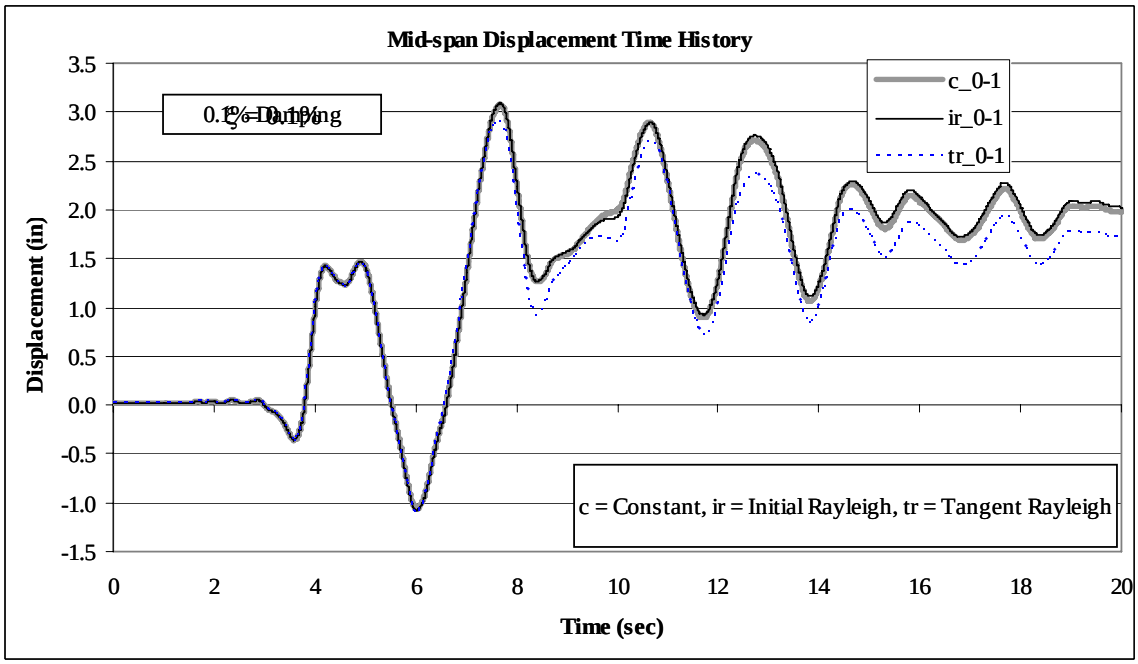

b) Midspan Deflection

Figure 2-13 Damping Model Time History Comparison (0.1% Damping Ratio)

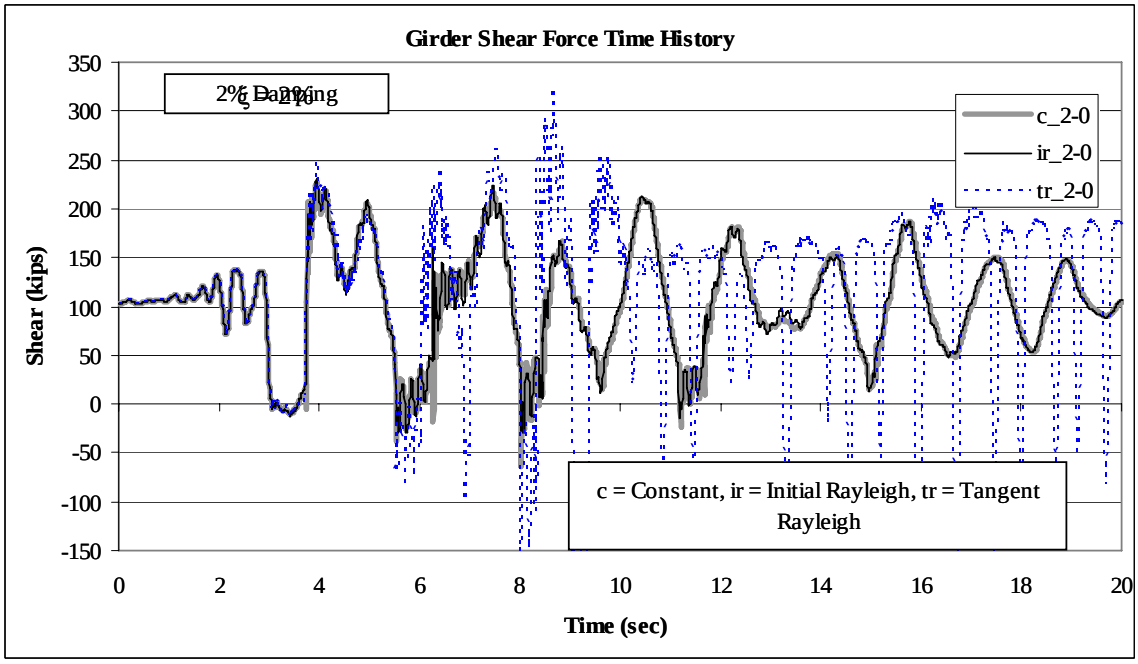

a) Girder Shear Force

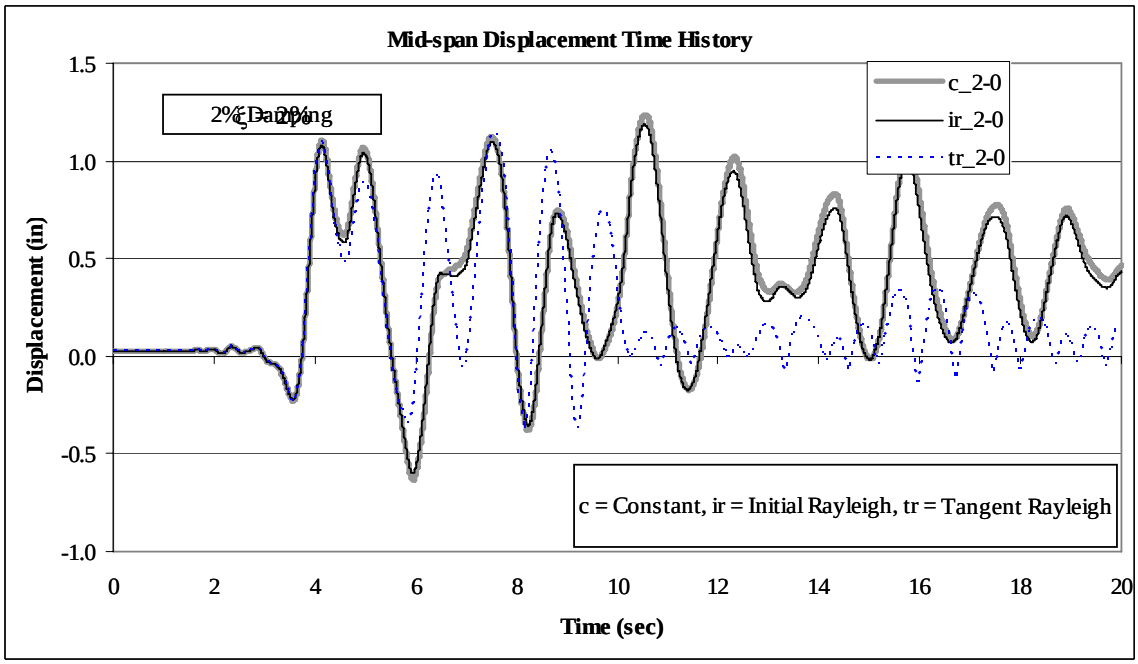

b) Midspan Deflection

Figure 2-14 Damping Model Time History Comparison (2% Damping Ratio)

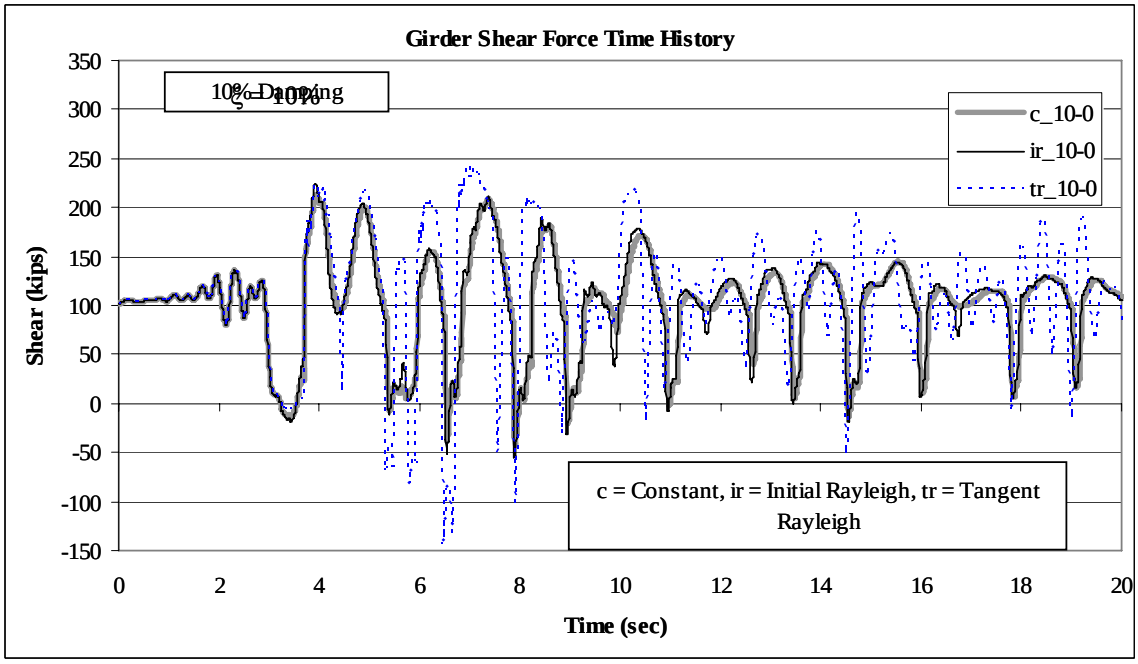

a) Girder Shear Force

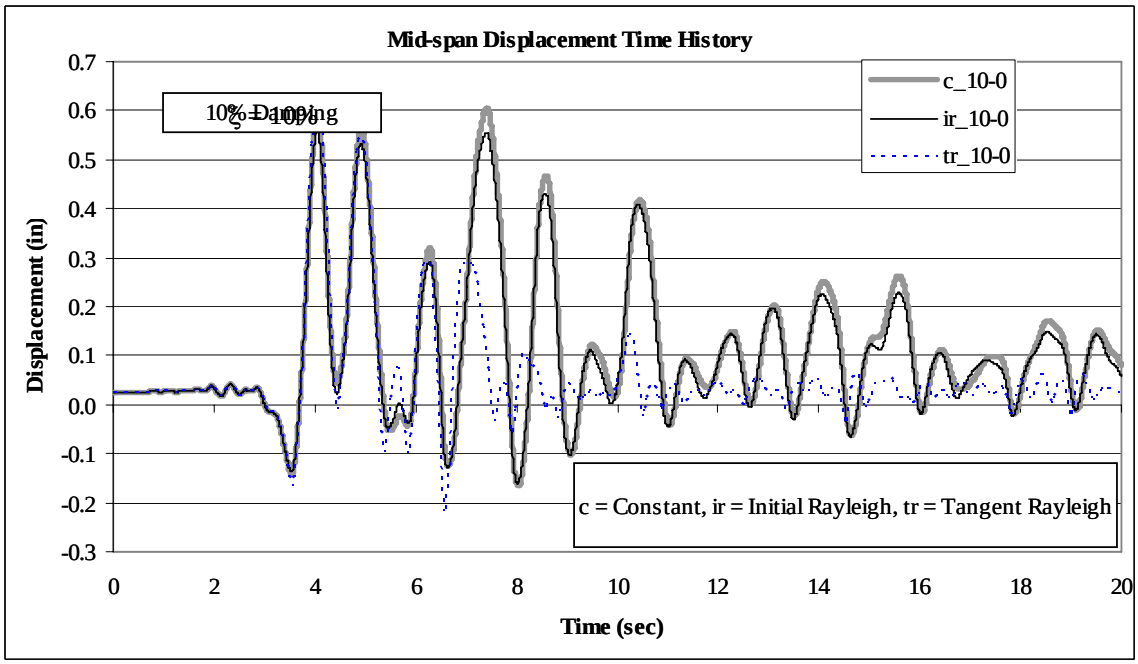

b) Midspan Deflection

Figure 2-15 Damping Model Time History Comparison (10% Damping Ratio)

3. Earthquake Excitations

Ten near field records were selected as input into the full scale bridge models. These records were considered to be representative of a significant seismic event in California. All records were within 25 kilometers of the fault rupture surface and many include significant near field effects (i.e. fling and forward directivity). These records were also selected because they showed significant vertical response in addition to their large lateral response. Table 2 lists the earthquakes used and summarizes various parameters of each event.

Table 2 - Summary of Earthquake Excitations

						Scaled to T=2 sec (N-S)					
Earthquake	Station	Abbr.	Date	Mw	Closest Dist to Rupture Surface (km)	Sa @ T=2.0 sec	Scale Factor	PGA - horiz (g)	PGV (cm/sec)	PGA - vert (g)	Duration (sec)
San Fernando	Pacoima Dam	PAC	2/9/1971	6.6	2.8	0.483	1.501	1.88	169	1.05	20.0
Iran	Tabas	TAB	9/16/1978	7.4	3.0	0.534	1.358	1.15	165	0.94	35.0
Irpinia, Italy	Calitri	CAL	11/23/1980	6.5	19.0	0.135	5.355	0.95	131	0.79	40.0
N. Palm Springs	Morongo Valley	MOR	7/8/1986	6	10.1	0.243	2.984	0.66	108	1.18	20.0
Superstition Hills	Wildlife Liquef.	WIL	11/24/1987	6.7	24.4	0.348	2.085	0.43	67.2	0.85	45.0
Northridge	Rinaldi	RIN	1/17/1994	6.7	7.1	0.574	1.262	1.06	210	1.07	15.0
Northridge	Sylmar	SYL	1/17/1994	6.7	6.4	0.619	1.171	1.00	152	0.63	40.0
Kobe	Takarazuka	TAK	1/16/1995	6.9	1.2	0.477	1.519	1.07	130	0.65	25.0
Chi Chi	TCU068	TCU	9/20/1999	7.6	1.1	0.627	1.156	0.54	204	0.57	60.0
Duzce	Bolu	BOL	11/12/1999	7.1	17.6	0.280	2.592	1.91	146	0.52	30.0

The earthquake records were scaled to match a Moment Magnitude 8, Soil Type D, 0.7g PGA design spectrum at a period of 2.0 seconds. The period of 2.0 seconds was selected because it is the primary longitudinal mode for both the 300 foot span and the 525 foot span bridge structures. Figure 3-1 shows the longitudinal and vertical acceleration response spectra for the scaled suite of earthquakes. Note that the median longitudinal spectra, matches the design spectra fairly well. Figure 3-2 shows the displacement response spectra for the scaled suite of earthquakes.

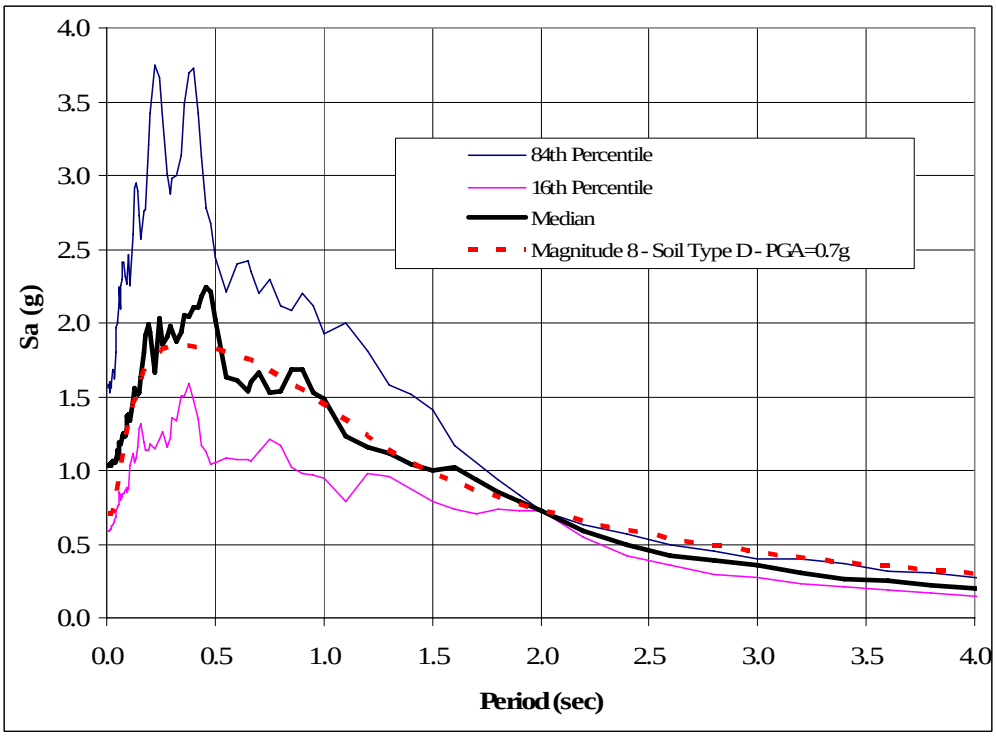

a) Longitudinal

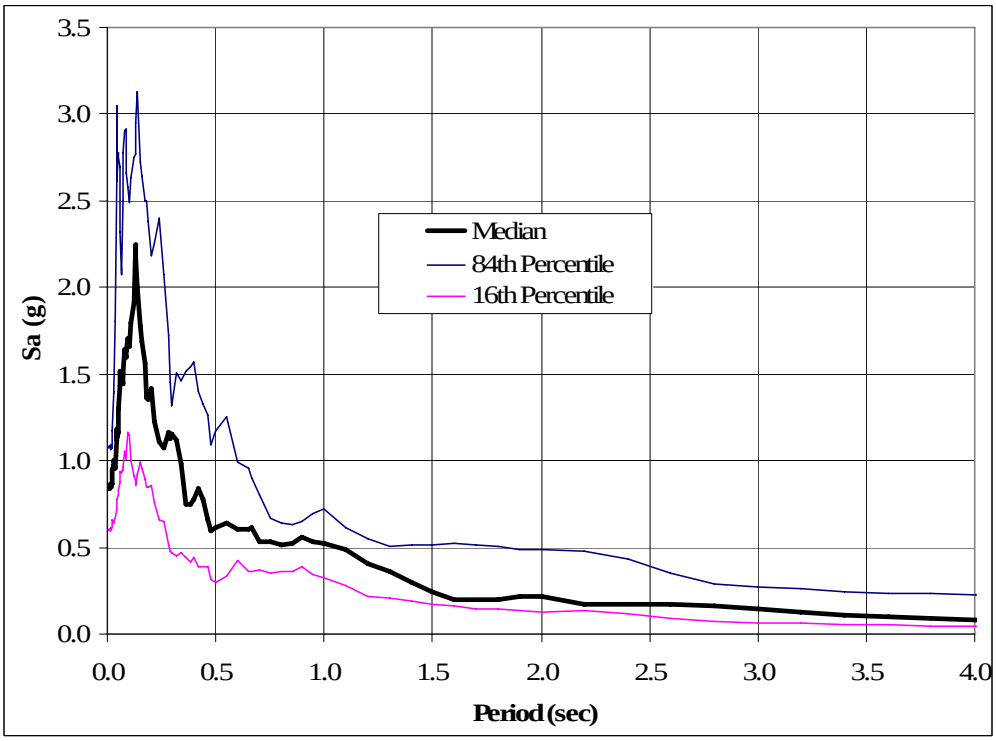

b) Vertical

Figure 3-1 Scaled Acceleration Response Spectrum

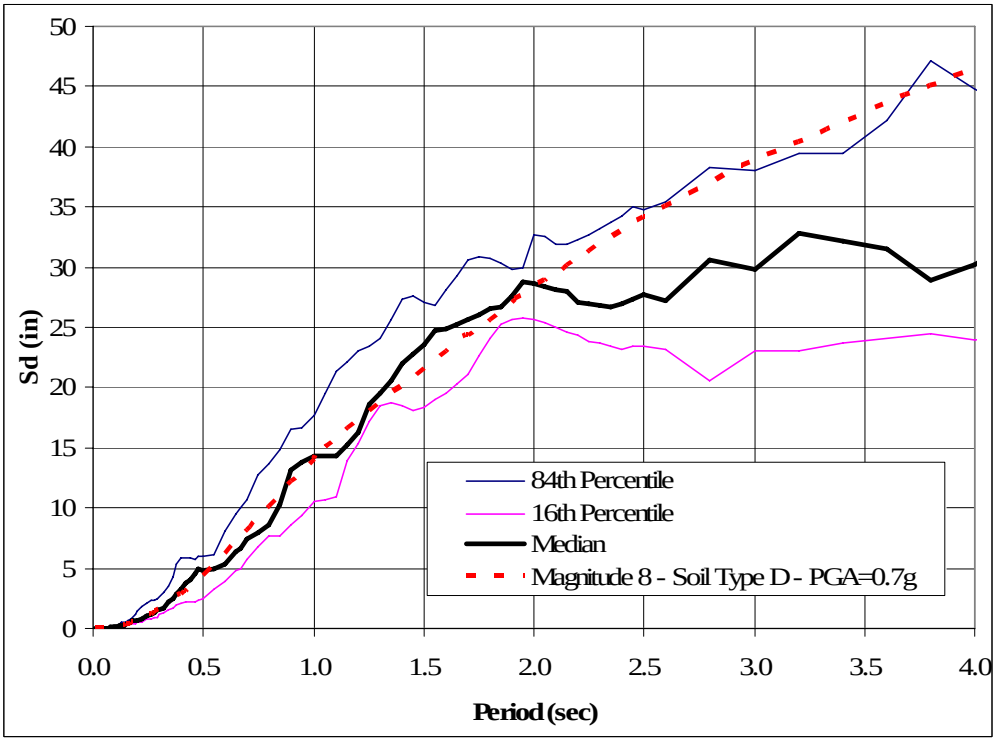

Figure 3-2 Scaled Displacement Response Spectrum

4. Full Bridge Models

Two full scale bridge models were developed. One with span lengths of 300 feet and the other with spans lengths of 525 feet. These spans were selected because they are considered to be within the range where precast segmental construction methods are the most economically competitive in California. Spans less than 250 feet will likely be under bid by conventional cast-in-place methods while spans greater than 525 feet will likely be competing with cable stayed bridges.

4.1. 300 Foot Span Prototype Bridge

The 300 foot span model is based on the Otay River Bridge, currently under construction in San Diego County. The Otay River Bridge is 0.6 miles long and consists of four longitudinal frames and eleven tapered piers. Figure 4-1 shows the bridge under construction. Figure 4-2 and Figure 4-3 show an elevation and a section of the full bridge, respectively. The bridge has two parallel precast segmental superstructures that are joined at the top flange with a cast-in-place closure. The superstructure segments are 36 feet wide and vary in depth from 10 feet at midspan to 16 feet at the piers. Thus the span-to-depth ratio varies from 19 to 30.

Figure 4-1 Otay River Bridge under Construction

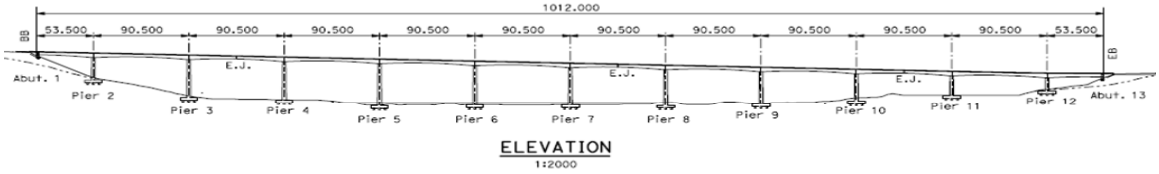

Figure 4-2 Otay River Bridge Elevation

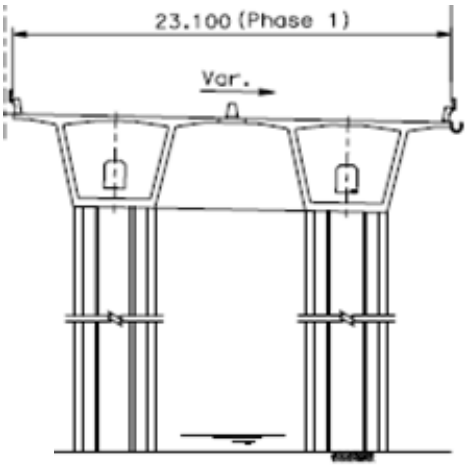

Figure 4-3 Typical Section of Otay River Bridge

4.2. 300 Foot Span Model Discretization

An analytical model of a five span frame was developed as shown in Figure 4-4. The interior spans are 297 feet and the exterior spans are 176 feet. Since only vertical and

longitudinal motions were considered, the model was limited to 2D and only one of the two parallel precast superstructures was considered. Approximately 40% (11 of 29 joints per span) of all superstructure segment joints were modeled. Piers 2 and 3 of the Otay River Bridge were chosen for the model and used to create a symmetric structure as if the frame were spanning a deep ravine.

4.2.1. Boundary Conditions

The beginning and end of the frame were modeled as abutments. Vertically they have a roller support and longitudinally they have a non-linear spring to capture the response of the soil behind the abutment, see Figure 4-5a. The abutment soil spring properties were calculated based on the Caltrans Seismic Design Criteria (Caltrans, 2004) using an initial stiffness of 20 kips per inch and an ultimate force of 5 ksf. The compression only abutment springs are not engaged until the 9.8 inch thermal expansion gap is closed.

The base of the piers were modeled as fully fixed with no consideration for soil structure interaction.

4.2.2. Piers

The top and bottom of the piers were modeled with non-linear 2-component Giberson beam hinging elements as shown in Figure 4-5b. These elements did not capture axial-moment coupling, thus the yielding moments were increased by 25% above the dead load moment capacity to account for the fact that vertical earthquake motion will increase the dead load on the piers which will in turn increase the moment capacity of the piers. A 25% increase is based on a preliminary run of the model using 100% of the Rinaldi record of the 1994 Northridge earthquake.

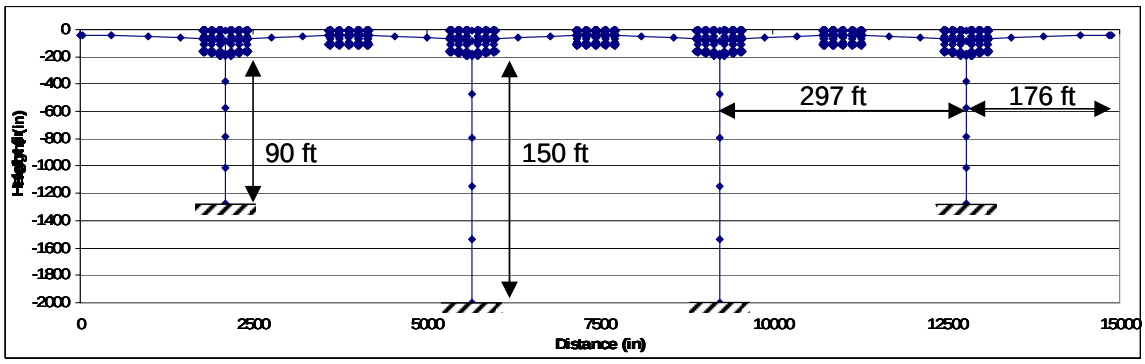

Figure 4-4 300 Foot Span Model

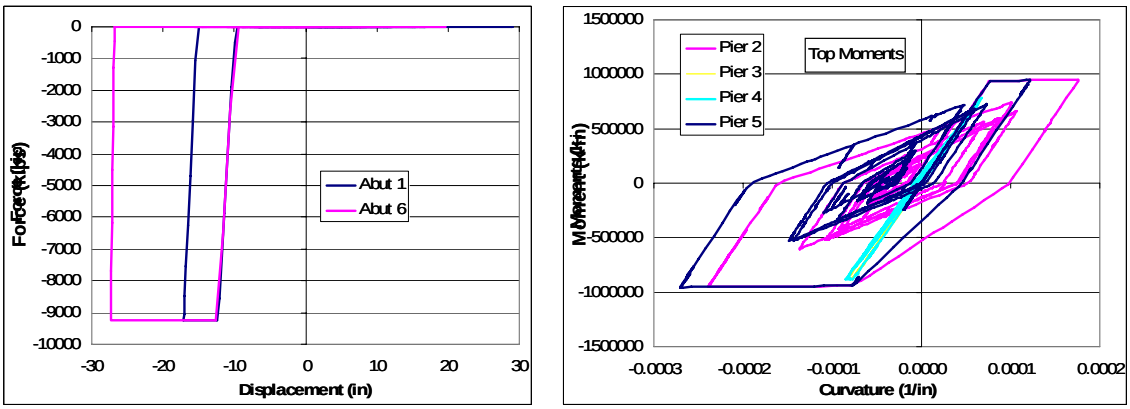

a) Abutment Hysteresis

b) Pier Hinge Hysteresis

Figure 4-5 300 Foot Span - Abutment and Pier Hystereses Behavior

4.2.3. Superstructure Joints

The superstructure was modeled with six segment joints at each pier and five segment joints at midspan as shown in Figure 4-6 and Figure 4-7. These joints were modeled in a similar manner as the validation models except that they utilized both top and bottom tendons. Non-linear shear deformations of the superstructure were neglected because the shear spans are very large. Cracking of the segments between joints was also neglected to simplify the model. This may slightly over estimate the rotation of the segment joints as all flexural cracking will be concentrated at the segment joints. This is considered to be conservative and acceptable.

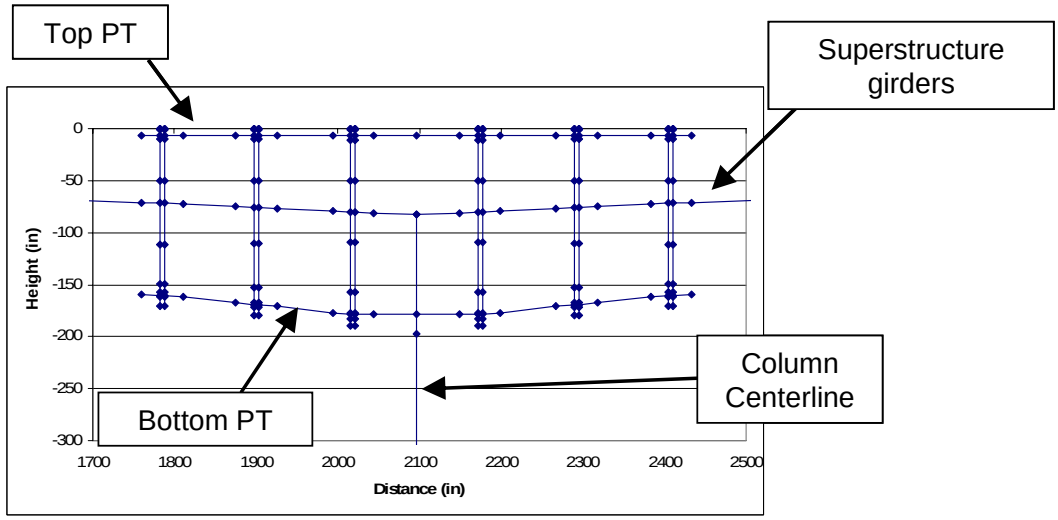

Figure 4-6 300 Foot Span Model Adjacent to Piers

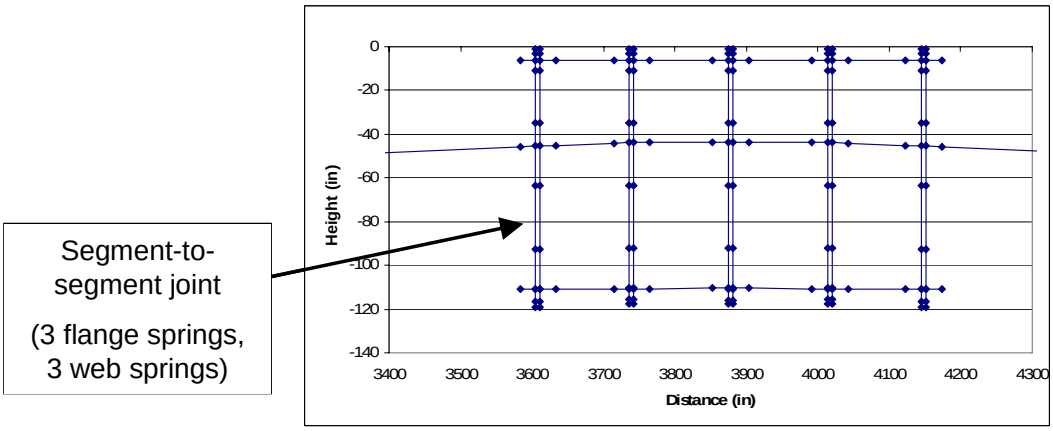

Figure 4-7 300 Foot Span Model Near Midspan

4.2.4. Superstructure Tendons

The post tensioning tendons were preloaded in the model according to the jacking forces shown on the Otay River Bridge design drawings. The model inherently accounts for elastic shortening losses, but not for losses due to friction or anchorage seating. In order to address this issue, the PT losses due to friction and anchorage seating was estimated for all tendons. A sample tendon stress diagram is shown in Figure 4-8. Figure 4-9

summarizes the tendon losses based on their length. The losses for all tendons crossing a joint were averaged and the pretension load reduced accordingly. For example Joint 1 (i.e., closest to the pier) has all 14 cantilever tendons crossing the joint. The average loss in the PT member in the model is thus the average loss of all 14 tendons and is 17.8 ksi. This approach was used for all joints in the model. The losses range from 16 ksi to 21 ksi depending on the joint. It is important to note that time dependant losses (i.e. creep, shrinkage, and relaxation) were not considered in the analyses presented herein.

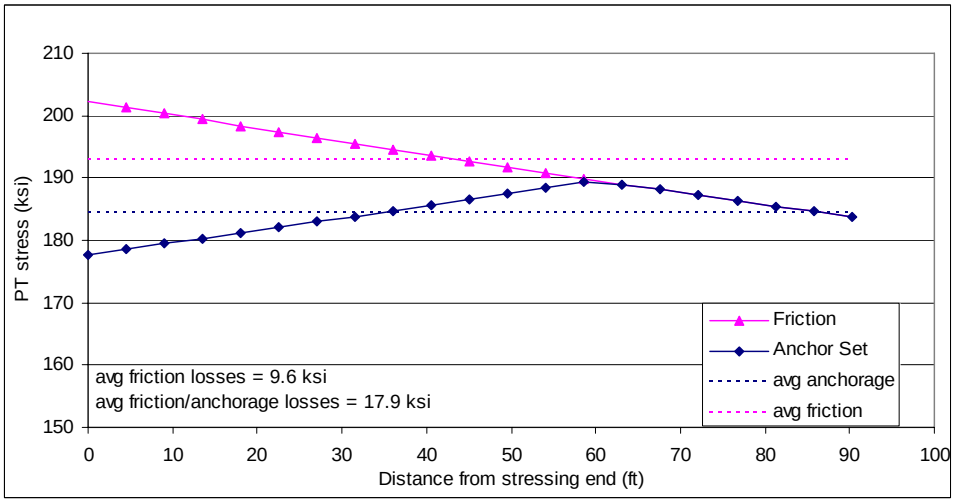

Figure 4-8 300 Foot Span - Anchorage and Friction Losses of a Typical Tendon

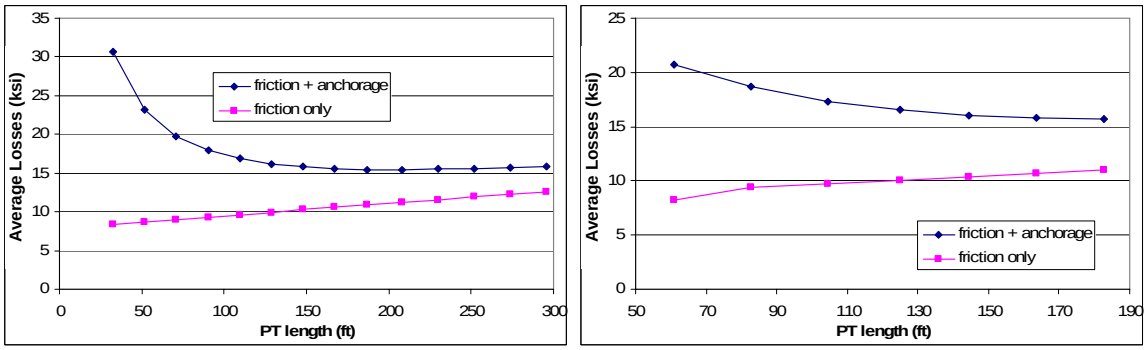

a) Cantilever Tendons b) 'B' Tendons

Figure 4-9 300 Foot Span - Summary of Tendon Losses

4.3. 300 Foot Span Model Results

4.3.1. Dead Load Joint Stresses

The state of stress in the segment joints prior to a seismic event will likely affect the response of the joint. The stress profile of the segment joints at Pier 3 and Span 3 are shown in Figure 4-10. These profiles included dead load, PT loads, and losses due to elastic shortening, friction and anchorage seating. Construction staging effects on the stress profile of the segment joints are beyond the scope of this project and was not incorporated in the model. The stress profiles shown are typical of all segment joints in the model and are considered reasonable. The stress profiles exhibit nearly uniform compression from top to bottom, thus allowing for maximum bending capacity. The peak stresses are well below the AASHTO limit of 0.45 $f_c^{'}$ (AASHTO, 1999). The average compression stresses across the joints are approximately 18% of $f_c^{'}$ adjacent to the piers and 13% of $f_c^{'}$ near midspan.

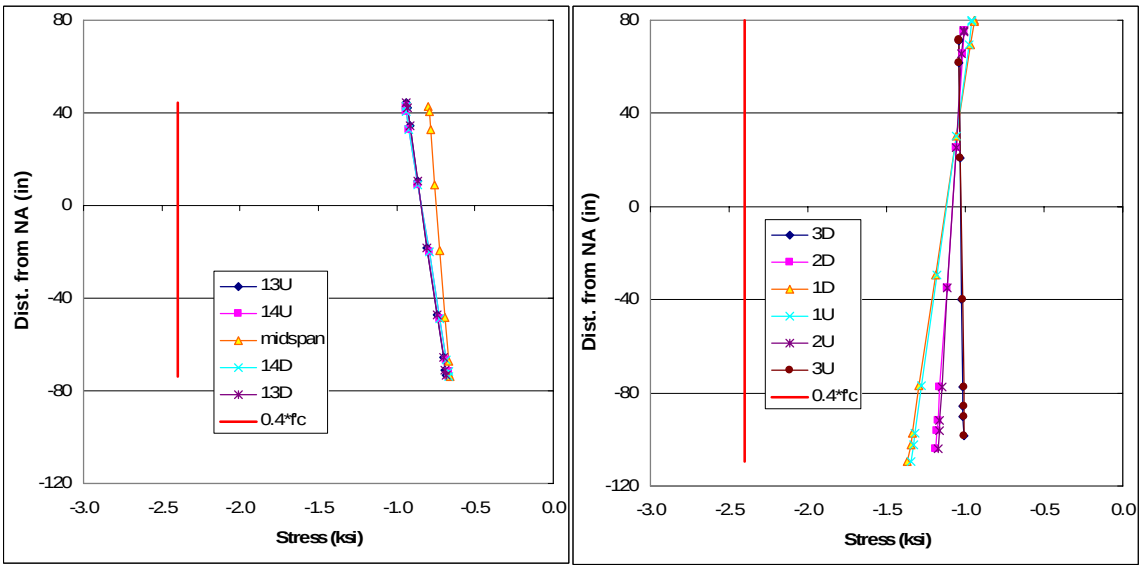

a) Near Midspan b) Adjacent to Pier

Figure 4-10 300 Foot Span - Typical Dead Load Stress Profiles of Segment Joints

4.3.2. Mode Shapes

The primary longitudinal mode has a period of 2.0 seconds and captures 86% of the mass (see Figure 4-11). The dominant vertical modes, shown in Figure 4-12 and Figure 4-13, have periods of 0.5 and 0.3 seconds and capture 18% and 22% of the mass, respectively.

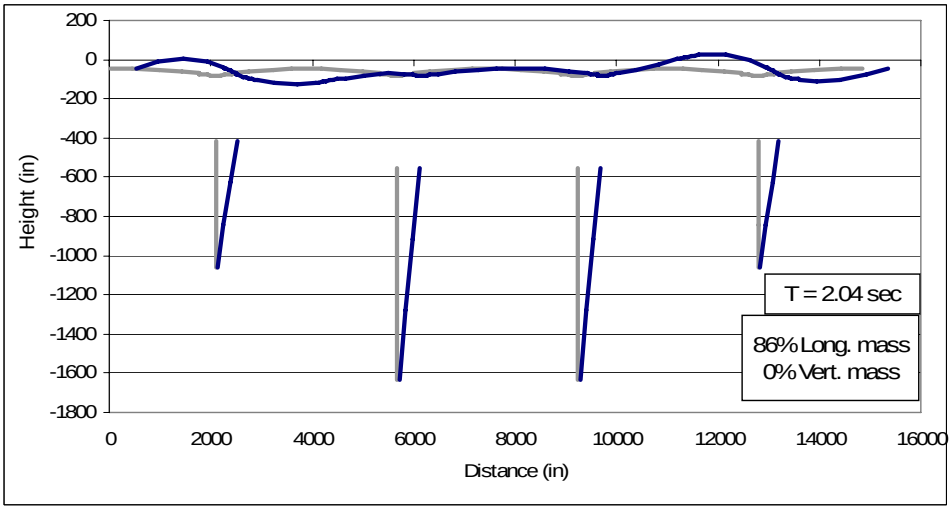

Figure 4-11 300 Foot Span - Primary Longitudinal Mode Shape

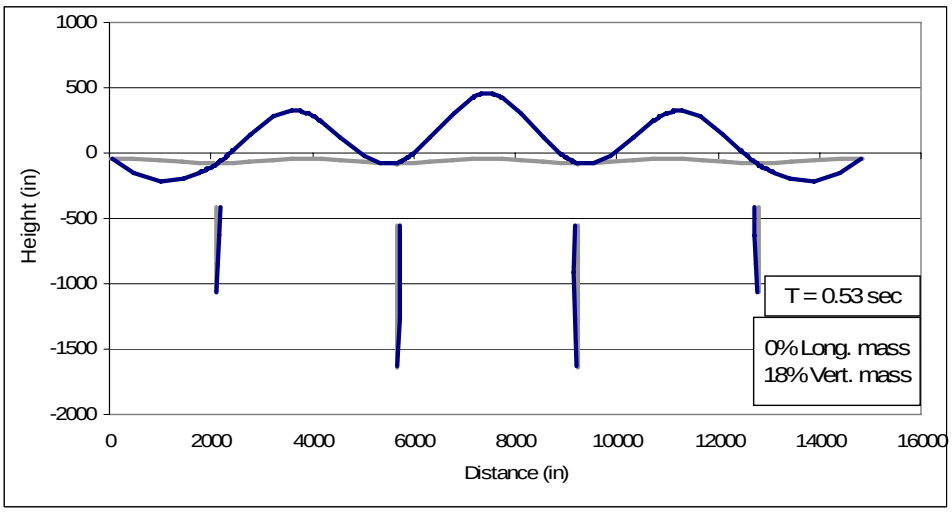

Figure 4-12 300 Foot Span - Primary Vertical Mode Shape – Mode 4

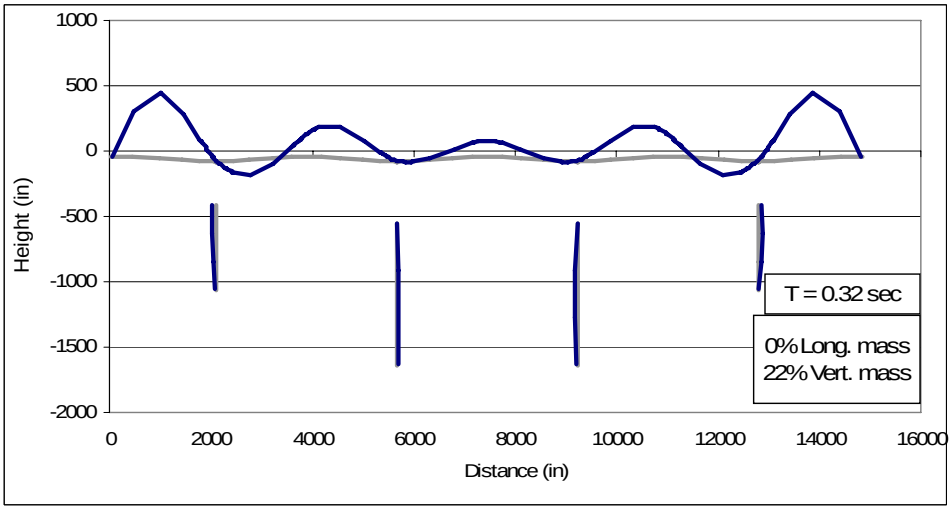

Figure 4-13 300 Foot Span - Primary Vertical Mode Shape – Mode 8

4.3.3. Longitudinal Push Analysis

A longitudinal pushover analysis was performed to understand the hinging sequence of the frame. The results of this analysis are shown in Figure 4-14. It is clear that the abutment soil spring is engaged prior to any column hinging, however the short piers and the abutment soil, yield at a similar displacement. The tall piers begin to yield when the short pier has reached a displacement ductility of about 2. Note that a 10 inch superstructure displacement corresponds to a short pier drift of 1%.

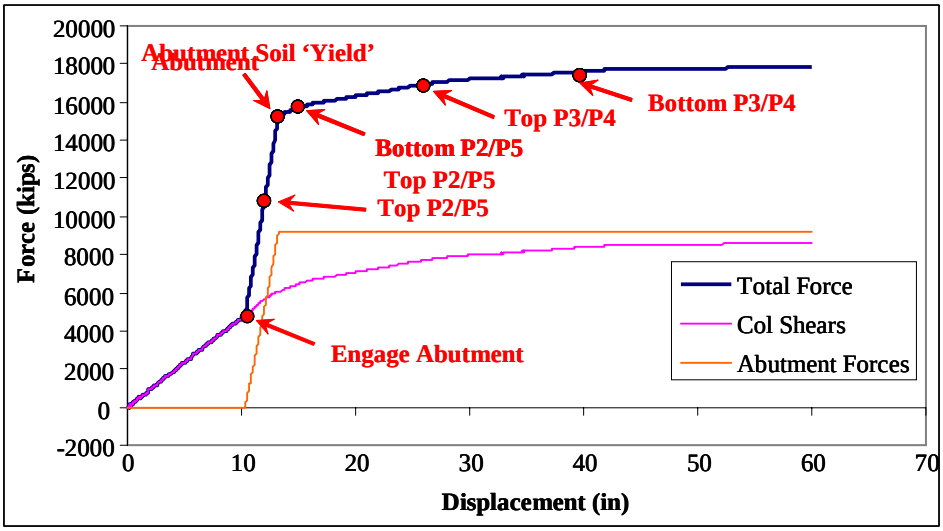

Figure 4-14 300 Foot Span - Longitudinal Push Results

4.3.4. Vertical Cyclic Push Analysis

A series of vertical reversed cyclic pushover analyses were performed in order to verify the moment-rotation behavior of the segment joints. Results from segment joint 1 (i.e., nearest the pier) and segment joint 15 (i.e., midspan) are shown in Figure 4-15. The response captures joint opening, concrete crushing and PT yielding for both positive and negative bending directions.

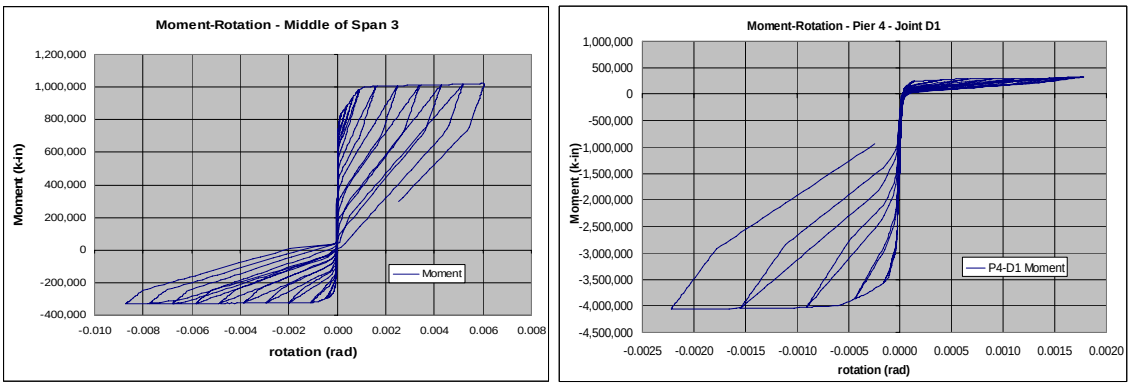

a) Joint 15 - Midspan b) Joint 1 – Adjacent to Piers

Figure 4-15 300 Foot Span - Typical Moment-Rotation Diagram from Cyclic Push Analysis

4.3.5. Earthquake Time History Analyses

4.3.5.1. Contribution of Vertical Earthquake Motion

In order to quantify the contribution of vertical motion on the joint response, the model was subjected to longitudinal motions only, as well as simultaneous longitudinal and vertical earthquake motions. Figure 4-17 and Figure 4-18 summarize the maximum (i.e. positive bending) joint rotations for all segment joints and all earthquake records. The horizontal axis of each chart shows the six different joint families. D1/U1 represents the first joint downstation or upstation of the pier, while D14/D14 is fourteen segment joints away from the pier and is adjacent to midspan, see Figure 4-16. Each vertical bar represents the peak rotation for a segment joint geometry due to a particular earthquake. The median earthquake response of each joint family is also shown. Figure 4-17 shows the results for only longitudinal earthquake motion, while Figure 4-18 shows the results for both longitudinal and vertical motion. It is clear that the vertical component significantly increases the joint response. By taking the median of the ratio of the segment joint median responses, we find that the median positive bending rotations have increased by 400%. From similar plots, shown in Appendix A, we find that negative bending rotations have increased by 90% and the residual rotations increased by only 9%.

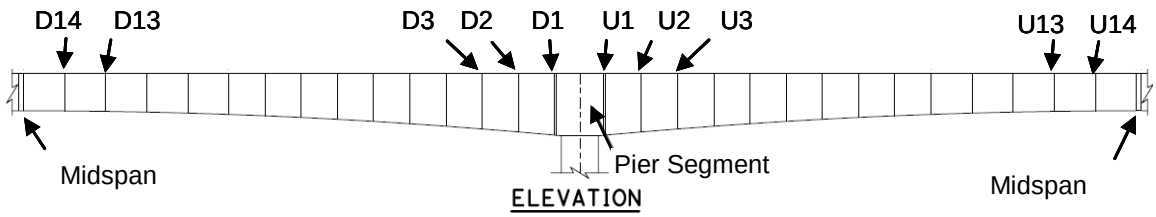

Figure 4-16 300 Foot Span - Segment Joint Identification

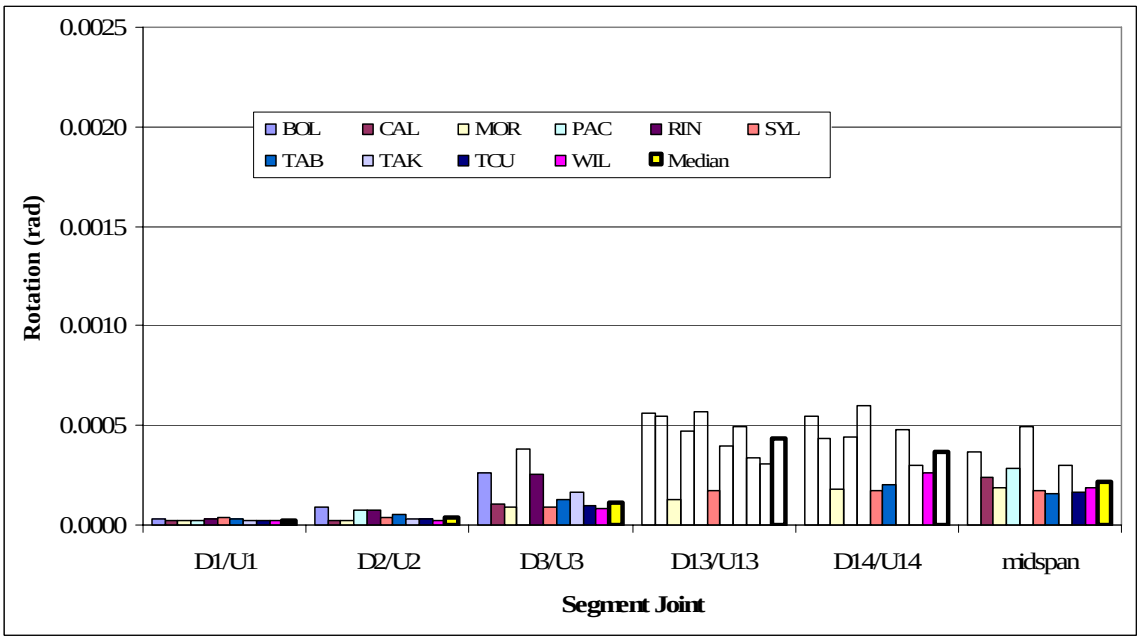

Figure 4-17 300 Foot Span – Max. Segment Joint Rotations – Longitudinal Ground Motion Only

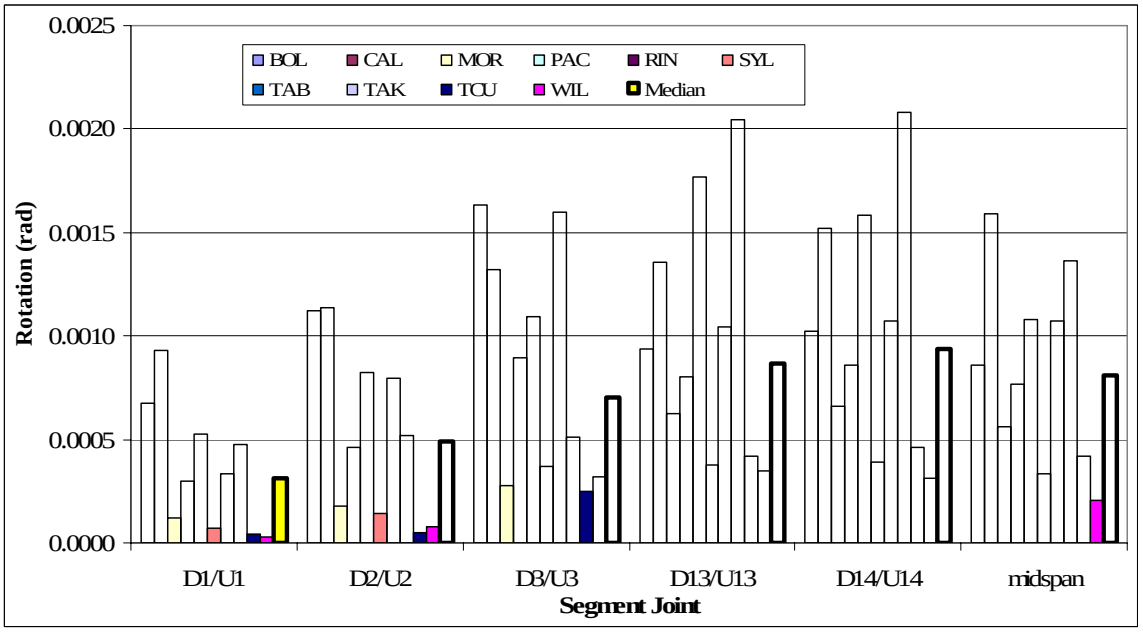

Figure 4-18 300 Foot Span – Max. Segment Joint Rotations – Long. and Vert. Input Ground Motion

4.3.5.2. Longitudinal Response of Piers

The longitudinal response of the piers is shown in Figure 4-19. The vertical bars represent the longitudinal drift ratio for each earthquake record. The median drift ratios

are indicated with horizontal lines and are 2.4% and 1.5% for the short and tall piers, respectively. These drift levels are easily achieved using current design practices. The median residual drifts are 0.14% and 0.08% for the short and tall piers respectively.

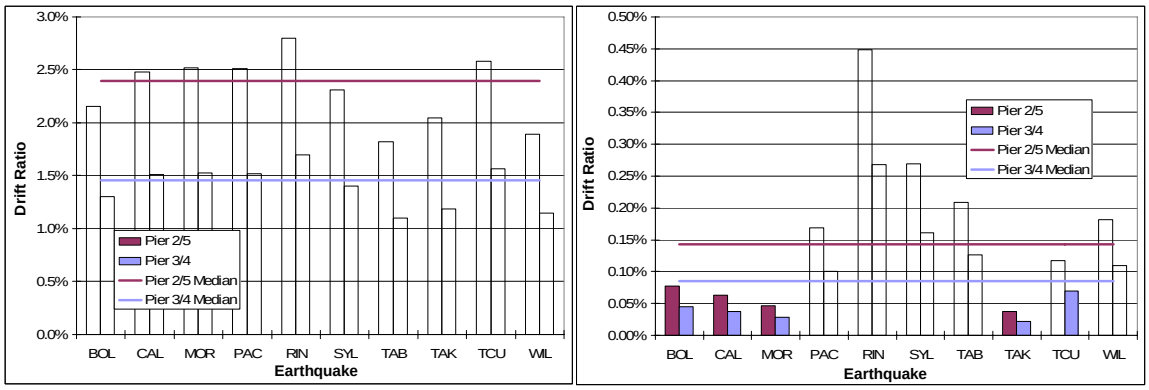

a) Peak Drift b) Residual Drift

Figure 4-19 300 Foot Span - Pier Longitudinal Drift Response

It is important to note that, based on the displacement response spectra, shown in Figure 3-2, the median short pier drift of an elastic structure with a period of 2.0 seconds is approximately 2.8%. Recall from the longitudinal push analysis that the abutments are engaged at a short pier drift of 1%, yet yields at a drift of 1.2%. The fact that the model did not achieve the expected purely elastic drift limit, despite significant inelastic behavior of the piers, suggests that the abutment played a role in reducing the longitudinal drifts.

4.3.5.3. Response of Superstructure Segment Joints

The moment rotation response of selected segment joints is shown in Figure 4-20. These diagrams do not necessarily represent the median response, rather they are closer to the 84th percentile response. They were selected because they show non-linear response and document the dynamic behavior of the model.

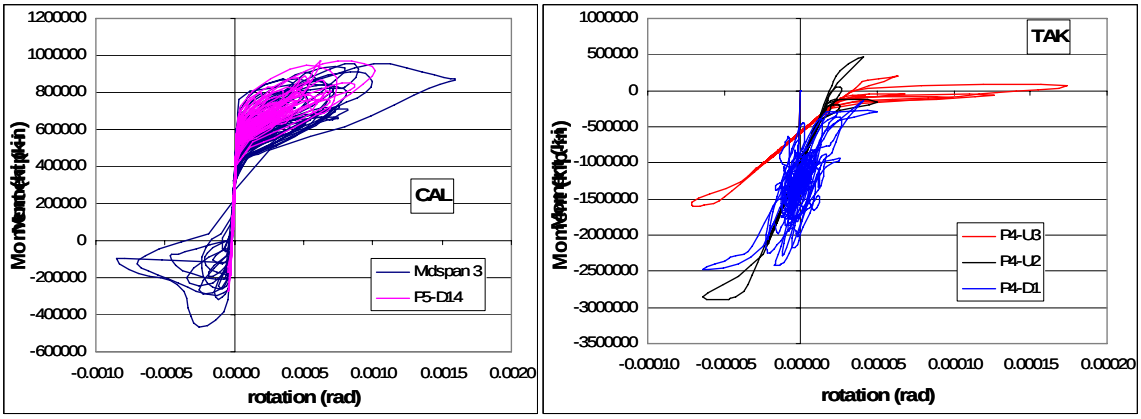

a) Near Midspan b) Adjacent to Pier

Figure 4-20 300 Foot Span - Sample Moment-Rotation Response

A summary of the segment joint response is shown in Figure 4-21. The 16th, 50th (median), and 84th percentile response are shown on top of the cyclic push results to assist in visualizing the amount of non linear response.

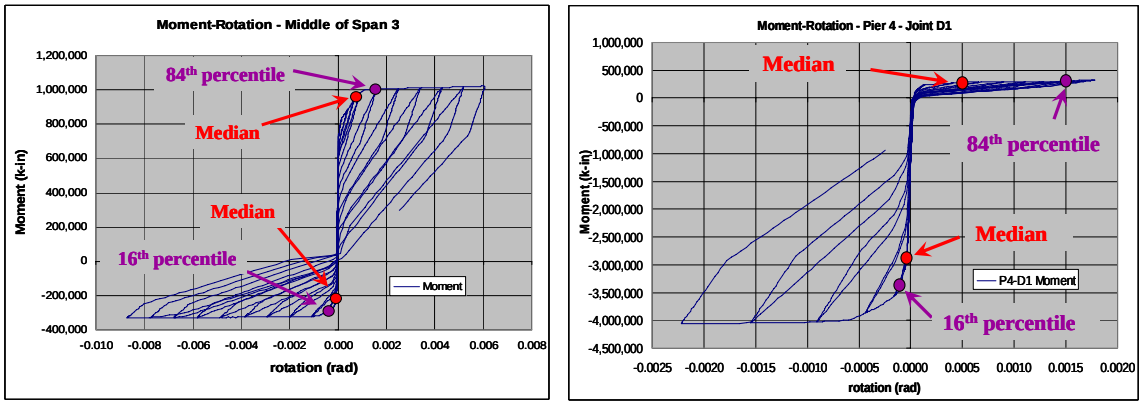

a) Near Midspan b) Adjacent to Pier

Figure 4-21 300 Foot Span - Summary of Segment Joint Response shown on Cyclic Push Results

The results indicate that the median response will open joints at the piers and midspan. The expected gap opening is about 0.1 inches. The median response will yield the positive bending (ie. bottom) PT tendons at the piers, but no tendons will yield anywhere else. Furthermore, there will be no residual joint openings for the median or 16th/84th percentile responses.

4.4. 525 Foot Span Prototype

The 525 foot span model is based on the San Francisco-Oakland Bay Bridge (SFOBB) Skyway, currently under construction in northern California. The SFOBB Skyway is 1.25 miles long and consists of four longitudinal frames and fourteen piers. Figure 4-22 shows the bridge under construction. Figure 4-23 shows an elevation of a typical pier cantilever and Figure 4-24 shows a typical pier section. The bridge consists of two parallel precast segmental superstructures that behave completely independent of each other. The superstructure segments are 87 feet wide and vary in depth from 18 feet at midspan to 30 feet at the piers. Thus the span-to-depth ratio varies from 18 to 29.

Figure 4-22 San Francisco Oakland Bay Bridge Skyway under Construction

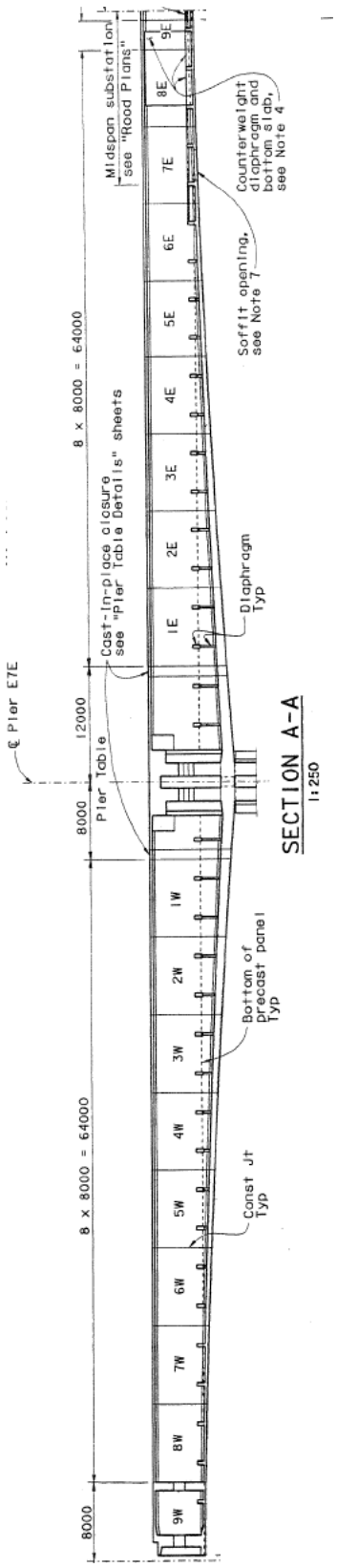

Figure 4-23 - San Francisco Oakland Bay Bridge - Typical Cantilever

Figure 4-24 - San Francisco Oakland Bay Bridge Skyway Pier Section

4.5. 525 Foot Span Model Discretization

The framework for the 525 foot span model is essentially the same as that of the 300' span model. Thus all modeling assumptions discussed in Section 4.2 apply to the 525 foot span model as well. Only one frame, similar to Frame 2 of the prototype structure, was modeled as shown in Figure 4-25. Internal spans extended 525 feet in length while external spans stretched 350 feet. Pier heights varied from 80 feet to 110 feet. Approximately 60% (i.e., 11 of 19 joints per span) of all superstructure segment joints were modeled.

The end spans of the frame were adjusted to emulate the global continuity of the bridge. The ends spans in the prototype frame have expansion joints at midspan for ease of construction. In addition, the prototype bridge utilizes large diameter pipe mbeams across the expansion hinges to develop moment and torsion continuity while at the same time allowing for thermal expansion. Moment continuity in the superstructure will shift

the inflection point away from midspan. To accurately capture this shift in the Ruaumoko model, the end spans of the frame were stretched to 350 feet (0.67 times the typical span length). Furthermore, this modeling adjustment will more accurately capture the vertical mode shapes of the frame.

4.5.1. Boundary Conditions

As in the 300 foot span model, the beginning and end of the frame were modeled as abutments. The non-linear compression only longitudinal abutment springs, were engaged upon closing of the 19.7 inch thermal expansion gap.

The prototype structure sits on deep pile foundations in very soft bay mud, thus a fixed base assumption is inappropriate. Foundation soil springs were obtained through the contractor of the SFOBB skyway and incorporated into the model. These soil springs were also used by the designers of the prototype bridge. Coupling of the axial and bending springs was not considered in the model. While this is not strictly correct, this approach was considered acceptable for the purposes of this investigation.

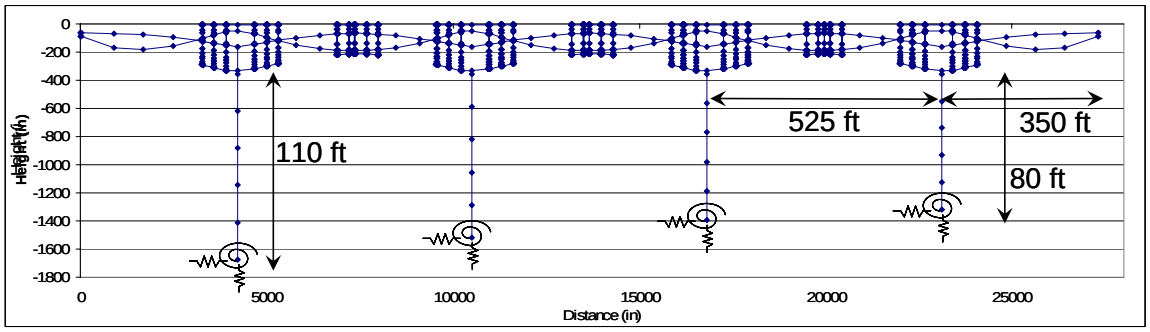

Figure 4-25 525 Foot Span Model

4.5.2. Piers

As discussed in Section 4.2.2, the piers were allowed to develop plastic hinges top and bottom. The moment capacity of the piers was increased by 13% to account for the axial load effect due to vertical earthquake motion.

4.5.3. Superstructure Joints

The superstructure was modeled with six segment joints adjacent to the piers and 5 segment joints near midspan, shown in Figure 4-26 and Figure 4-27, respectively. To improve numerical stability and to ensure accurate representation of the moment of inertia across the segment joints (see Section 2.3.2), three additional web springs were added to the joint modeling of the tall pier segment joints.

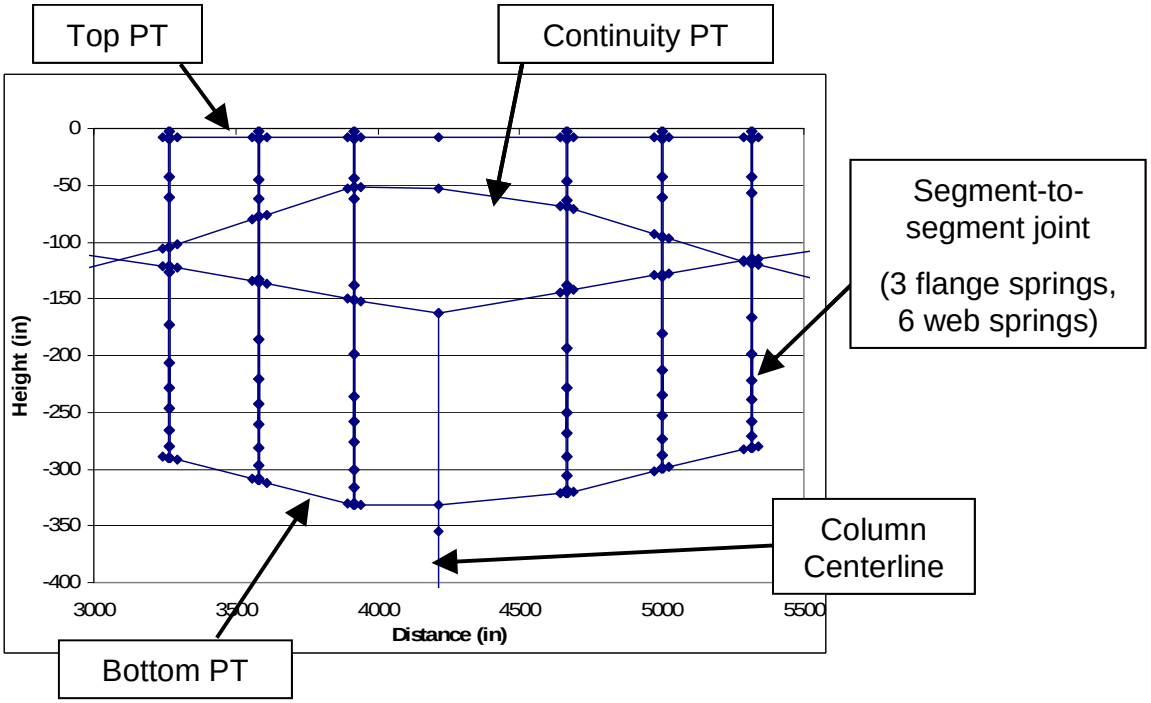

Figure 4-26 525 Foot Span Model Adjacent to Piers

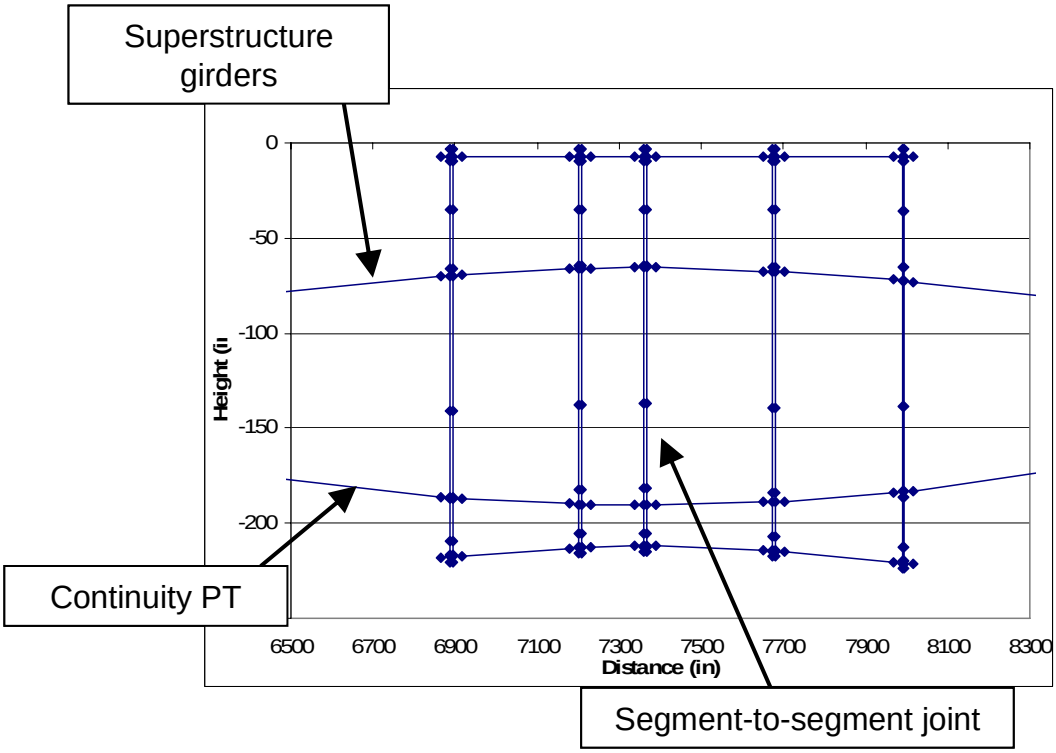

Figure 4-27 525 Foot Span Model Near Midspan

4.5.4. Superstructure Tendons

The prototype bridge utilizes various types of tendons (i.e., cantilever tendons, continuity tendons, top tendons, bottom tendons, 'D' tendons and 'P' tendons), each with different jacking stresses. These various tendons were lumped together in the model to generate three categories of PT; top tendons, bottom tendons and continuity tendons. Depending on when each tendon was stressed during the construction process, the tendon forces varied greatly. We obtained the tendon losses from the contractor's engineer. In order to ensure that the tendons have accurate initial forces, the initial jacking foresee in the Ruaumoko model was adjusted until the losses at the end of construction matched those calculated by the contractor's engineer. The average results for all tendons at various segment joints are shown in Figure 4-28. On average the losses from the Ruaumoko model and those determined by the contractors engineer are within 5%.

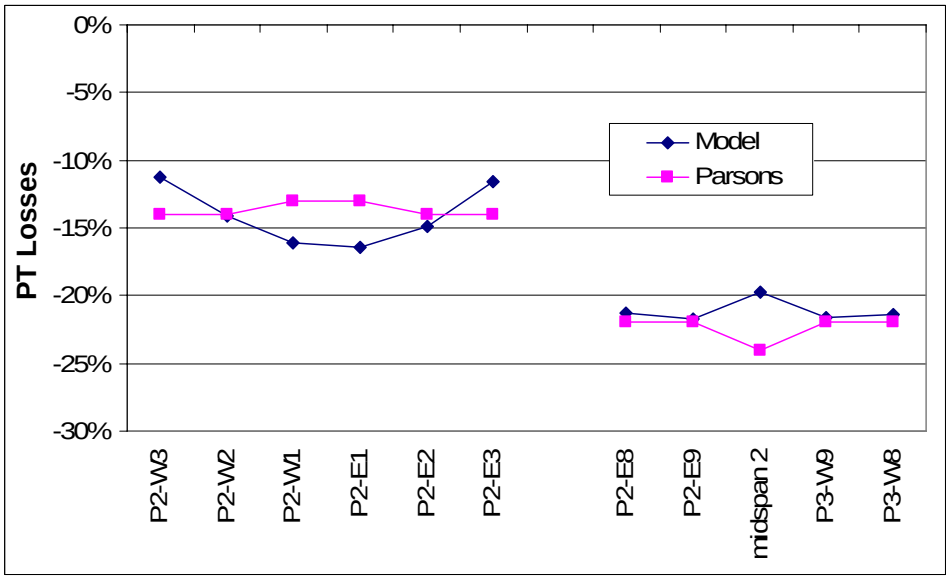

Figure 4-28 Comparison of Average PT Posses

4.6. 525 Foot Span Results

4.6.1. Dead Load Stress Profile

The results from a full longitudinal construction staging analysis of the SFOBB skyway were obtained from the contractor. A comparison of the top and bottom superstructure stresses, at the end of construction, between the Ruaumoko model and the contractor's BD2 model are shown in Figure 4-29 and Figure 4-30, respectively. In the Ruaumoko model, the concrete is effectively placed and all the PT tendons stressed for the entire bridge simultaneously. The Ruaumoko model grossly overestimates the top stress and underestimates the bottom stresses. Clearly this is not correct and must be adjusted.

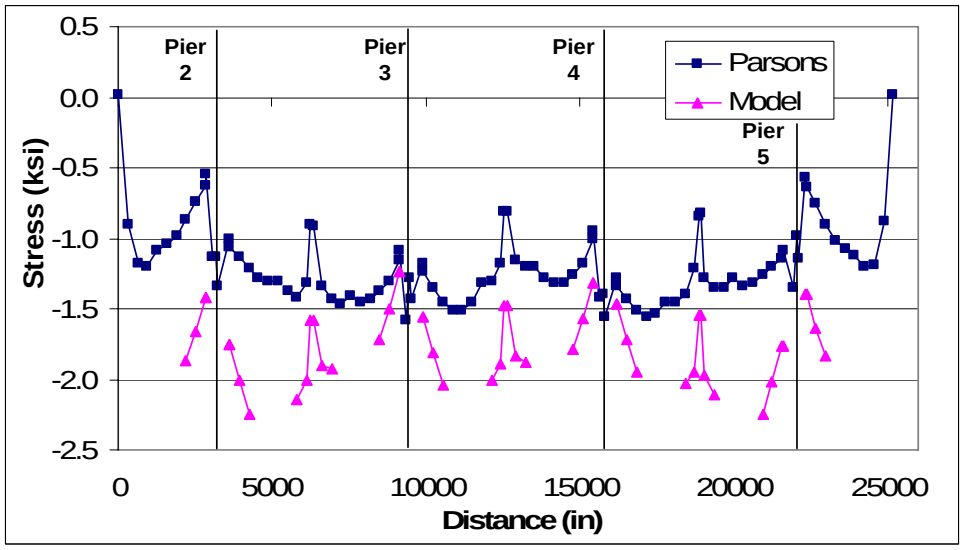

Figure 4-29 Comparison of Superstructure Top Stresses Prior to Calibration

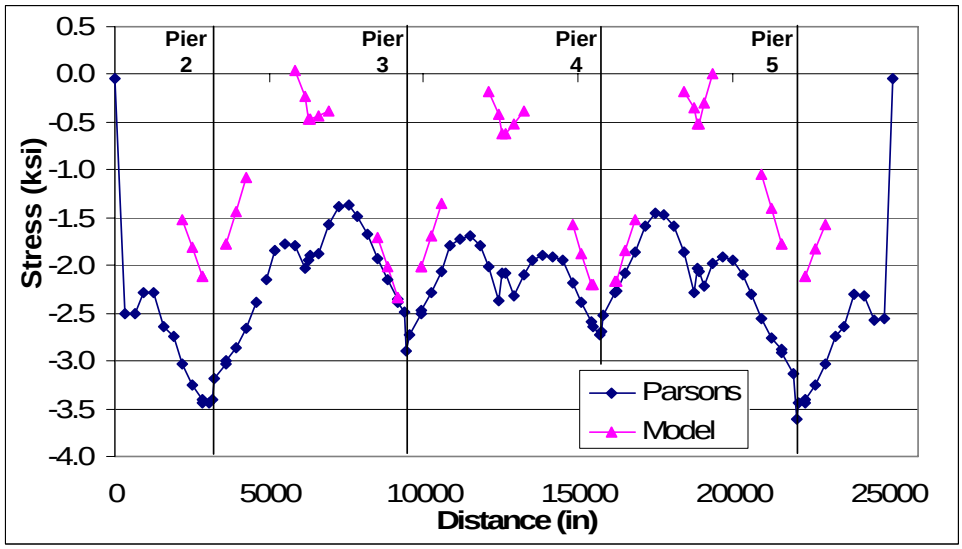

Figure 4-30 Comparison of Superstructure Bottom Stresses Prior to Calibration

To more accurately represent the stress state of the joints after construction, equal and opposite forces and moments were applied across each joint in the Ruaumoko model. The value of these forces was iterated until convergence with the contractor's stress state was achieved. Figure 4-31 and Figure 4-32 show a comparison of the top and bottom stresses after accounting for the longitudinal construction staging effects. The dead load

superstructure stress profiles achieved through this process are shown in Figure 4-33 for segment joints various piers and spans. The stress profiles on exterior piers exhibit a steep gradient while the interior piers and spans are near uniform. All stresses are below the AASHTO limit of 0.45 $f_c^{'}$ (AASHTO, 1999). The average compression stress across both pier and span segment joint is 22% of $f_c^{'}$.

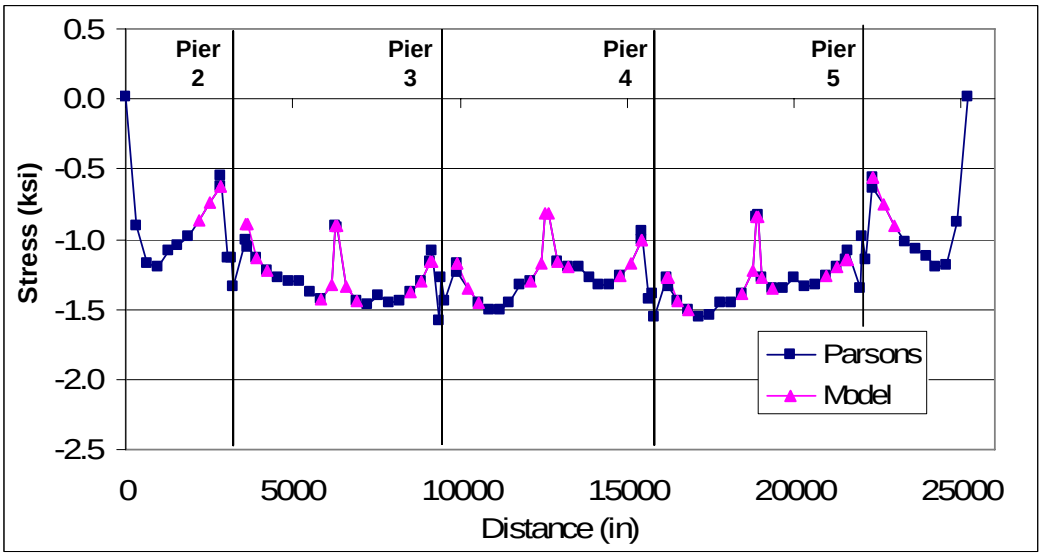

Figure 4-31 Comparison of Superstructure Top Stresses after Calibration

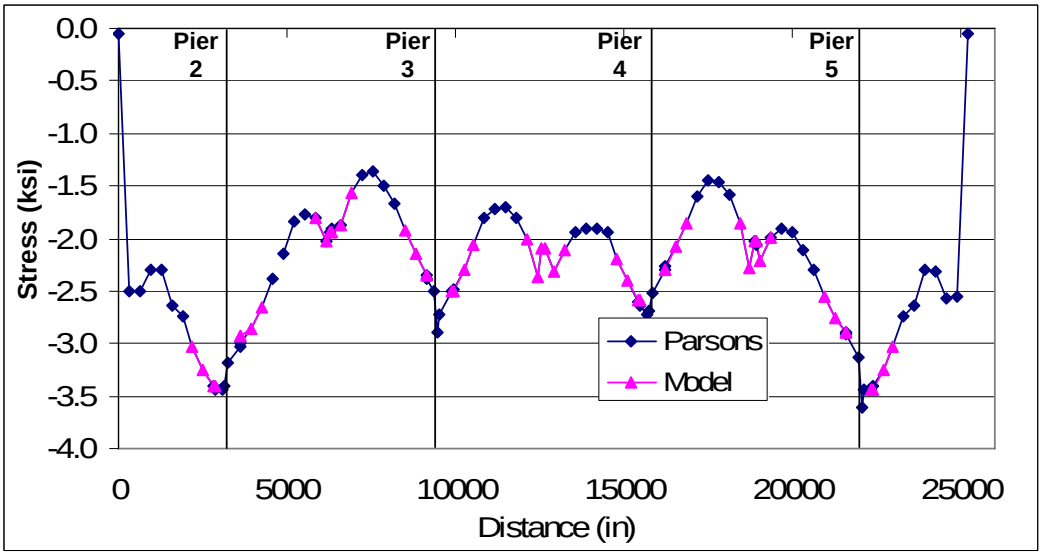

Figure 4-32 Comparison of Superstructure Bottom Stresses after Calibration

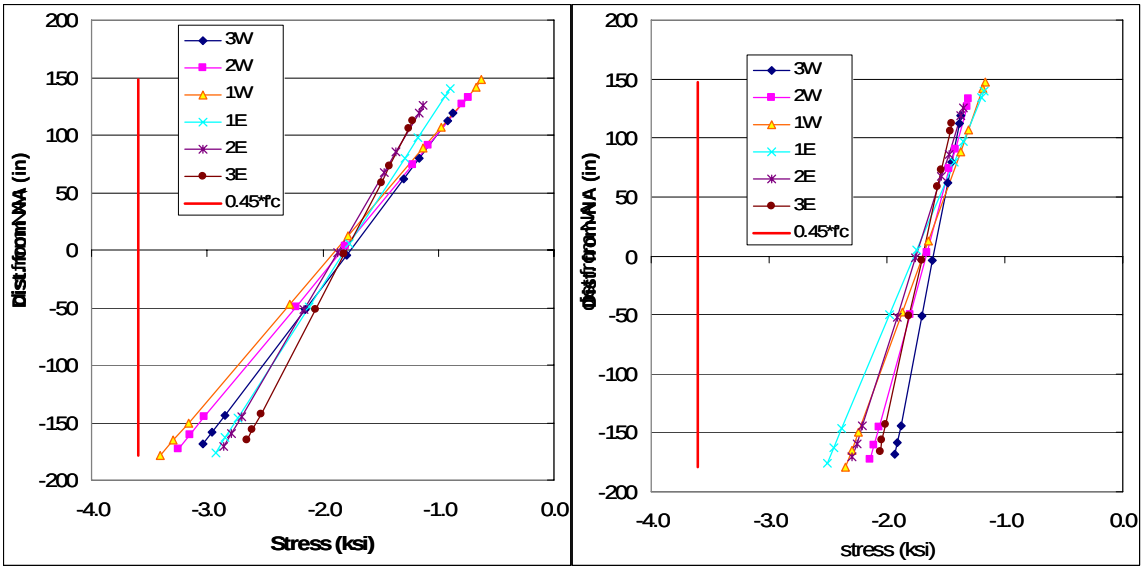

a) Pier 2 b) Pier 3

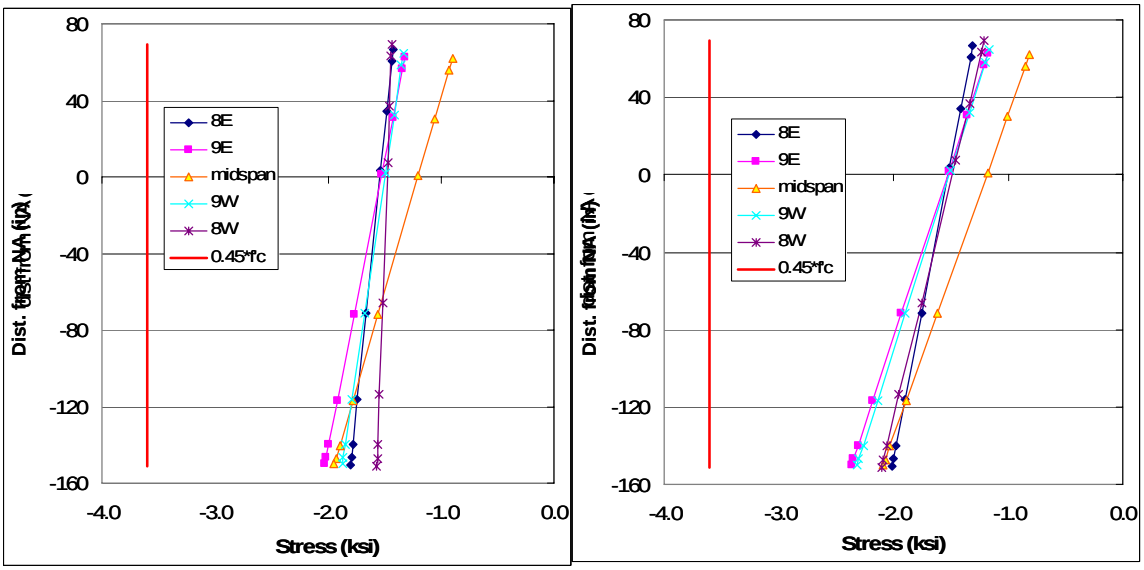

c) Span 2 d) Span 3

Figure 4-33 525 Foot Span - Dead Load Superstructure Stress Profile for Typical Piers and Spans

4.6.2. Mode Shapes

The primary longitudinal and vertical mode shapes are shown in Figure 4-34 and Figure 4-35, respectively. The primary longitudinal mode had a period of 2.0 seconds and engaged 93% of the mass. The dominant vertical mode had a period of 0.66 seconds and captured 41% of the mass.

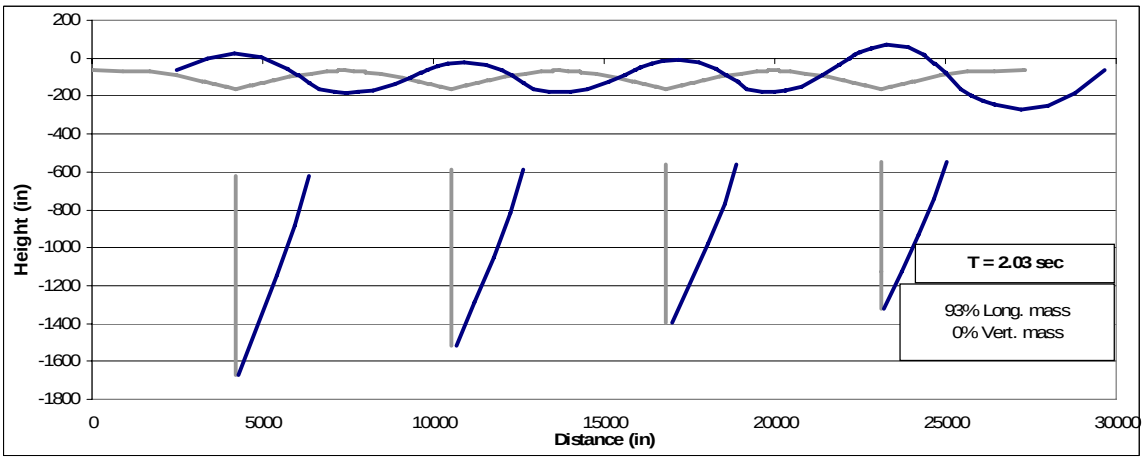

Figure 4-34 525 Foot Span - Primary Longitudinal Mode

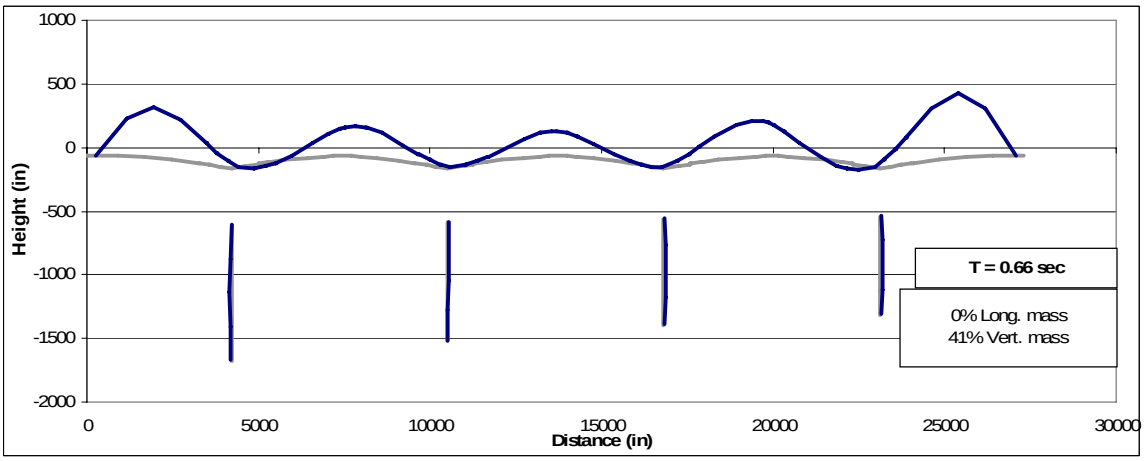

Figure 4-35 525 Foot Span - Primary Vertical Mode

4.6.3. Longitudinal Push Analysis

A longitudinal push-over analysis was performed in order to understand the hinging sequence of the frame, see Figure 4-36. The top of the piers hinge first, prior to engaging the abutment soil springs. The bottom of the piers hinge when the top hinges reach a displacement ductility of about 4. It is important to note that the foundations soil springs reduce the initial stiffness by approximately 75% and change the hinging sequence.

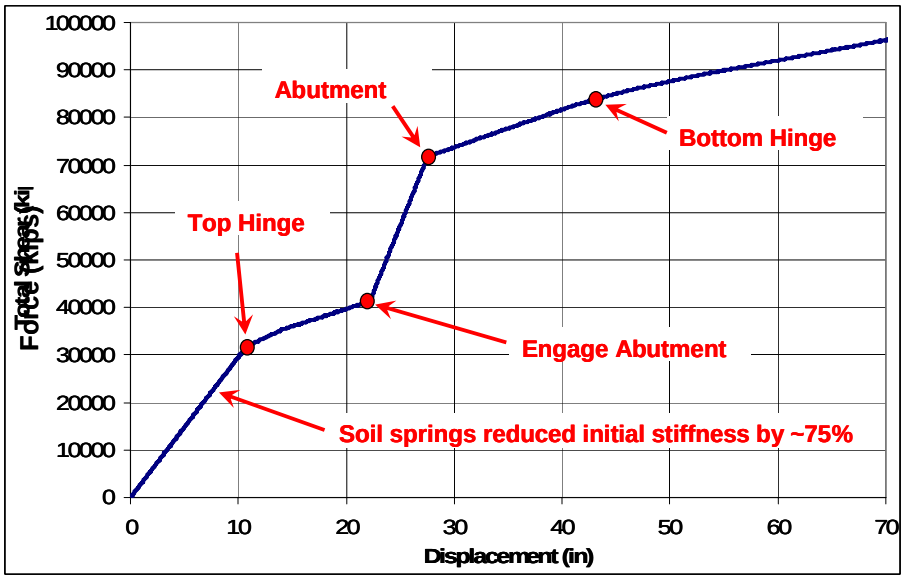

Figure 4-36 525 Foot Span - Longitudinal Push Analyses

4.6.4. Vertical Cyclic Push Analysis

A series of vertical reversed cyclic pushover analyses were performed in order to verify the moment-rotation behavior of the segment joints. Results from segment joint W1 (i.e., nearest the pier) and segment joint 10 (i.e., midspan) are shown in Figure 4-37. The response captures joint opening, concrete crushing and PT yielding for both positive and negative bending directions.

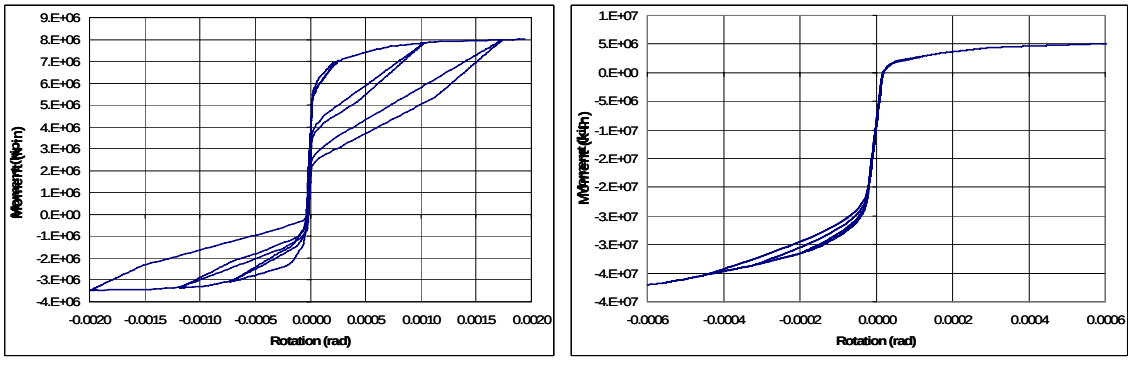

a) Joint 10 - Midspan b) Joint W1 – Adjacent to Piers

Figure 4-37 525 Foot Span - Typical Moment-Rotation Diagrams from Cyclic Push Analysis

4.6.5. Earthquake Time History Analyses

4.6.5.1. Contribution of Vertical Earthquake Motion

To quantify the contribution of vertical motion on the joint response, the model was subjected to longitudinal motions only, as well as simultaneous longitudinal and vertical earthquake motions. Figure 4-39 and Figure 4-40 summarize the maximum (i.e. positive bending) joint rotations for all segment joints and all earthquake records. The horizontal axis of each chart shows the six different joint families. W1/E1 represents the first joint west or east of the pier, while W9/E9 is nine segment joints away from the pier and is adjacent to midspan (see Figure 4-38). Each vertical bar represents the peak rotation for a segment joint family due to a particular earthquake. The median earthquake response of each joint family is also shown. Figure 4-39 shows the results for only longitudinal earthquake motion, while Figure 4-40 shows the results for both longitudinal and vertical motion. It is clear that the vertical component significantly increases the joint response. By taking the median of the ratio of the segment joint median responses, we find that the median positive bending rotations increased by 575%. From similar plots, shown in Appendix A, we find that median negative bending rotations increased by 200% and the median residual rotations remain unchanged.

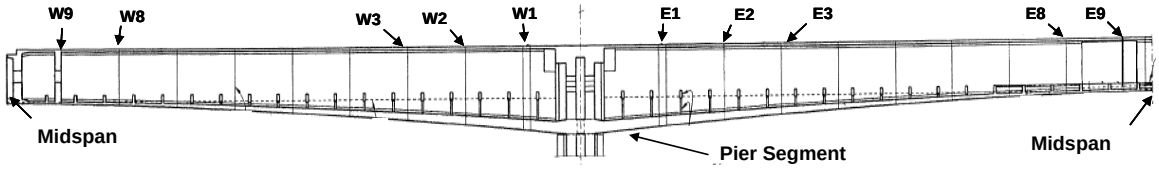

Figure 4-38 525 Foot Span - Segment Joint Identification

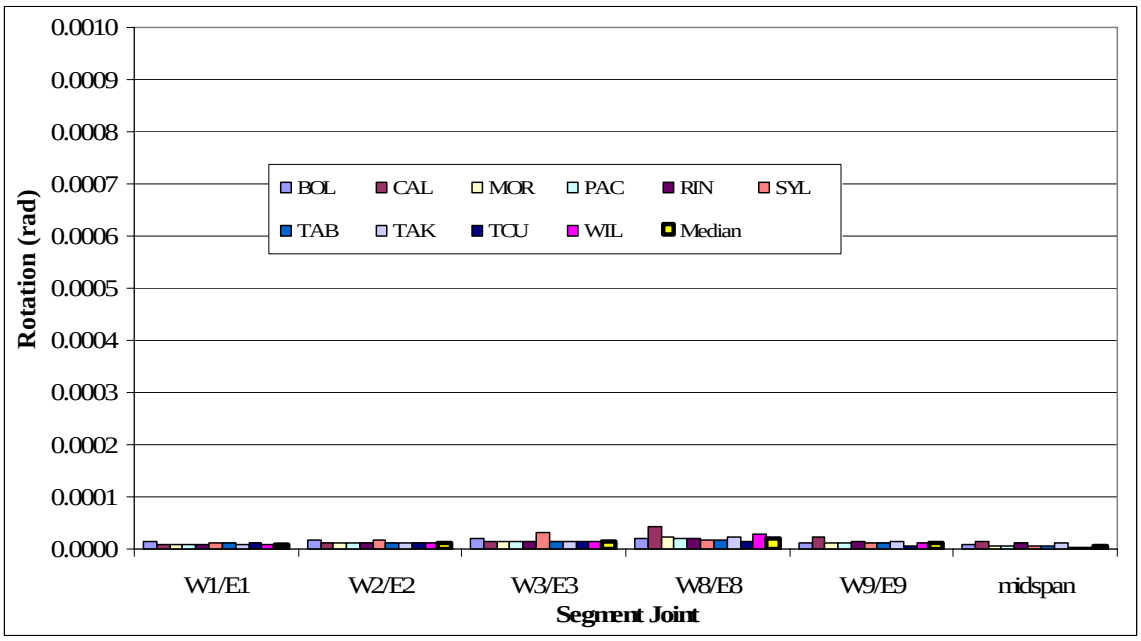

Figure 4-39 525 Foot Span – Max. Segment Joint Rotations – Long. Input Ground Motion Only

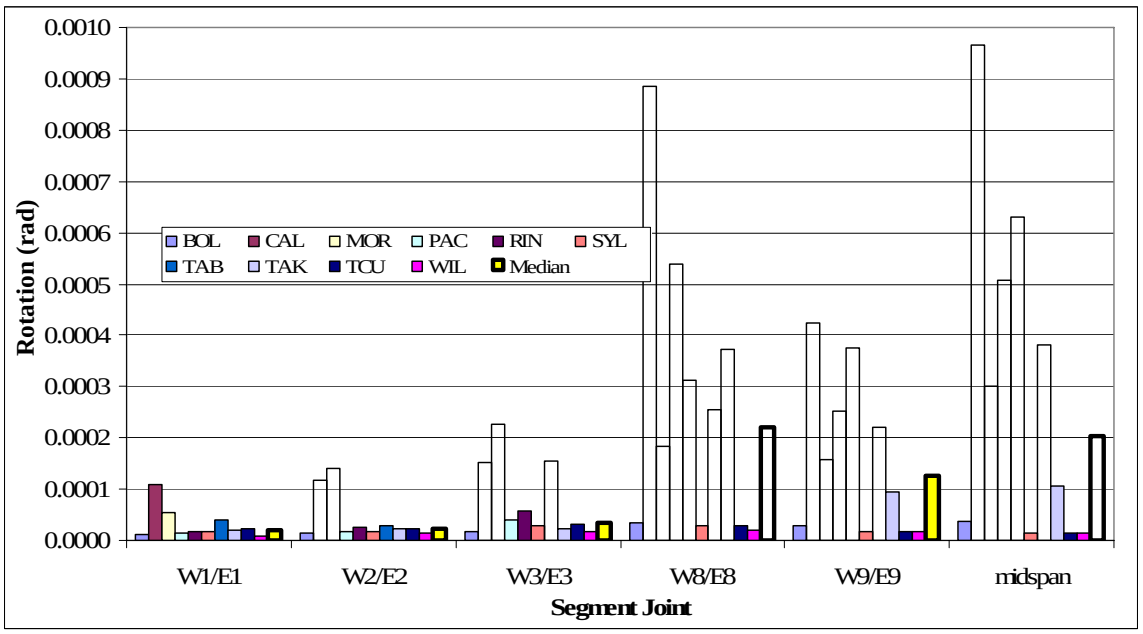

Figure 4-40 525 Foot Span – Max. Segment Joint Rotations – Long. and Vert. Input Ground Motion

4.6.5.2. Longitudinal Response of Piers

The longitudinal response of the piers is shown in Figure 4-41. The vertical bars represent the longitudinal drift ratio for each earthquake record. The median drift ratios

are indicated with horizontal lines and are 2.7% and 2.0% for the short and tall piers, respectively. These drift levels are easily achieved using current design practices. The median residual drifts are 0.20% and 0.19% for the short and tall piers respectively.

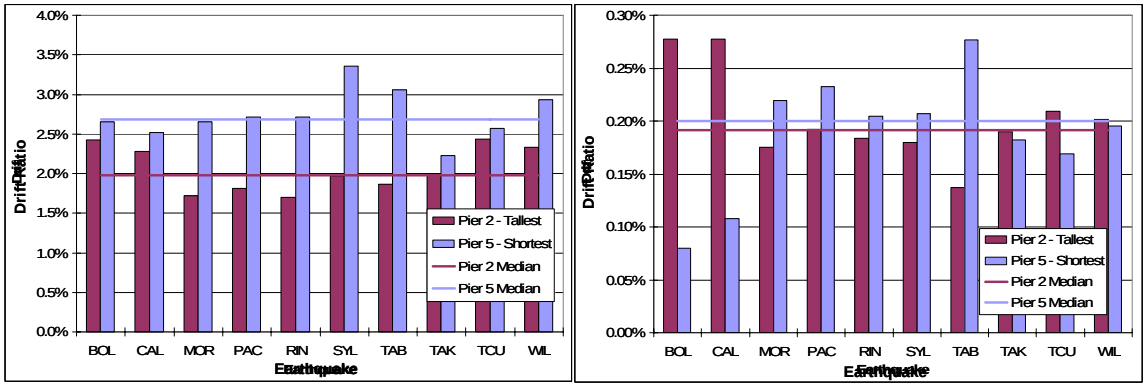

a) Peak Drift Ratios b) Residual Drift Ratios

Figure 4-41 525 Foot Span - Pier Longitudinal Drift Response

4.6.5.3. Response of Superstructure Segment Joints

The moment rotation response of selected segment joints is shown in Figure 4-42. These diagrams do not necessarily represent the median response, rather they are closer to the 84th percentile response. They were selected because they show non-linear response and document the dynamic behavior of the model.

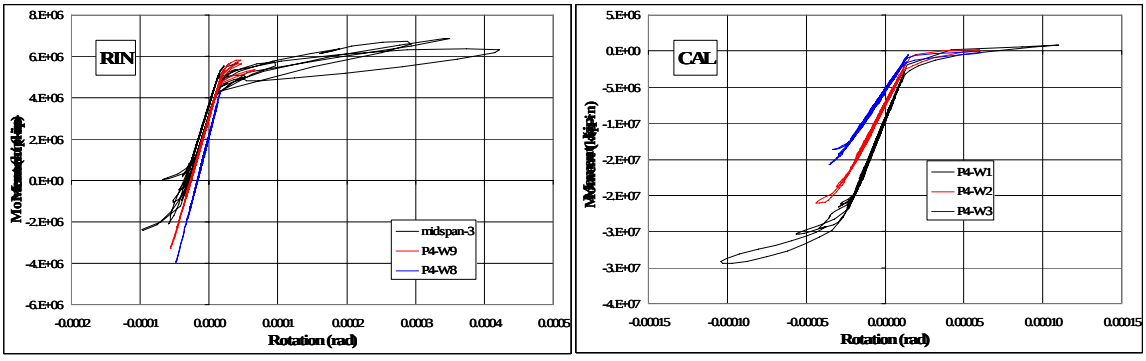

a) Near Midspan b) Adjacent to Pier

Figure 4-42 525 Foot Span - Sample Moment-Rotation Response

A summary of the segment joint response is shown in Figure 4-43. The 16^{th}, 50^{th} (i.e., median) and 84^{th} percentile response are shown on top of the cyclic push results to assist in visualizing the amount of non linear behavior.

The results indicated that the median response opened joints at the piers and midspan with an expected gap opening of about 0.05 inches. Yielding of the PT tendons did not occur. Furthermore, the results showed that the segment joints closed completely after the seismic event and generated no residual joint openings for the median or 16^{th}/84^{th} percentile responses.

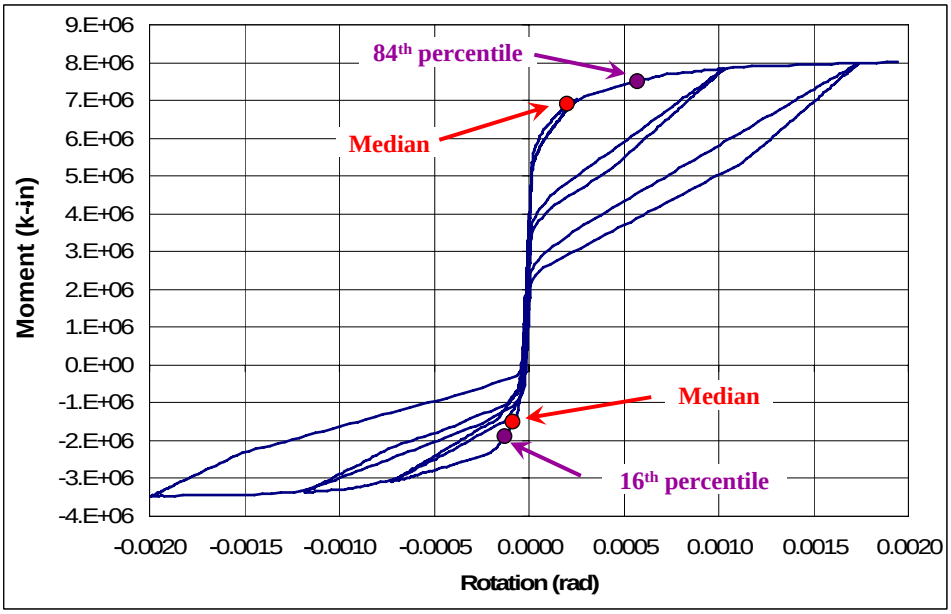

a) Near Midspan

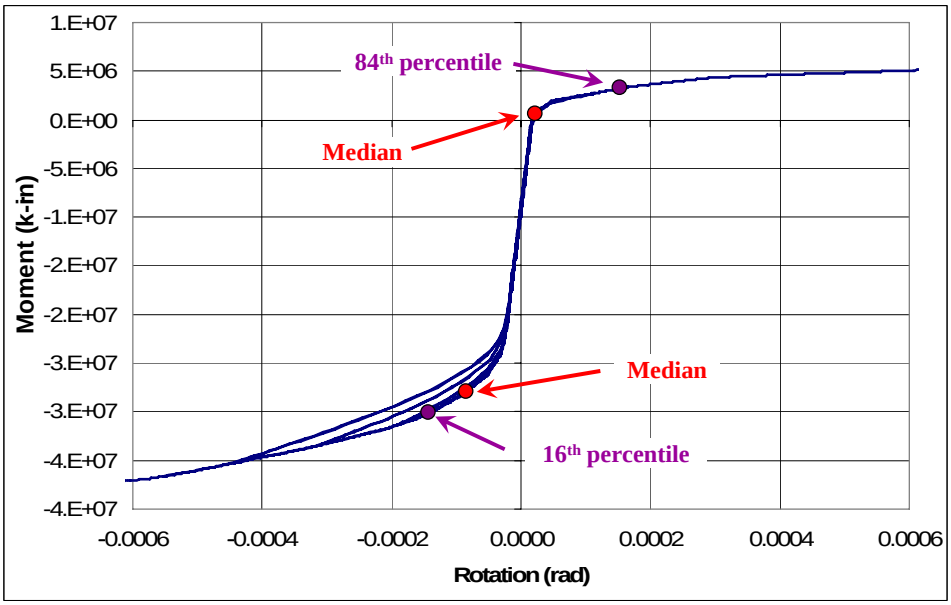

b) Adjacent to Pier

Figure 4-43 525 Foot Span - Summary of Segment Joint Response shown on Cyclic Push Results

5. Model Limitations

The results presented above are better understood when one fully comprehends the limitations of the model. The limitations are as follows.

- The stress state of the joints for the 300 foot span model is approximate and does not account for construction staging effects or time dependant effects such as creep, shrinkage or relaxation. These effects will likely change the values presented modestly. But the general conclusions are expected to remain unchanged.
- The focus of this investigation was limited to superstructures using bonded tendons.
- 3D effects were not considered at this time. It is important to first understand the 2D response before looking into the contributions of transverse earthquake motions on the segment joint response.
- The pier bases for the 300 foot span model were assumed to be completely fixed, thereby neglecting soil-foundation structure interaction. Accurate foundations soil springs were not easily accessible for this bridge and determining them was beyond the scope of this paper. Regardless, the general conclusions presented will likely remain unchanged because the vertical earthquake motion dominates the bridge response and soil structure interaction will predominately affect the longitudinal bridge response.
- Both the 300 foot span and 525 span bridges were modeled with longitudinal abutment soil springs. Most segmental bridges are very long, thus the contribution of the abutment to the global response of the bridge will likely be

very small. Instead there may be interaction between adjacent frames, in the form of pounding. In the end the response is expected to be similar.

- While all the earthquake motions used are records of historic earthquakes with the horizontal component scaled to a design spectrum that is compatible with a 2500 year return period, it remains to be seen what the return period of the vertical motion represents. We have targeted records with strong vertical components, thus we may be subjecting the model to vertical motions that are rarer than a 2500 year return event. Defining the vertical return period is beyond the scope of this report.
- The models were subjected to coherent earthquake excitation. Given the long spans of the bridges investigated herein, and the possibility for varying soil conditions, particularly at the SFOBB skyway site, the seismic wave may not enter the base of the piers in a synchronized manner. Thus the assumption of coherent earthquake motion may not be correct. Incoherent ground motions may increase the demands on the segment joint.
- The unbonded length of the PT tendons was based on large scale experiments with 16 strand tendons (Megally et al., 2002). This should be very close to the unbonded length for the 15 strand tendons used in the Otay River Bridge, but will likely be smaller than the unbonded length of the 34 strand tendons of the SFOBB Skyway. This underestimate of the unbonded length will underestimate the yield rotation of the segment joints, thus the rotation capacity of the 525 foot spam bridge presented herein, are likely underestimated.

6. Conclusions

Detailed 2D analytic models of a single frame of two unique precast segmental bridges were developed, and subjected to a number of non-linear analyses. The models were based on the Otay River bridge and the San Francisco-Oakland Bay Bridge Skyway and have typical span lengths of 300 feet and 525 feet, respectively. The models accurately captured the non linear response of superstructure segment joints and were subjected to a suite of ten near field earthquake records with the goal of obtaining the median seismic response of the segment joints. The span-to-depth ratios of the two bridge models were similar, with the 525 food span bridge being slightly more slender.

The results indicate that vertical earthquake motions significantly contributes to the joint response, increasing the peak negative moment joint rotations by over 400%, the peak positive moment rotations by at least 90%, with only a marginal (less than 10% increase) effect on the residual rotations. In general, the influence of vertical motion on the joint response increased as span length increased.

Based on both longitudinal and vertical earthquake motions, the results indicated that the median response opened joints adjacent to the piers and near midspan and that the maximum gap width was approximately 0.15 inches. In addition, the bottom PT tendons adjacent to the piers may yield in the smaller span length; however there were no residual joint openings anywhere on the bridge. In general, the joint demands on the 300 foot span bridge were larger than the 525 foot span bridge. This was likely due to the fact that the 525 foot span bridge has comparatively more compression across the segment joints.

The superstructure axial load ratio, due to longitudinal PT, of the 525 foot span was greater than the 300 foot span by 23% adjacent to the piers and 69% near midspan.

The results clearly indicated that the superstructure segment joints opened during a significant seismic event. The median response, however, was not sufficient to cause crushing of the extreme concrete elements. Yielding of the PT only occurred in the bottom tendons near the piers of the 300 foot span model. These tendons, however, were only a small percentage of the TP at that location. Therefore no significant permanent damage was observed in the bridge superstructure and the stresses and strains in the concrete and PT remained essentially as they were prior to the seismic event.

Debris on a bridge deck is unavoidable and it may be possible for debris to fall into a segment joint should one open during a seismic event. Given the maximum observed segment joint gap width of 0.15 inches, however, it is very unlikely that debris of sufficient size and strength can fit into the gap and prevent full closure of the segment joint. Debris that is small enough to fit into the gap will likely be pulverized by the significant compression forces across the segments joint due to the longitudinal PT. Any residual cracks that may be created in all likelihood will be approximately the size of shrinkage cracks. Thus, this unlikely occurrence will not cause the bridge to be more maintenance dependant than a typical prestressed concrete bridge with shrinkage cracks.

Based on the results and limitations presented above, it appears that the current design practices in California, which are based on capacity design procedures, prevent significant damage to segmental bridge superstructures.

7. Design Recommendations

Based on the results and conclusions presented above, the following design recommendations are proposed.

- The top and bottom flange thickness must be large enough to ensure that the neutral axis of the superstructure does not migrate into the webs upon joint opening and crushing of the extreme concrete fibers. In other words, the top flange at the piers must be able to take the jacking force of the top and continuity tendons plus the yield force of the bottom tendons. Similarly, the bottom flange at the piers must be able to take the jacking force of the bottom tendons plus the yield force of the top and continuity tendons. Likewise for the midspan joints. This is especially relevant under 3D loading and confinement of the corners should be considered, see Figure 7-1.

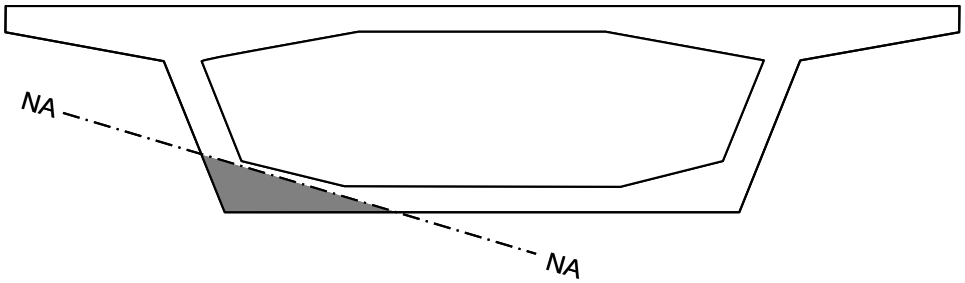

Figure 7-1 Schematic of Neutral Axis Depth due to 3D loading

- While the results indicated that critical PT tendons were unlikely to exceed the full yield limit state, the possibility of loss of prestressing due to yielding of tendons warrant the recommendation that new segmental bridges allow for the possibility of future tendons in the design. The AASHTO Guide Specifications for Design and Construction of Segmental Concrete Bridges (AASHTO, 1999) requires provision for access and anchorage attachment of future tendons with a

PT force not less than 10% of the positive and negative moment primary PT forces. While this provision was intended to be an allowance for the addition of future dead load or to adjust for cracking or deflection of the bridge, it will likely be acceptable for seismic concerns as well.

- Continue using capacity design principles to design precast segmental superstructures as this approach appears to prevent permanent joint opening and significant yielding of the PT tendons adjacent to the piers. Capacity design principles are essential to control the seismic performance of the column-superstructure connection. The current capacity design approach considers over-strength of the column in the design of the superstructure but does not consider the column axial force increase due to vertical excitation and the corresponding increase in the column moment capacity. This approach is thus not a truly rigorous capacity design approach, but it appears to be acceptable and considerations for the effects of vertical earthquake motion on the column moment capacity are not recommended for the capacity design of the superstructure.

8. Future Research

Possible avenues for further study are briefly outlined in this chapter.

- The research presented herein focused solely on the two dimensional response of segmental superstructures. It is possible that the transverse earthquake response may increase the demands on the segment joint and the PT tendons. Since yielding of the PT and the subsequent loss of prestressing force can have a significant influence on the serviceability of bridges, the 3D response of precast segmental superstructure warrants further study.
- The initial stress state will change through out the life of the bridge due to creep, shrinkage, relaxation and temperature. Yet an earthquake may occur at any time during the life of a bridge. Thus it is important that the impact of the pre-earthquake stress state on the response of the segment joints be better understood, through further analyses and sensitivity studies. It is expected that this effect will be more relevant to cast-in-place segmental since the concrete in the segments is less mature at the time of stressing.
- The detailed analysis presented herein utilized a joint model that is based on an unbonded length from a 16 strand tendon. Most segmental bridges utilize larger tendons. The development length of full scale tendons has never been fully investigated, and warrants further study, in the form of large scale testing, to more accurately assess the response of segmental bridge joints.
- Long span bridges are susceptible to increased seismic demands caused by incoherent ground motion. It has been shown that segment joints of precast segmental bridges are sensitive to coherent vertical ground motion. Incoherent

ground motion may excite anti-symmetric modes that may increase segment joint demands and influence the serviceability of the bridge after a significant seismic event. Thus further research into this effect is warranted.

- The emphasis of this report is on the scaling of records to match the horizontal response spectra, because no guidelines exist for matching the vertical response spectra. Further studies are necessary to develop vertical acceleration design spectra as well as guidelines for scaling ground motions to vertical design spectra.
- This report focused on the response of segmental bridges with bonded tendons. The use of external unbonded PT tendons may increase the possibility of reducing the amount of PT required in the superstructure as unbonded tendons have significantly larger rotation capacity. Thus further studies into the response of unbonded tendons are warranted.

9. References

1. AASHTO, “Guide Specifications for Design and Construction of Segmental Concrete Bridges”, American Association of State Highway and Transportation Officials, Washington, D.C., 1999.
2. Burnell, K.P., Megally, S.H., Restrepo, J.I., and Seible, F., “Seismic Testing of Precast Segmental Systems Bridges: Phase III, Bridge Systems Test”, Structural Systems Research Project SSRP 2005/01, University of California at San Diego, La Jolla, CA, June 2005.
3. Caltrans, “Seismic Design Criteria”. California Department of Transportation, Sacramento, CA, Version 1.3, February 2004.
4. Carr, A.J., “RUAUMOKO – Users Manual”. University of Canterbury, Christchurch, New Zealand, February 2004.
5. Megally, S.H., Garg, M., Seible, F, and Dowell, R.K., “Seismic Performance of Precast Segmental Bridge Superstructures”, Structural Systems Research Project SSRP 2001/24, University of California at San Diego, La Jolla, CA, May 2002.

Appendix A – Effect of Vertical Ground Motion on Joint Rotation

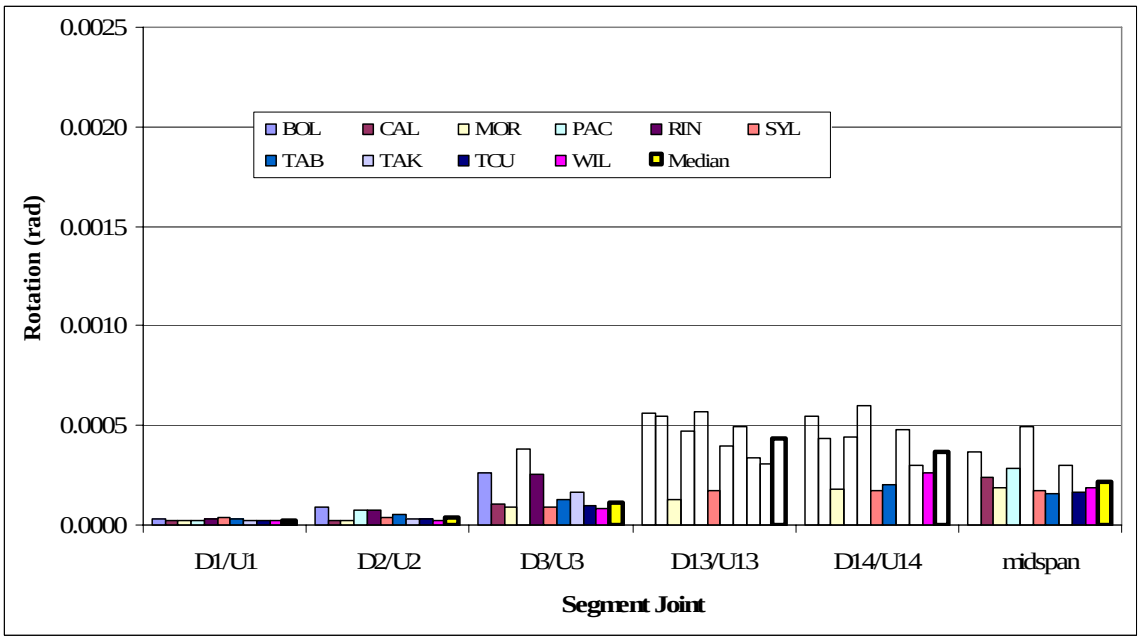

Figure 9-1 300 Foot Span - Maximum Segment Joint Rotations – Long. Only

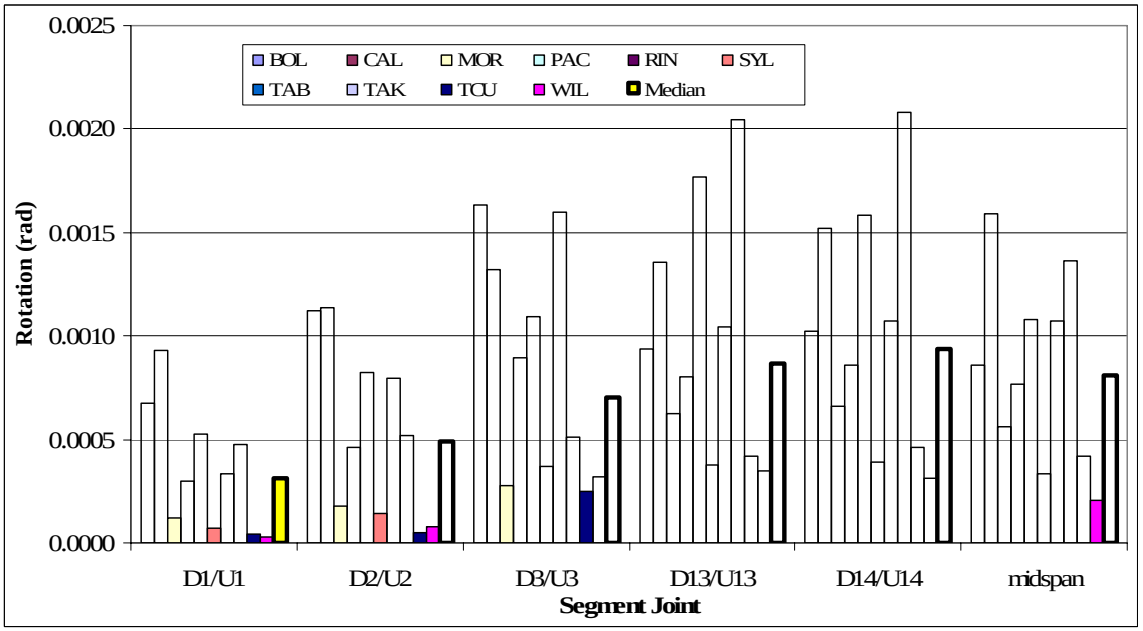

Figure 9-2 300 Foot Span - Maximum Segment Joint Rotations - Long. and Vert.

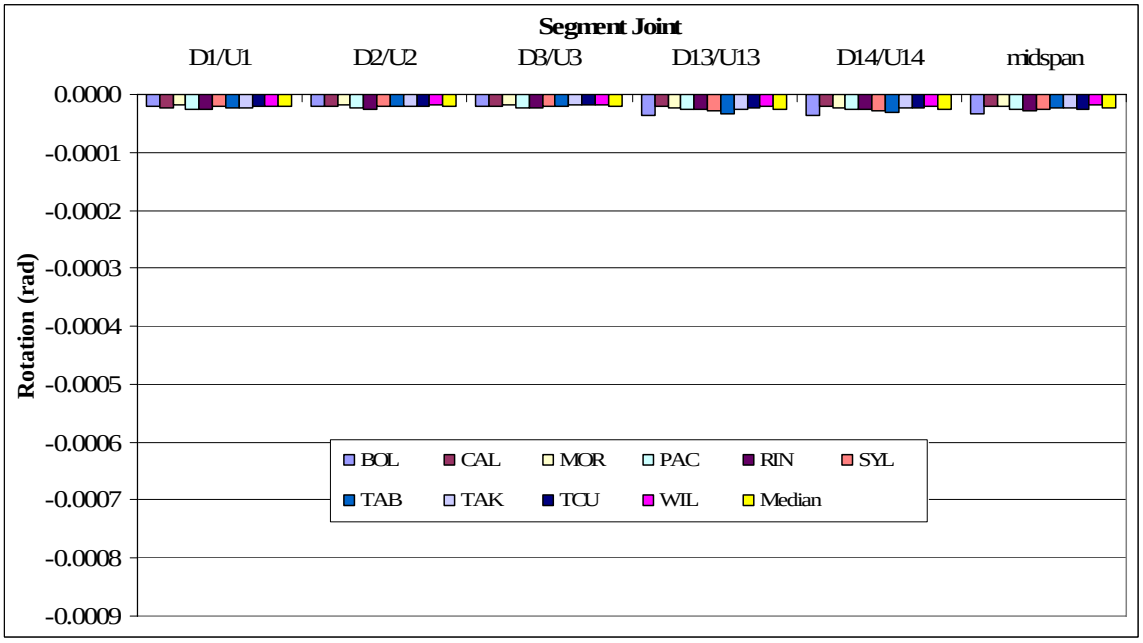

Figure 9-3 300 Foot Span - Minimum Segment Joint Rotations - Long. Only

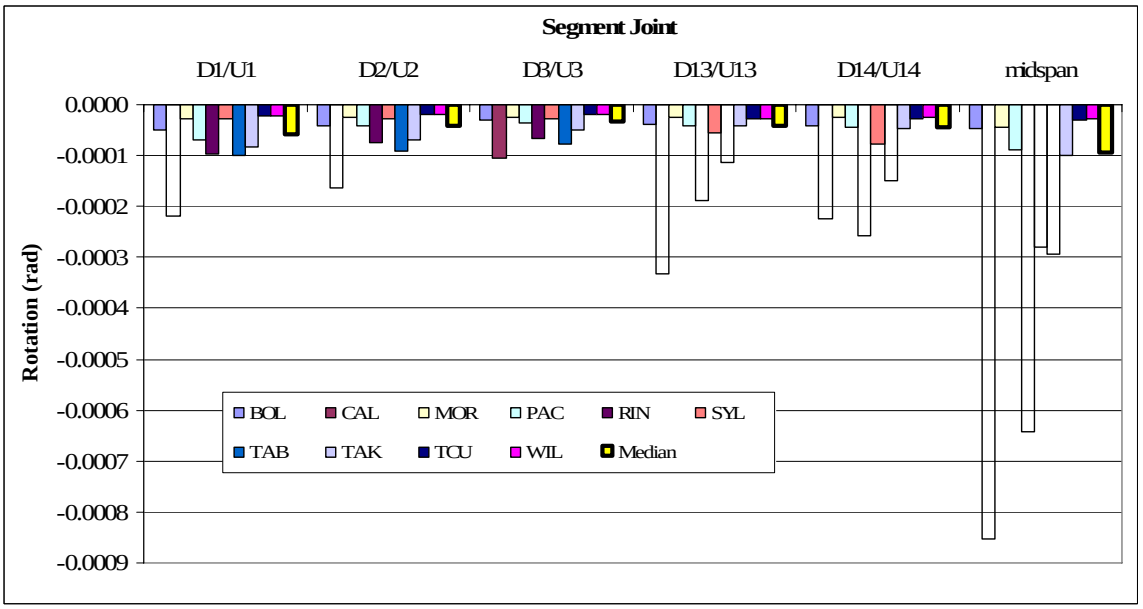

Figure 9-4 300 Foot Span - Minimum Segment Joint Rotations - Long. and Vert.

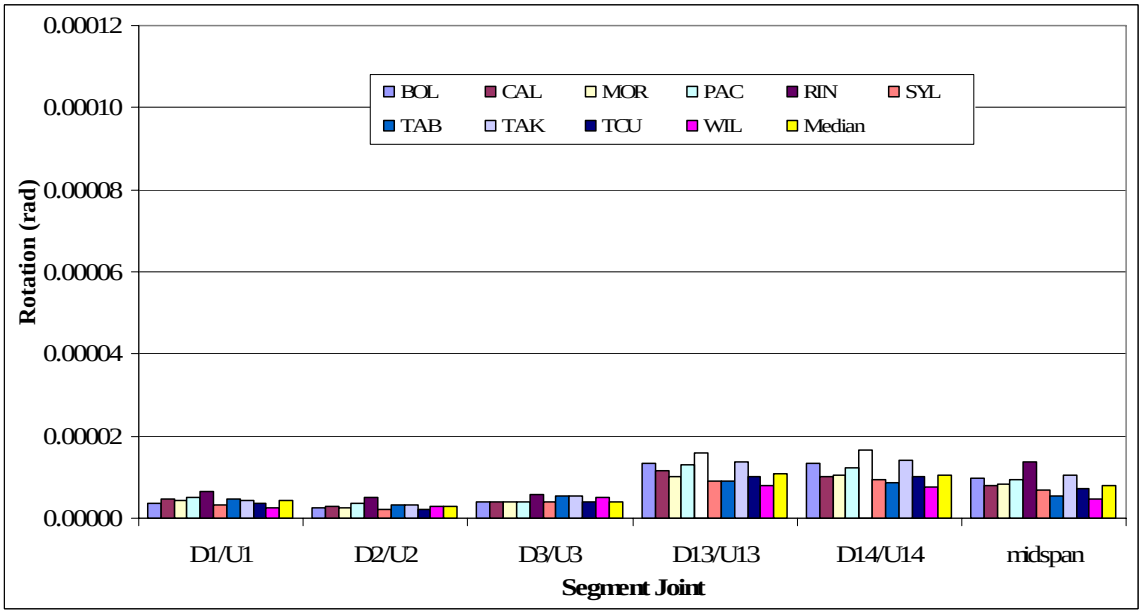

Figure 9-5 300 Foot Span - Residual Segment Joint Rotations - Long. Only

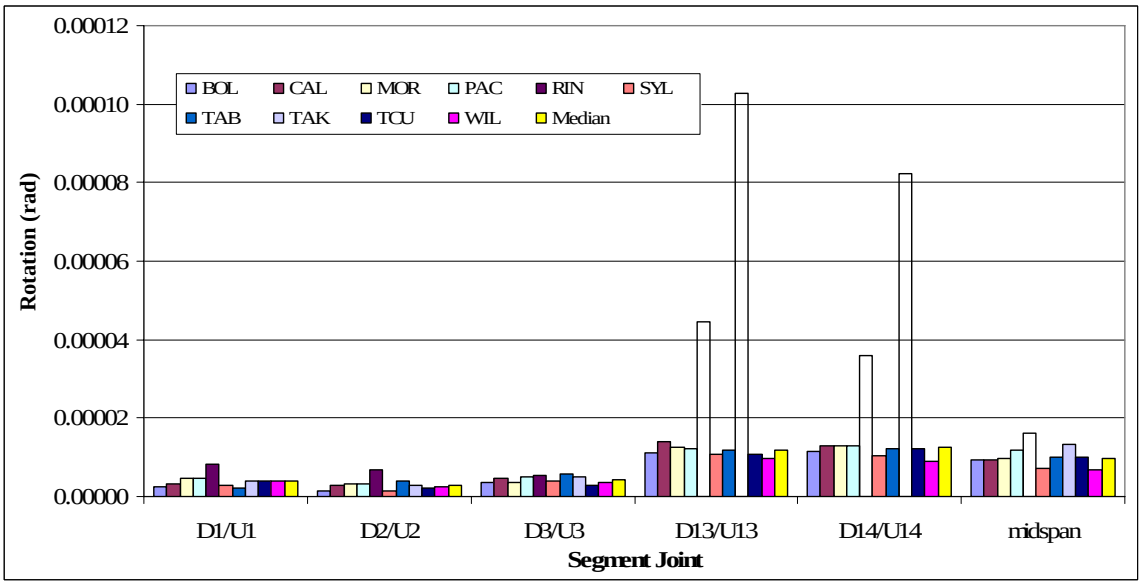

Figure 9-6 300 Foot Span - Residual Segment Joint Rotations - Long. and Vert.

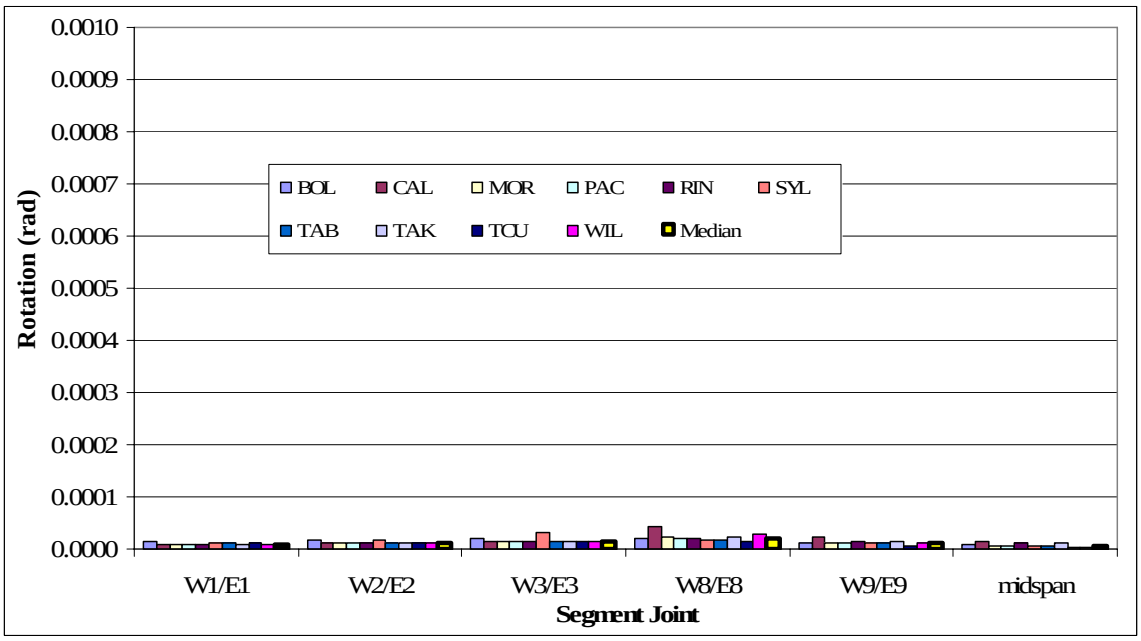

Figure 9-7 525 Foot Span - Maximum Segment Joint Rotations - Long. Only

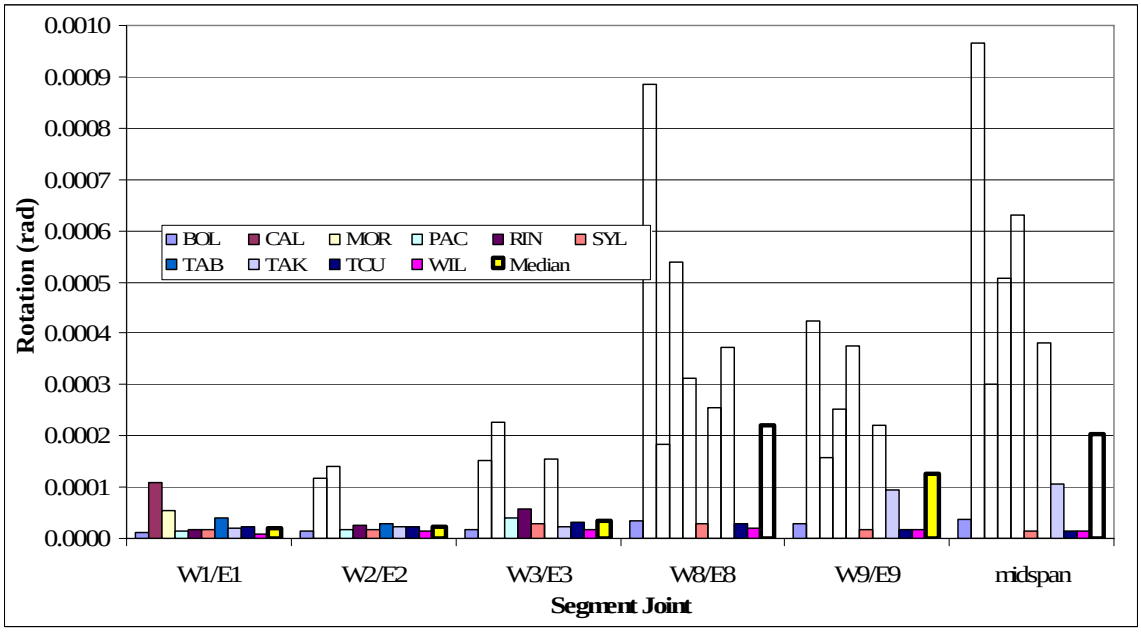

Figure 9-8 525 Foot Span - Maximum Segment Joint Rotations - Long. and Vert.

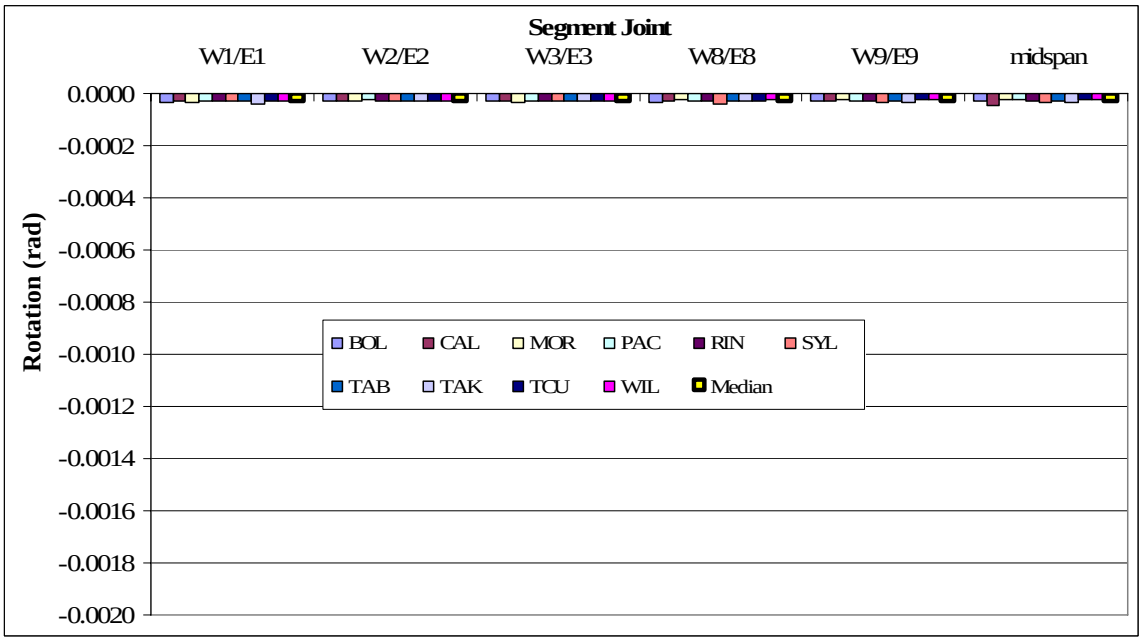

Figure 9-9 525 Foot Span - Minimum Segment Joint Rotations - Long. Only

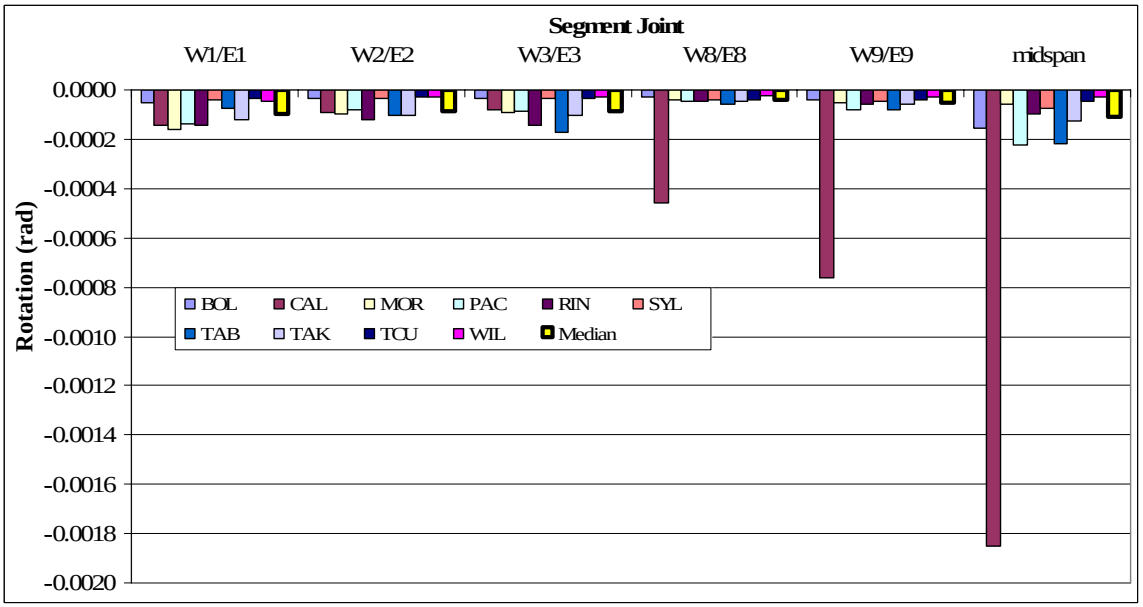

Figure 9-10 525 Foot Span - Minimum Segment Joint Rotations - Long. and Vert.

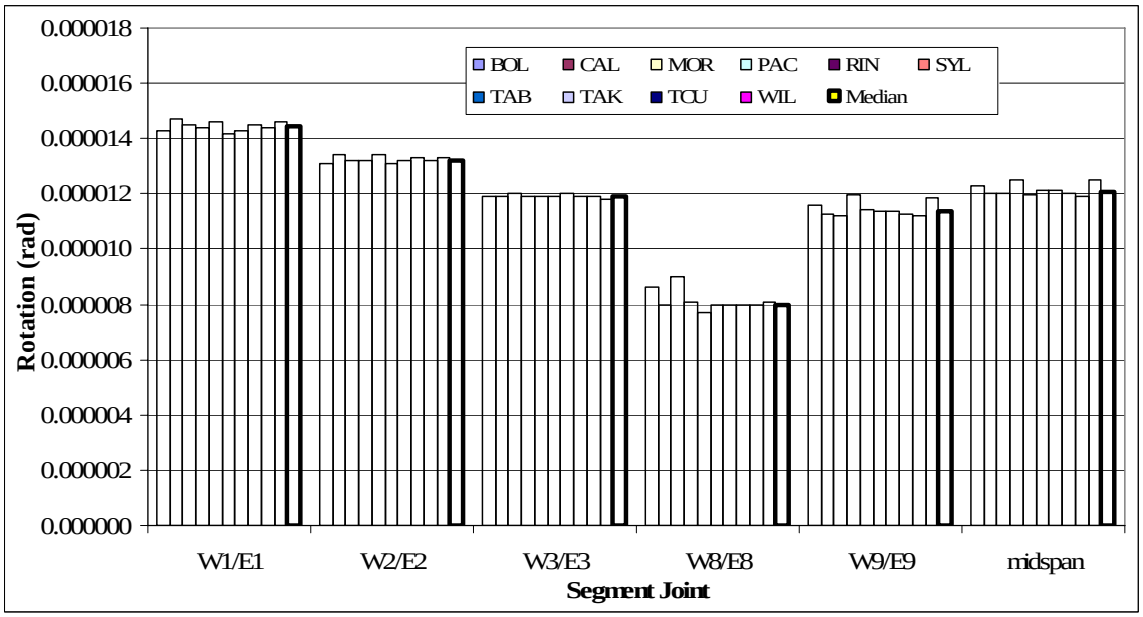

Figure 9-11 525 Foot Span - Residual Segment Joint Rotations - Long. Only

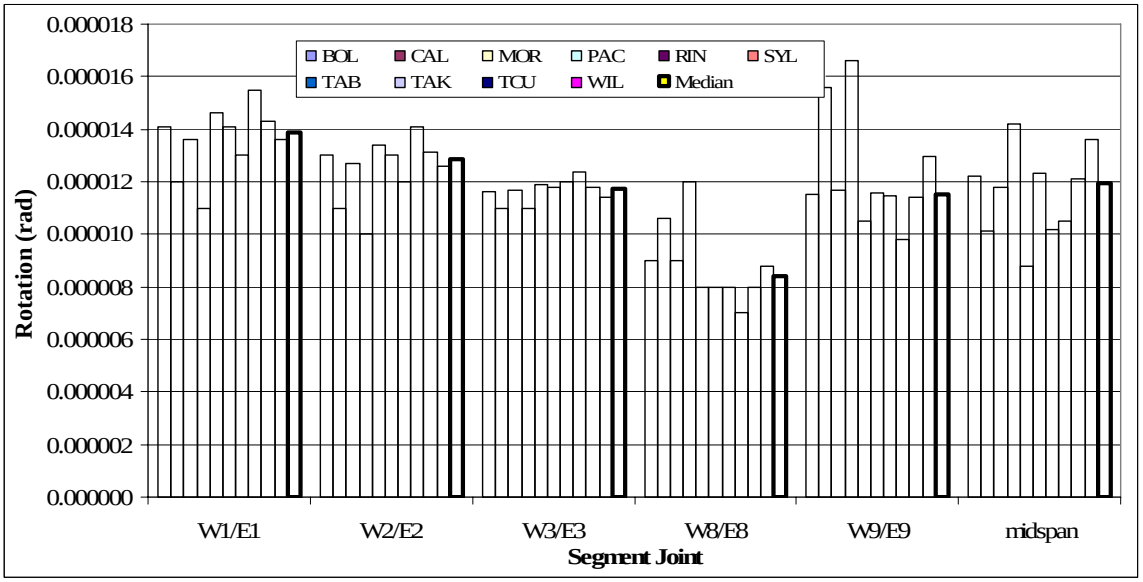

Figure 9-12 525 Foot Span - Residual Segment Joint Rotations - Long. and Vert.

Appendix B – Ruaumoko Description (Carr, 2004)

RUAUMOKO

The Maori God of Volcanoes and Earthquakes

Athol J. Carr

The program **Ruaumoko** is designed to carry out the analysis of structures, in particular buildings and/or bridges, subjected to earthquake and other dynamic excitation. The program is used for earthquake excitation studies including modeling of base-isolation systems and for studies on earthquake excited pounding between buildings. The program can also be used to carry out static or dynamic pushover analyses. The original program was designed for two-dimensional structures, and has been renamed **Ruaumoko-2D** but the three-dimensional version **Ruaumoko-3D** has now been released. This version has all the features of the original program but with the capability of full modeling of three-dimensional structures.

Analysis types:

1. Static analysis.
2. Modal or eigenvalue analysis to find the frequencies and mode shapes of free vibration. The programs also computes the fractions of critical damping associated with each natural mode of free-vibration as a result of the chosen damping model.
3. Dynamic earthquake analysis with horizontal and/or vertical earthquake inputs as well as the initial static loads. The earthquake excitation may be applied to the foundation as is normally done in such analyses where the displacements computed are those of the structure relative to the foundation. There is the option to regard the input excitation as a travelling ground motion where the input arrives at different nodes with a time delay based on the wave velocities of the soil foundation and the distance between nodes. A random motion may be added to the input at subsequent nodes to apply dispersion to the input motion based, again, on the distance between supporting nodes. In all of these traveling wave analyses a total displacement approach is used.
4. Dynamic response with dynamic force histories as well as the initial static loads. A push-over analysis is a special version of this analysis option. If there are no masses or damping in a push-over analysis then the pushover is a static pushover.
5. Adaptive Pushover analysis where the load pattern changes as the structure changes its properties. This is a static pushover but the masses are used in a Rayleigh process to generate the next step load increment. The final solution is independent of the initial loading pattern used and is in effect an incremental displacement process with all the displacement increments being virtually constant in magnitude. The process terminates automatically when the maximum capacity of the structure is reached.
6. A Cyclic Adaptive Pushover analysis where an adaptive loading, as above, is applied to the structure until the desired displacement is exceeded for a specified degree of freedom. The direction of the load is then reversed and a further adaptive response is followed until the displacement achieved reaches the next point on the specified displacement history.
7. A total displacement approach may be used to get the response to specified displacement history inputs at as many nodes as required. This may be used to analyze structures where different ground displacement histories are specified at different points in the foundation of the structure. Up to 99 different input displacement histories may be used in any one analysis.

Analysis Options:

1. Elastic analysis This over-rides all non-linear member and geometric options enabling an elastic analysis to be carried out without changing the structure data from that used for a non-linear analysis.
2. In-elastic or non-linear analysis.
3. Elastic Response Spectra Analysis. This over-rides all non-linear member and geometric options and obtains the response of the structure to a response spectrum for each of the earthquake components.

Geometric Options:

1. Small Displacement Analysis (Default). This is a conventional analysis where the initial geometry is used throughout the analysis.
2. Large Displacement Analysis. Here the coordinates of the nodes are updated at every time-step, the member transformation matrices are updated and the geometric stiffness (due to axial forces in the members) is updated using the current axial force in the member.
3. P-Delta Analyses. The original geometry is used in every time-step but after the static analysis the geometric stiffness matrices for the frame members are computed using the static axial force in each member. At each time-step the axial forces in the members and the slope of each member is used to correct the equilibrium of the structure to allow for the P-Delta effect. This gives generally similar results to the Large Displacement analyses but with a much reduced computational effort.

Mass Representation Options:

1. Lumped Mass model. This model gives a diagonal mass matrix with no inertia associated with the rotational degrees of freedom.
2. Diagonal Mass model. As above, but inertia is associated with the rotational degrees of freedom. The diagonal rotational terms for frame members are those from the member consistent mass matrices
3. Consistent Mass model. This generates for members with distributed mass a representation that is kinematically consistent with the deformation modes of the members.
   Note: If only input nodal masses are used then there is no difference between the Lumped and Diagonal Mass models.

Damping Options:

1. Rayleigh or Proportional Damping model using the Initial Elastic Stiffness matrix.
   Damping matrix [C] = alpha[M] + beta[K]
2. Rayleigh or Proportional Damping model using the current Tangent Stiffness matrix.
   Damping matrix [C] = alpha[M] + beta[K]
3. Linear variation of the fraction of critical damping with the frequencies of free vibration. This includes the case of constant damping over all frequencies.
4. Tri-linear Variation of the fraction of critical damping with frequency of free vibration.
5. General variation of the fraction of critical damping with frequency. This is a generalization of the Tri-linear model above.
6. Rayleigh or Proportional Damping with different members or sections of the structure having different amounts of damping.
   Damping matrix [C] = alpha[M] + beta[K]
   This is done member-by-member and different members or parts of the structural system may have differing alpha and beta values.
7. Damping members (dashpots, both linear and non-linear) may also be included in the computational model. The dashpots may have different damping values associated with each of the member deformation velocities, axial, shear, torsion and rotation.

Member Types:

All members are represented by a four-node definition, node **I**, **J**, **K** and **L**. These are the four corner nodal points for the Quadrilateral Finite Elements and the Masonry Panel Elements. For all other members, which are line or one-dimensional elements, the first two nodes **I** and **J** are the nodes that the member is connected to in the structure. The second two nodes **K** and **L**, which are usually dummy nodes with no displacement degrees of freedom, are used to define the inner ends of rigid links connected to first two or outer nodes. The deformable part of the member is that between the inner two nodes **K** and **L**. If these last two node numbers are 0, or omitted, they are taken to be the same as the first two nodes and the rigid links do not exist. This allows for the easy incorporation of rigid links in the structure removing the necessity of using stiff dummy members to model structural actions. Such stiff dummy members pose a great risk to the accuracy of the analysis. The default, with the last two nodes omitted from the data, provides the normal two-node definition of the one-dimensional members. In **Ruaumoko-3D** the line

members use a 5th node, node **M**, or a global coordinate direction i.e. +x, -x, +y, -y, +z or -z, to define the principal axis directions of the member cross-section. The local z axis lies in the plane of nodes **K**, **L** and **M**. The spring, dashpot and tendon members may also be of zero length when the member axes directions are assumed to be in the global axes directions. The frame and foundation members must have a non-zero member length.

1. Frame members:

The beam or frame members may allow for shear deformations and rigid end-blocks within nodes **K** and **L**.
They may be pinned to the joint at either end or at both ends.
A choice of almost any of the hysteresis rules available.
Strength degradation is permitted for most hysteresis rules.
Damage indices for the member may be computed for most hysteresis rules.
The shear in the frame members may be inelastic, using a SINA hysteresis to model the inelastic shear behaviour and the model also allows the shear strength to degrade with the shear deformations as well as with the plastic rotations at the ends of the members.
There is an option to allow inelastic slip rotation to occur at the ends of the members due to variations in the connection shear forces. This may be important in modeling shear link members in eccentrically braced frames etc.

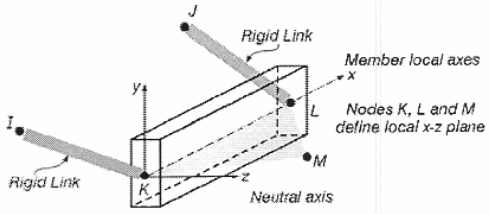

Ruaumoko-2D:

1: Giberson One-component beam member.
If the second moment of area **I** = 0.0 it acts as a truss member
2: Reinforced concrete beam-column member (Giberson)
3: Steel beam-column member (Giberson)
4: General beam-column member (Giberson)
5: Two-component beam member.
6: Variable flexibility beam member. (This model has a quadratic variation of flexibility along the in-elastic member length)
7: Four hinge beam member (Giberson)

Ruaumoko-3D:

1: Giberson One-component beam member.
2: Reinforced concrete beam-column member (Giberson)
3: Steel beam-column member (Giberson)
4: General beam-column member (Giberson)
5: Two-component beam member.
6: Variable flexibility beam member. (This model has a quadratic variation of flexibility along the in-elastic member length)
7: Reinforced concrete beam-column member with an alternative yield surface. (Giberson)

2. Spring Members:

May be used as a truss member where the Longitudinal stiffness = AE/L
A choice of almost any of the hysteresis rules available.
Strength degradation is permitted for most hysteresis rules.
Damage indices for the member may be computed for most hysteresis rules.

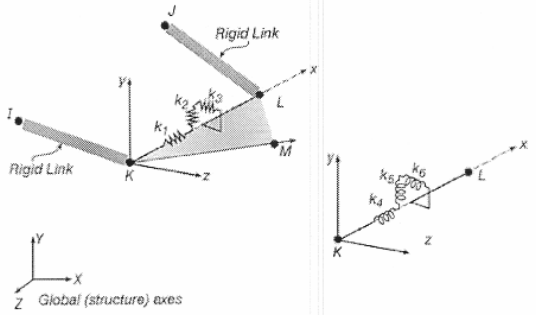

Ruaumoko-2D:

Three actions (longitudinal displacement, transverse displacement and rotation about the out-of-plane axis, i.e. z-rotation)

1: No Interaction between longitudinal and transverse components.
2: Quadratic Interaction between longitudinal and transverse components (Tri-linear hysteresis only).
3: Degradation in the transverse stiffness is a function of the rotational spring ductility. (Used to represent shear-flexure interaction and shear strength degradation due to flexure)
4: A model where there is an interaction between the axial force in the spring member and the yield moment about the z axis.

Ruaumoko-3D:

Six actions (longitudinal displacement, two transverse displacements, twist and rotations about the two transverse axes)

1: No Interaction between longitudinal and transverse components.
2: Quadratic Interaction between longitudinal and transverse components.
3: Degradation of the transverse stiffnesses as a function of the rotational spring ductilities. (Used to represent shear-flexure interaction and shear strength degradation due to flexure)
4: A model where there is an interaction between the axial force in the spring member and the yield moments about the y and z axes.

3. Wall Members: (**Ruaumoko-2D** only)

This is a filament type element used to represent reinforced concrete structural walls. The cross-section is represented by a series of segments, or filaments, each with its own concrete and steel areas. Plane sections are assumed to remain plane enabling a computation of the effective cross-sectional area, moment of inertia and location of the neutral axis. A Lobatto quadrature is used to integrate along the member length. Different concrete and steel models are allowed.

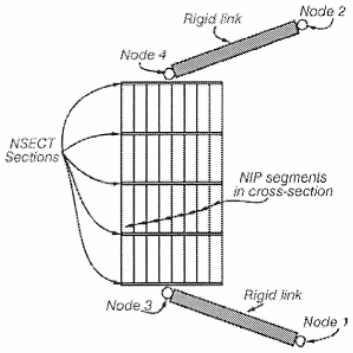

4. Viscous Dash-pot Members:

Linear or non-linear dashpot elements. Allows for gap in which no force is generated and may have different properties in positive and negative directions.

Ruaumoko-2D: Three actions, longitudinal, transverse and z-rotation velocities.

Ruaumoko-3D: Six actions, longitudinal and two transverse velocities, twist and rotational velocities about the two transverse axes.

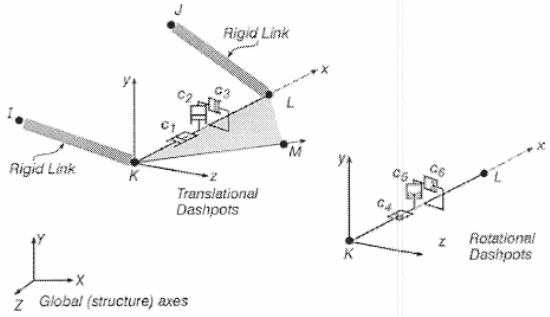

5. Contact Elements:

Three actions (Longitudinal contact spring, Transverse friction springs, Longitudinal dashpot)
'Hertzian Contact' hysteresis or 'Bi-linear with slackness' hysteresis rule.
User specified Initial Gap.
Compressive and/or Tensile action.
Friction and Damping attributes available when axial contact occurs.
Member only acts during time-history analysis

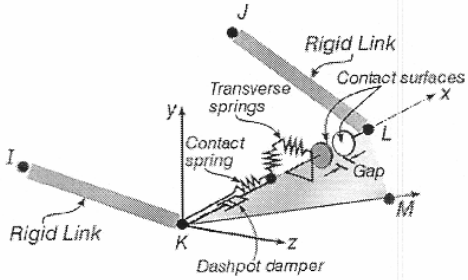

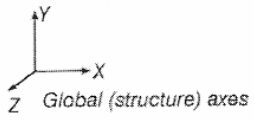

6. Tendon Elements:

One longitudinal action. The member has no stiffness but applies forces etc. to nodes **I** and **J**.

1: Constant forces depending on magnitude and sign of the member displacement.
2: Force proportional to nodal displacements, velocities or accelerations (with up to 10 contributions from different nodes and actions).
3: Re-settable Actuator (semi-active damper) model.

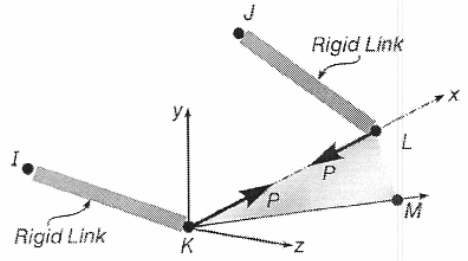

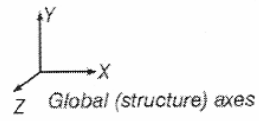

Quadrilateral Finite Elements:

Ruaumoko-2D:

1. Linear Elastic Hybrid-Stress (Type II) Plane Stress finite element with three degrees of freedom at each node (local x and y displacements and rotation about z axis). There is a cubic lateral displacement on each edge (this matches an adjoining beam or frame member displacement) and a linear longitudinal displacement on each edge.

Ruaumoko-3D:

1. Linear Elastic Hybrid-Stress (Type II) Plane Stress finite element with three degrees of freedom at each node (local x and y displacements and rotation about z axis). There is a cubic lateral displacement on each edge (this matches an adjoining beam or frame member displacement) and a linear longitudinal displacement on each edge.
2. Linear Elastic Hybrid-Stress Plate Bending finite element with three degrees of freedom at each node, an out-of-plane displacement and rotations about the two in-plane local axes. A plate shear deformation term may be added in this element.
3. A combination of the above two elements to form a shell finite element with six degrees of freedom at each of the four nodes.

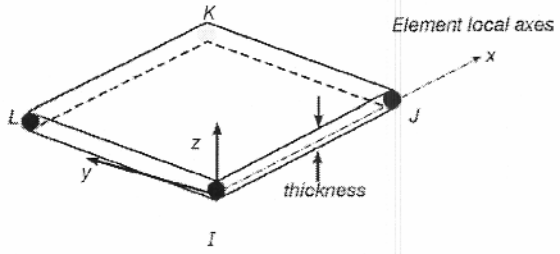

Masonry Panel Elements:

Four-strut model with a very detailed masonry hysteresis to represent the diagonal force transmission across the panel, the two struts in each direction transmit some of the force into moments at the joints. A fifth strut, with a bi-linear hysteresis, transmits part of the shear from the top to the bottom of the panel element. In **Ruaumoko-3D** an elastic plate finite element may be added to the panel to provide an out-of-plane stiffness.

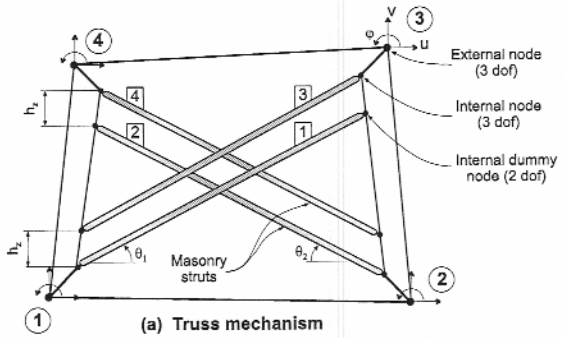

(a) Truss mechanism

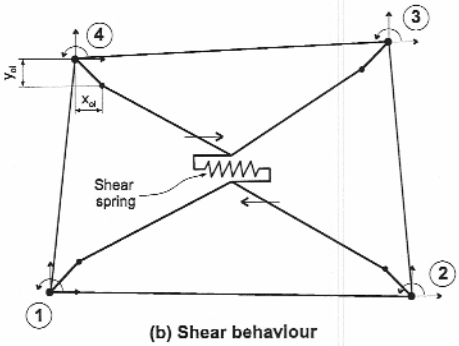

(b) Shear behaviour

9. Ground or Foundation Elements:

This is a beam-like element that is a form of distributed Winkler Spring in both the transverse and longitudinal actions. These can be used to represent foundation material under a structure or to represent through-soil coupling between structures.

Shear stiffness terms optional except for Vogt foundation model.

A choice of almost any of the hysteresis rules available.

Strength degradation is permitted for most hysteresis rules.

Actions are only provided in the local x-y plane of the element.

1. Vlasov soil model, linear variation with depth for shallow soils.
2. Vlasov soil model, hyperbolic variation with depth for deep soils.
3. Vlasov soil model, exponential variation with depth for very deep soils.
4: Pasternak soil model, this is a general two-parameter model.
5: Vogt soil model, a general model but with no shear term.

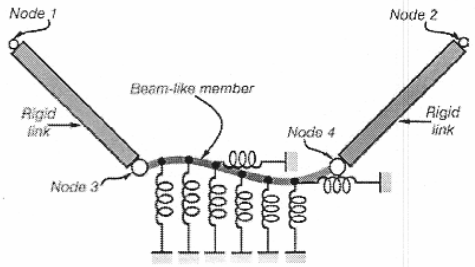

Hysteresis Models: (Stiffness degradation) (for Frame, Spring and Foundation Members)

Current Hysteresis Rules available are:

0. Linear Elastic
1. Elasto-Plastic
2. Bi-linear
3. RAMBERG-OSGOOD hysteresis (Original model)
4. TAKEDA Bi-linear Degrading Stiffness
5. Bi-linear with Slackness
6. KIVELL Degrading Stiffness (initially used for nail-plates in timber frames)
7. Origin Centered Degrading Stiffness
8. SINA Degrading Stiffness
9. STEWART Degrading Stiffness (initially used for modeling nailed panels to timber frames but also very successfully applied for reinforced concrete columns which use plain round reinforcement bars)
10. Degrading Bi-linear Stiffness
11. CLOUGH Degrading Stiffness
12. Q-HYST Degrading Stiffness
13. MUTO Tri-linear Degrading Stiffness
14. FUKADA Tri-linear Degrading Stiffness
15. Bi-linear Elastic
16. Non-linear Elastic (initially used for Un-Reinforced Masonry panels)
17. Degrading Elastic
18. Ring-Spring model. This has a flag-shaped hysteresis loop.
19. HERTZIAN Contact Spring
20. MEHRAN Degrading Stiffness
21. WIDODO Foundation Compliance Model
22. LI-XINRONG Reinforced Concrete Column hysteresis
23. BOUC-WEN hysteresis
24. REMENNIKOV Steel Brace model
25. TAKEDA with Slip (Otani)
26. AL-BERMANI Bounding-Surface model (Zhu)
27. Peak Oriented hysteresis
28. MATSUSHIMA Degrading Stiffness
29. KATO Degrading Shear model
30. Elastomeric Damper model
31. Composite Section SINA Degrading Stiffness
32. Different +/- Stiffness Bi-linear Stiffness
33. Masonry Strut hysteresis (Crisafulli)
34. Hyperbolic hysteresis
35. Degrading Bi-linear hysteresis with Gap
36. Bi-Linear +/- Stiffness
37. Non-linear Elastic Power Rule
38. Revised Origin Centered Degrading Stiffness
39. Dodd-Restrepo Steel hysteresis model
40. Ramberg-Osgood hysteresis (this is a bounded model, used since 1984)
41. Ramberg-Osgood hysteresis (this uses the "Pyke" range to bound forces)
42. HERA-SHJ Steel Beam sliding-joint model (under development with HERA(NZ))
43. Re-settable Actuator (semi-active damper) hysteresis.

Strength Degradation:

Many of the hysteresis rules allow for degradation of the strength of the members. The Yield Forces or Yield Moments may degrade as a function of the member ductility or the number of cycles of inelastic action. This is independent of the stiffness degradation associated with the hysteresis rule. There are some hysteresis rules with their own built-in degradation of strength.

Damage Indices:

Many of the hysteresis rules used in the Frame and Spring Members allow for the computation of the following damage indices for the members.

1. Number of inelastic cycles of member action
2. Ductility
3. Park and Ang Damage Index
4. Bracci et. al. Damage Index.
5. Roufaiel and Meyer Damage Index
6. Cosenza, Manfredi and Ramasco Damage Index
7. Banon and Venezziano Damage Index
8. Krawinkler and Zohrei Damage Index
9. Dissipated energy

Slaving of Nodal Degrees of Freedom:

Nodal degrees may be slaved to the matching degrees of freedom of other nodes in the structure. This feature removes the necessity to place dummy stiff members in the structure as required by so many other programs with the ensuing risk to the accuracy of the analysis. This feature, together with the four-node definition of the linear members means that complicated systems may be modeled with the minimum of effort and computational cost. In **Ruaumoko-3D** there is also the ability to model floor diaphragms that are rigid in their own planes.

Travelling Wave Input (Earthquake analysis only):

The analysis may be the normal single foundation ground motion model for earthquake analyses or instead allow for a traveling wave input, in the x, y and z directions using a wave velocity in each direction to calculate the time delay for the wave input at each base node in turn. In these travelling wave analyses a Total Displacement formulation is used rather then the conventional Relative (to the ground) Displacement formulation. A random dispersion option exists to modify the motion at subsequent input supports to allow for a dispersion, or incoherence, in the motion to allow for distance from the first arrival support.

Displacement Limits:

The user may specify displacement limits, which will trigger termination of the analysis if they are exceeded during the time-history response.

Input Data:

The program prompts for all input data but in most analyses the user using an editor program such as Windows Notepad prepares a data file, which is in a free-format. If input is made interactively all input keystrokes may be logged to a file thus creating a data file for later use.

Number of Excitation Components:

In **Ruaumoko-2D** up to 2 input ground accelerograms may be input. In **Ruaumoko-3D** up to 3 input ground accelerograms may be input in any specified directions. Up to 99 different time-histories may be specified for dynamic force pattern loadings or displacement histories if specified nodal displacement time-histories are being used.

Excitation Input Formats:

The excitation (earthquake, dynamic force time-histories or displacement time-histories) may be input in one of six different formats. Other acceleration records may be easily converted to one of these formats. The excitations may be input from separate files or attached as part of the data file.

Program Output:

The output file contains:

1. Image of all input data:
2. Results of computed masses from member self-weight.
3. Nodal displacements and member forces and moments from the static analysis.
4. Natural frequencies and periods of free-vibration together with the fraction of critical viscous damping associated with each mode.
5. Participation Factors and Effective Modal Masses for each mode of free-vibration for each component of the earthquake excitation. (Only for accelerogram excitation)
6. Each requested mode shape of free-vibration.
7. If required: Nodal displacements and member actions as requested for any node or member specified at specified time-step intervals.
8. If requested: At the end of the time history analysis the residual nodal displacements and members actions can be output.
9. If requested: The envelope of inter-storey drifts may be output.
10. Envelopes of nodal displacements and the times of peak response.
11. Envelopes of member forces and moments and the times of peak response.
12. Envelopes of member deformations and the times of peak response.
13. Envelopes of member ductilities for all members that exceed yield actions.
14. If required: Damage indices for specified members
15. Analysis statistics

Mode of Program Execution:

The program runs in an interactive mode by default. However, the user may set up a batch file to run the program in batch mode. This is very useful if a large number of analyses are to be run for, say, a large scale parameter study.

Graphical Output:

The Structure Mesh, Excitations and Mode-Shapes of Free Vibration may be plotted. Real-time plots of the deflected shape of the structure showing locations of inelastic action may also be shown during the dynamic time-history.

Post-processor Output File:

These post-processor output files holding structure data and nodal and member results may be output at specified time-step intervals. These files are either Binary files (default) or ASCII text files for input to the post-processor program **Dynaplot**. The ASCII text file format may also be used as input to a user written post-processor program.

Post-Processor Programs:

All results from **Ruaumoko-2D** and **Ruaumoko-3D** may be passed to the post-processor program **Dynaplot**.

1. All of the graphics produced by **Ruaumoko** during the analysis may also be reproduced in **Dynaplot** and the deflected shape/plastic hinge pictures may be run as a continuous movie as in **Ruaumoko** or in a frame-by-frame mode which is useful if they are to be produced in hard-copy form.
2. Time-history plots of nodal actions, i.e. displacements, velocities, accelerations, nodal damping forces, nodal inertia forces and nodal applied loads can be produced.
3. Time-history plots of member forces, deformations and relative stiffnesses can be produced.
4. Hysteresis loops for member actions may be plotted.
5. The mode shapes of free vibration can be plotted as can deflected shapes of the structure.
6. Plots of Kinetic Energy, Damping Work Done, Strain Energy, Plastic Work Done and Applied Work Done are available.
7. Time-history plots and Hysteresis loops may also be plotted for combinations of nodal and member inputs (with up to 50 contributions per line).
8. Plots of the member and nodal point meshes are also able to be output.
9. Output plots are produced as bit-maps for printing or saving to files.
10. Output plot data may also be saved as ASCII files for input to other programs such as spreadsheets.

Dynaplot can convert Relative displacements, velocities and accelerations to Total displacements, velocities and accelerations or conversely from Total to Relative responses.

Dynaplot can produce Response Spectra from the Nodal Acceleration histories. These use the same routines as used by the program **Spectra** described below. Both Displacement Response Spectra and Acceleration Response Spectra are produced. This may be very useful if the inputs are the total acceleration histories at a node as then the spectra produced are *floor spectra* which are useful in the design of parts or portions of a structure.

There is a second post-processor program **Combplot** that takes the output from **Dynaplot** for different analyses or different structures and enables the graphs to be combined for comparisons of the different analyses. The program will also take input from **Spectra** (see below) so those Response Spectra from different earthquakes may be compared.

Spectral Analysis Program:

The program **Spectra** computes response spectra for earthquake records in any of the formats accepted by **Ruaumoko-2D** and **Ruaumoko-3D**.
Six different spectra are computed and plotted:

1. Spectral Displacement
2. Spectral Velocity
3. Psuedo-Spectral Velocity
4. Spectral Acceleration
5. Psuedo-Spectral Acceleration
6. Equivalent Velocity (this is related to energy input from the earthquake)
7. The earthquake accelerogram is also plotted

Accelerogram Plotting Program:

The program **Pquake** plots the accelerogram for earthquake records in any of the formats accepted by **Ruaumoko**.

Generation of Synthetic Accelerograms Program:

The program **Simqke** computes an artificial earthquake accelerogram to match a prescribed Acceleration Response Spectra. This program was developed from the Simqke program that came from MIT in the 1970s. Various time envelopes for the white noise seed may be used to control the time-wise shape of the acceleration record. The input and final spectra are plotted as is the final acceleration history or accelerogram.

Hysteresis Rule Exerciser Program:

The program **Hysteres** takes a displacement history and computes the associated hysteresis loop for a specified stiffness, yield strength and post-yield behaviour. Nearly all of the hysteresis models available in **Ruaumoko** may be specified.

This program may be used to see how a particular rule works but may also be used to determine the best choice of loop parameters to obtain the most suitable hysteresis loop, matching observed experimental test results, for use in a **Ruaumoko** analysis.

A choice of displacement histories is available:

1. Built-in displacement history (this has 100 points)
2. Laboratory-like Displacement History with cycles of increasing ductilities. (155 points)
   1 cycle at ductility 0.75
   3 cycles at ductility 1.00
   2 cycles at ductility 2.00
   2 cycles at ductility 3.00
   2 cycles at ductility 4.00 then increasing to ductility 6.00
3. User specified Sine wave displacements (Input Period, duration and amplitude)
4. User specified Incremental Displacement History
5. User specified Displacement History
6. User specified Displacement History with experimental Force History.
   In this case comparative plots of experimental and calculated force histories and hysteresis loops are produced.
7. CUREe Abridged Loading History.
8. CUREe Near-Field Loading History.
9. CUREe Standard Loading History.
10. ISO Loading Protocol.
11. SPD Loading Protocol.
12. ATC-24 Loading Protocol.

Program Developments:

Ruaumoko and its associated programs are seldom the same from one week to the next as there is a continuous series of developments taking place. However, backwards compatibility of input data and models is maintained. Any difficulties with earlier data sets are covered in the release notes supplied with the cdrom, email or diskettes if replacement executable files are being sent out. If new versions of the post-processor program **Dynaplot** do have a change of data, because of the requirements of new options, then the old versions of **Dynaplot** may be retained, with an alternative name, until all the old post-processor files have been finished with.

Ruaumoko has been developed as an object-oriented program. The control program knows nothing about the operation of any of the members or elements or of their databases. All data transfer in the program is passed via the subroutine call lists except for the member database that comes from a disk file written by the member routines. Only the member routines know the structure of that member type database. All hysteresis rules are called from one subroutine, this means that new rules can be added to the program with minimal programming effort, once the rule is tested for reliability (say by using the **Hysteres** program) then about 10 minutes work is required to add the rule into the **Ruaumoko** (and **Hysteres)** programs. New member types also have minimal changes required in the program, at most, probably half a days work.

If a user wishes to see new features added to the program please contact me. Where possible, it will be done here by me provided all the details are supplied. The alternative approach is that the development process can be done by the user, leaving the task of interfacing the new features into the program here at Canterbury. A sample hysteresis rule subroutine is supplied on the cdrom explaining the rules for such subroutine development.

Program Language:

The programs are written in ANSI FORTRAN77 with one or two features from ANSI FORTRAN90 and FORTRAN95, i.e. the program minimizes the possible effects of compatibilities in compilers. All the graphics is handled via interface subroutines so that the calling programs know nothing of the graphics package structure used in different computer operating systems. There are interface routines for all the different graphics systems that have been used. For PC operating systems the graphics uses the Microsoft Graphics Library originally supplied with the Microsoft compilers and for Windows95/98/NT/2000/XP now supplied with the Digital (Compaq) Visual Fortran 5.0 and 6.X compilers. On Digital/Compaq Alpha unix workstations the graphics is GKS (Graphics Kernel System) or PHIGS graphics. Work is being done to convert the GKS graphics to OpenGL graphics. This would remove the necessity of having GKS or PHIGS installed on the workstation in order for the graphics to work but would also enable the same graphics interfaces to be used on the Microsoft Windows platforms. However, OpenGL introduces its own problems with the general lack of availability of fonts except in the Microsoft version.

Pre-Processor Program.

For **Ruaumoko-2D** only, a **Ruaumoko User Interface** program **Rui** has been prepared in Visual Basic 6.0 to provide a simpler means of preparing or editing the data files. The **Rui** uses a series of templates requesting the appropriate data and showing all the appropriate options at each stage of the data preparation. For the choice of hysteresis loops the shape of the chosen loop is drawn and the user is prompted for the loop data if any extra data is required. There is also a **Rui_Master program**, also written in Visual Basic 6.0 which enables the **Ruaumoko-2D, Dynaplot, Spectra** and **Simqke** programs to be run from within the User interface itself once a data set has been selected or created. These programs are still a little experimental but have been in use by graduate students for some months. However, they have proved to be difficult to upgrade to include all the latest features from **Ruaumoko** and experience has shown that, despite the claims of Visual Basic and other software suppliers that the screen resolutions of different computers are mapped automatically there have been difficulties with screen resolution, particularly on some laptop computers and the programs have also appeared to be slow and *clunky*. The data files generated under the output limitations of Visual Basic are difficult to read in other editors and with Visual Basic, only files generated by the **Rui** can be edited by the **Rui.** For this reason it is difficult to see continued development of this version of the interface. There are further worries. Initial work done in Visual Basic 5.0 had to be started afresh when Visual Basic 6.0 was released and there is considerable concern about what will happen with the next release of Visual Basic if Microsoft continues its policy of not having backwards compatibility of its software. Investigation of better options for the user interface programs is under way.

Information and Help in Use of Ruaumoko etc.

Help is available by E-mail: a.carr@civil.canterbury.ac.nz

This is the most convenient method in that data sets can be attached to the E-mail where there appears to be a difficulty in the data or program. Help is also available by fax, however data sets will require keying-in which takes time and introduces the risk of error. However, plots can be sent by fax if they are useful in showing strange behaviour though as long as they are not too large as bitmaps they could also be emailed. In New Zealand we pay for emails that we send as well as for the ones we receive. I am a little wary of opening Microsoft Word or Excel documents as they pose a considerable risk of carrying viruses.

The Fax number is: International: +64-3-364-2758, or from New Zealand: (03)-364-2758

License Arrangements:

Licenses for all the suite of **Ruaumoko** programs are covered by the following license fees. The programs are sent on a cdrom and two copies of the manuals are supplied with every license. The programs are not transferable and are not to be distributed outside the licensed organization.

Universities, Teaching Institutions, etc.
NZ$2,500.00 for unlimited research and teaching use within the institution. Not for commercial use.

Consulting Practices, Research Organizations, etc.
NZ$6,750.00 for unlimited research and consulting use within the organization.

The licenses will be notified of program upgrades. These occur at approximately 18 month intervals. The initial upgrade will be sent out free of charge with future upgrades being available at a cost of NZ$350 for each upgrade.

Extra manuals are available for NZ$30.00 plus postage. However, the manuals are included as .pdf files on the cdrom with the programs so that extra copies may be printed locally.

For New Zealand purchasers 12.5% Goods and Services Tax (GST) must be added to all prices.

The programs will run on any of the Microsoft Windows operating systems. (Windows95, Windows98, WindowsNT, Windows2000 or WindowsXP).

Source code for the programs or supporting libraries is **not** supplied.

If desired, a free trial version of the programs can be forwarded for evaluation. These are standard versions of Ruaumoko with a reduced amount of memory allocated and the programs will run for approximately 3 months.

For universities and other teaching institutions a student version can also be supplied, at no extra cost, which will only work for a limited period of time such as a semester or academic year. This has been popular where it is desired to make the program readily available to students without the worry of un-authorized copying of the programs. This is particularly the case where there is not a protected computer network. This student version would require replacing every year or semester etc. but this can be done easily by email.

The **Ruaumoko** cdrom contains:

1. Versions of the programs for Windows95, Windows98, WindowsNT, Windows2000 or WindowsXP together with the supporting Windows graphics help file.
   - **Ruaumoko-2D,** Two dimensional dynamic analysis
   - **Ruaumoko-3D,** Three dimensional dynamic analysis
   - **Dynaplot,** Post-processor program for **Ruaumoko-2D** and **Ruaumoko-3D**
   - **Combplot,** Post processor program for **Dynaplot**
   - **Hysteres,** Hysteresis loop exerciser and tuning program
   - **Inspect,** Inelastic response spectra program
   - **Spectra,** Earthquake Response Spectra program
   - **Simqke,** Generation of artificial earthquake acceleration records
   - **Pquake,** Plotting of earthquake acceleration records
   - **Inspect**, Earthquake In-elastic Response Spectra program
   - **Fprint**. Printing of **Ruaumoko** output with FORTRAN carriage controls.
2. A series of data sets for different structures that include the example and pushover data files used in the **Ruaumoko** manual.
3. A selection of earthquake accelerograms.
4. The Ruaumoko User Interface **Rui.**
5. The Ruaumoko User Interface Master Program **RuiMaster.**
6. Sets of results files for the examples in the **Ruaumoko** manual. This includes the post-processor files which can be used in **Dynaplot**.
7. A set of desktop icons for Windows Desktop shortcuts.
8. An example Subroutine for hysteresis rules together with the conditional editor that I use before passing the programs to the compiler
9. A **Readme.pdf** text file. This covers installation.
10. An **ASCII.pdf** file which describes the contents of an ASCII version of the post-processor files so that users who wish to write their own post-processor files, for instance, if they are doing a large number of parameter studies and only which to abstract a small amount of data from each analysis.
11. A complete set of updated manuals in .pdf format which can be printed from Adobe Acrobat.

To order a **Ruaumoko** license, contact Dr Athol J. Carr by E-mail, Fax or mail. Normal practice is to include an invoice and license agreement with the cdrom and manuals when they are forwarded to the licensee.

Dr Athol J. Carr
Reader in Civil Engineering,
University of Canterbury,
Private Bag 4800,
Christchurch,
NEW ZEALAND.
Telephone: +64 3 377 6001 Extension 6246
Fax: +64 3 364 2758
Email: a.carr@civil.canterbury.ac.nz
Or athol.carr@canterbury.ac.nz

Web site:

There are two web sites for Ruaumoko

http://www.ruaumoko.co.nz or http://www.civil.canterbury.ac.nz/ruaumoko